

POLITECHNIKA POZNAŃSKA  
WYDZIAŁ ELEKTRONIKI I TELEKOMUNIKACJI  
KATEDRA TELEKOMUNIKACJI MULTIMEDIALNEJ I MIKROELEKTRONIKI

MAGISTERSKA PRACA DYPLOMOWA

# Synteza dźwięku instrumentów dętych metodą falowodową

Michał Junczyk

Promotor:

**dr inż. Maciej Bartkowiak**

Poznań. 2010

The dissertation deals with an implementation of the woodwind instrument physical model using the digital waveguide modelling technique. An essential theory concerning acoustical properties of woodwind instruments and applicable modelling methods is discussed. This includes an analysis of two existing models of clarinet and flute instruments, which serves as a starting point for the implementation of the "Irish whistle" physical model in Matlab. The final result is the "Irish whistle" application capable of producing a whistle-like sound. Graphical User Interface allows a convenient control over the model and excitation source parameters. The evaluation of the model consists of various comparison tests with a real Irish whistle and an examination of the most interesting model parameters.

Praca dotyczy implementacji modelu fizycznego instrumentu dętego metodą falowodową. W pracy przedstawiono podstawowe informacje teoretyczne na temat właściwości akustycznych instrumentów dętych oraz możliwe techniki ich modelowania. Na podstawie dostępnej literatury dokonano analizy istniejących modeli fizycznych fletu oraz klarnetu, które posłużyły jako punkt wyjścia do implementacji modelu fletu irlandzkiego w środowisku Matlab. Rezultatem projektu jest aplikacja „Irish whistle” pozwalająca na produkcję dźwięków o brzmieniu zbliżonym do oryginału. Graficzny interfejs użytkownika umożliwia wygodną kontrolę nad parametrami źródła pobudzenia oraz modelu instrumentu. W celu ewaluacji modelu przeprowadzono szereg testów porównawczych z prawdziwym instrumentem oraz przetestowano wpływ najbardziej interesujących parametrów.

<b>1</b>	<b>INTRODUCTION .....</b>	<b>5</b>
1.1	PREFACE .....	5
1.1.1	<i>Thesis outline .....</i>	5
1.1.2	<i>Why physical modelling? Limitations of other sound synthesis methods. ....</i>	5
1.1.3	<i>Physical modelling .....</i>	7
1.2	PROBLEM STATEMENT .....	9
1.3	METHODOLOGY: .....	9
1.3.1	<i>Introduction to the topic.....</i>	9
1.3.2	<i>Example code analysis .....</i>	10
1.3.3	<i>Irish flute implementation .....</i>	10
1.3.4	<i>GUI creation and tuning .....</i>	10
1.3.5	<i>Evaluation and testing .....</i>	11
1.4	ASSUMPTIONS.....	11
1.4.1	<i>Physical modelling and audio compression.....</i>	11
1.4.2	<i>Desired outcome .....</i>	12
1.4.3	<i>Limitations .....</i>	12
<b>2</b>	<b>THEORY .....</b>	<b>14</b>
2.1	ACOUSTIC WAVES .....	14
2.1.1	<i>Acoustic waves propagation in space .....</i>	14
2.1.2	<i>D'Alembert Solution.....</i>	14
2.1.3	<i>Digital Waveguide .....</i>	15
2.2	DIGITAL WAVEGUIDE ACOUSTIC MODELLING .....	16
2.2.1	<i>Lumped acoustic systems.....</i>	16
2.2.2	<i>Acoustic impedance, admittance and their electrical analogies .....</i>	17
2.2.3	<i>Wave propagation in cylindrical tubes .....</i>	18
2.2.4	<i>Load Impedances and discontinuities .....</i>	23
2.2.5	<i>Input impedance .....</i>	26
2.3	TONE HOLES AND OTHER PRACTICALITIES .....	27
2.3.1	<i>Two port junction model.....</i>	28
2.3.2	<i>Three-port junction model .....</i>	32
2.3.3	<i>Dynamic three-port filter model .....</i>	33
2.3.4	<i>Wave digital filter model.....</i>	35
2.4	INTERPOLATION .....	37
2.5	EXCITATION MODELS .....	38
2.5.1	<i>Clarinet nonlinear excitation mechanism .....</i>	39
2.5.2	<i>Models of clarinet excitation mechanism.....</i>	43
2.5.3	<i>Excitation mechanism of transverse flute and recorder.....</i>	46

2.5.4	<i>Perry's Cook STK flute excitation model</i> .....	50
2.5.5	<i>Chris's Chafe vortex noise model</i> .....	53
2.6	CLARINET AND FLUTE PHYSICAL MODELS.....	54
<b>3</b>	<b>IMPLEMENTATION OF AN IRISH FLUTE PHYSICAL MODEL.....</b>	<b>57</b>
3.1	INTRODUCTION.....	57
3.2	IRISH TIN WHISTLE CONSTRUCTION AND ACOUSTIC PROPERTIES.....	57
3.3	BLOCK DIAGRAM OF THE TIN WHISTLE PHYSICAL MODEL.....	59
3.4	GRAPHICAL USER INTERFACE .....	64
3.4.1	<i>Global parameters and display properties</i> .....	65
3.4.2	<i>Input signal parameters</i> .....	66
3.4.3	<i>Physical model parameters</i> .....	66
<b>4</b>	<b>EVALUATION OF THE IRISH TIN WHISTLE PHYSICAL MODEL.....</b>	<b>68</b>
4.1	INTRODUCTION.....	68
4.2	EVALUATION METHODOLOGY .....	69
4.3	MOST INTERESTING CONTROL PARAMETERS .....	70
4.3.1	<i>Model adjustments</i> .....	70
4.3.2	<i>Stability control</i> .....	71
4.3.3	<i>Timbre control</i> .....	72
4.3.4	<i>Overblowing</i> .....	78
4.4	REAL VS. VIRTUAL TIN WHISTLE COMPARISON.....	81
4.4.1	<i>Tuning</i> .....	81
4.4.2	<i>Resonances and timbre</i> .....	83
4.4.3	<i>Transient and stationary characteristics</i> .....	88
4.5	IMPERFECTIONS OF THE TIN WHISTLE MODEL .....	94
<b>5</b>	<b>CONCLUSIONS AND FUTURE RESEARCH .....</b>	<b>96</b>
5.1	RESEARCH SUMMARY .....	96
5.2	RECOMMENDATIONS AND FUTURE RESEARCH.....	96
<b>6</b>	<b>BIBLIOGRAPHY .....</b>	<b>97</b>

# 1 Introduction

## 1.1 Preface

### 1.1.1 Thesis outline

This work aims at exploring the topic of physical modelling of woodwind instruments using the digital waveguide modelling synthesis. Simple models of clarinet and flute were implemented using the available literature and web resources. The Irish flute instrument (also known as “tin whistle” or “penny whistle”) has been chosen for the most detailed implementation and evaluation.

The thesis consists of three main parts in chronological order starting with theory, through implementation and finishing with evaluation of the model. First two chapters contain some fundamental theory concerning musical sound, acoustic waves and modelling using digital waveguides (DWG synthesis). The most common building blocks of DWG physical models are discussed using clarinet and flute models from the open-source STK Synthesis Toolkit library. Chapter three presents a new Irish flute DWG model implementation in Matlab. Chapter four deals with the evaluation of the Irish flute model. The most interesting model parameters affecting the produced sound, as well as the stability of the system are examined and described in more details. Subsequently, results of the model tuning process are discussed. Finally, comparison tests between obtained sounds of the real instrument and its model are conducted, with some comments about model imperfections. The last fifth chapter contains conclusions on conducted research and discusses possible future improvements.

### 1.1.2 Why physical modelling? Limitations of other sound synthesis methods

For centuries the classical music and traditional instruments make our lives pleasant with non decreasing power. On the other hand, the theoretical study of musical acoustics is a relatively young part of science, considering the long history of musical instrumentation. The most amazingly sounding instruments e.g. Stradivarius violin were designed mostly by empirical means. Tools and methods to analyze acoustical differences between such a masterpiece and its mediocre counterpart came afterwards. Before

mathematical models and helpful test equipment were available, the knowledge about instrument design was handed down from generation to generation over many centuries and design improvements were obtained mostly empirically. It's only the past century when the musical acoustics reached the level enabling the cooperation between instrument designers and physicists. Through the in-depth analysis performed by scientists, designers achieve a better understanding of many complex instrument properties, helping them improve their products.

Music synthesis differs from musical acoustics principally with its design oriented goals, which can be summarized as the creation of new sounds and instruments using electronic devices or computers. The most popular sound synthesis techniques are based on pre-recorded sounds of original instruments (sampling) or creation of new sounds using waveform and noise generators, filters, envelope generators, modulators and various effect processors (e.g. additive, subtractive and fm synthesis) [1]. All this contemporary technology delivered into creative hands of musicians yields fruits in the development of new music genres e.g. techno, hip-hop and almost infinitely big field for an experimentation and creation of completely new, sometimes strange musical sounds. While the electronic music brought many excitement and freshness to our lives, traditional instruments and acoustical music is doing very well and has the most powerful impact on listeners.

Hence, another goal set for companies and hobbyist involved into musical synthesis world is the recreation of the traditional acoustic instruments sounds, which turned out to be a non-trivial task. The outcome should be a "better" version of the original instrument which is easier to play, cheaper, more portable and more flexible.

Results of the simplest synthesis method called "sampling" are not satisfying, because produced sound elongates and shortens in an unnatural manner along with the pitch changes. Moreover the natural instrument property to change its timbre depending on the musician's expression is difficult to realise on the synthesizer based on few samples only. The solution called "multisampling" (recording a complete set of samples of natural instrument representing various types of expressions) is very time consuming and demands many gigabytes of storage space, e.g. Alicia

Keys's piano library contains 17 GBs of samples recorded with 12 different discrete velocities.

The frequency domain based methods like additive or subtractive synthesis try to recreate the spectrum of the original sound using basic waveforms and filters. However reproduction of all original spectral characteristics demands plenty of available signal paths, manipulators etc., and creates a cost of an increased components/computational power requirements. Moreover if the instrument becomes too complex, less experienced users may be muddled up in plethora of parameters. Finally, realistic spectrum changes in time are difficult to obtain, because sound processing and generation components have stationary characteristics.

### **1.1.3 Physical modelling**

Starting back in the eighties of the last century, musical acoustics and synthesis worlds turned into new, very attractive approach called physical modelling, which lays at the crossroads of these two fields. Its strength in simulating sounds of traditional instruments lies in the fact that, "rather than trying to directly reproduce the sound by an acoustical system, physical modelling aims, relying on the physical properties of the system, at simulate its functioning" [2]. It took about twenty years before the PCs computing power became sufficient to perform real-time processing demanded by virtual instruments mathematical models. Nowadays most professional audio software companies invest time and money into the physical modelling research and equip new versions of their popular *DAW (Digital Audio Workstation)* software with new playful instruments. Arturia Brass, Propellerhead Reason Kong or Image Line Sakura are the most popular programs able to realistically synthesize sounds of most chordophones, idiophones and some aerophones.

The sound produced by a digital physical model is calculated as its response to a given input, such as the blowing pressure in the mouth of a musician. By simulating the behaviour of the acoustical model itself, it is possible to obtain realistic reproduction of the physical features of the output e.g. changing the timbre with the register of the notes played. Therefore it is much easier for the player to actually interact with the virtual instrument.

Comparing to the previously mentioned synthesis schools, which rather produce sounds of non changing spectrum characteristics within time, physical modelling deals very well with the reproduction of transients, crucial from the perceptual point of view. Most of the music and speech sounds are transient in nature, with very abrupt spectrum and amplitude changes during the attack phase of a note. Effects like vibrato (amplitude or frequency modulation) or natural expression with varying dynamic levels are hard to reproduce by additive synthesis or sampling, because it would lead to an analysis and synthesis of many different sound spectra or playing many different samples for even a single note [2].

The main difficulty and biggest drawback of the physical modelling method is the complexity of sound production processes and physical properties of simulated instruments. Therefore modelling demands a serious number of experiments and solid theory background. Toshifumi Konimoto, leader of the Yamaha physical modelling research team responsible for the legendary VP1 and VL1 synthesizers puts more light on the time consuming evaluation process, explaining that "rather than relying on frequency response graphs and other "precision" measurements to evaluate final performance, many critical performance decisions are made using the trained ears of top-level music and sound specialists" [3]. Considering practicality and computational cost the biggest goal for designers and physicist is to find the "optimal trade-off between the convenience of the model and its perceptual relevancy" [2]. More complex model means an increased processor usage and leads to problems with the real-time performance, by increasing latency while using e.g. MIDI wind controller or keyboard. Hence, if the particular physical property of the instrument is imperceptible, it can be skipped/simplified in the model to save a computing power. Another drawback from the end user point of view is the high risk of making a model unplayable, by tweaking accessible parameters in the wrong way. Instruments create sound because of the occurrence of an acoustic resonance, which is the result of an acoustic feedback. Digital systems containing feedback are very prone to unstable behaviour for even tiny changes of model parameters. Therefore PM synthesizer very often demand painstaking approach when designing new patches and are recommended to experienced synthesizer's users.

## **1.2 Problem statement**

The goal of this thesis is the creation of the woodwind instrument physical model using digital waveguide synthesis method. The research is conducted based on the available web resources and literature. Matlab is the programming environment of choice. Irish Flute is the instrument of choice for most detailed implementation with GUI (Graphical User Interface). Final stage of this project is the evaluation of the implemented model consisting of comparison tests with the Feadog Irish whistle and analysis of the most interesting model parameters.

## **1.3 Methodology:**

All the actions leading to the desired outcome can be divided into five essential stages:

- 1) Introduction to the topic
- 2) Example code analysis
- 3) Irish flute implementation
- 4) GUI creation and tuning
- 5) Evaluation and testing

### **1.3.1 Introduction to the topic**

Introduction to the topic stage starts with the analysis of materials concerning acoustics of the woodwind instruments, acoustic wave propagation and digital waveguide synthesis theory background. The best available resource materials treating of a digital waveguide modelling are made accessible online by its inventor, Julius O. Smith from the Stanford University [4]. Another great source of information is provided by Smith's colleagues from the Stanford's University CCRMA department – Perry Cook and Gary Scavone. Starting with the ultimate open-source library STK (Synthesis ToolKit), which is a "set of open source audio signal processing and algorithmic synthesis classes written in the C++ programming language" [5], through the Scavone's highly educational PhD thesis about single-reed woodwind instruments [6], finishing at Cook's reader-friendly book "Real Sound Synthesis for Interactive Applications" [7]. .

Reference materials concerning woodwind instruments and acoustics in general were found mostly in the internet: [8], [9], [10] and [11].

### **1.3.2 Example code analysis**

After obtaining theoretical understanding of how woodwind instrument physical models work, the next stage was to implement and run a simple model of such instrument in Matlab environment. The STK clarinet and STK flute source codes from the open-source STK library were analyzed and rewritten using Matlab, thus allowing stage-by-stage analysis of the signal flow and better understanding of the sound generation process.

### **1.3.3 Irish flute implementation**

Unfortunately the author of this thesis does not possess any experience playing a clarinet or a transverse flute. Both instruments are quite expensive and hard to master for a beginner. Furthermore their physical models are constantly improved by specialists from mentioned Stanford University CCRMA (Center for Computer Research in Music and Acoustics) department or Marseille's laboratory of mechanics and acoustics of the CNRS (Centre National de la Recherche Scientifique) [12]. To keep the project down to earth, the Irish flute (also known as the Tin Whistle or Scottish flageolet) has been purchased; hence allowing the author to conduct comparison tests between the real instrument and its model using self played and recorded sounds. Tin whistle with its simple construction, almost perfectly cylindrical bore and only six finger holes seemed to be the perfect choice for the creation of a new physical model and further research.

### **1.3.4 GUI creation and tuning**

After creating an Irish flute physical model in Matlab using building blocks and filter design functions from previously mentioned STK programs, the next step was the initial evaluation of obtained sounds. Implementation was a success in terms of generating "some" flute-like sounds, but the differences between the real Irish flute and its model's timbre, attack character and spectrum were easily perceivable. Therefore in order to make parameters adjustment easier, a graphical user interface in Matlab was created. The sound samples of a real Irish flute were recorded and made

available in the application to allow a quick comparison between virtual and real-world sounds during calibration process. There is no doubt that this part of the project was the most challenging and arduous one. Firstly the author had to overcome problems with an unexpected behaviour of the model introduced by a feedback in the system, finding a set of parameters ensuring stability for most standard musician's finger configurations on the instrument (fingering). Moreover the amplitude, frequency, randomness or noise character etc. of an incoming pressure from a player's mouth are equally important factors affecting obtained sound. Hence it was not a trivial task to adjust a plethora of parameters in a way to closely reproduce real instrument sounds. Last but not least every generation of the couple seconds long sound was taking about 20-30 seconds, which made a process of tuning quite tedious.

### **1.3.5 Evaluation and testing**

Last part of the project was focused on the model tuning, analysis of various parameters affecting timbre and stability and finally various comparison tests with real Irish whistle. Due to perceptible discrepancies between synthesized and recorded sounds the idea of performing MOS listening tests was abandoned

## **1.4 Assumptions**

### **1.4.1 Physical modelling and audio compression**

The goal of the project formulated as the creation of a woodwind instrument physical model, could be put in the wider context connected with audio compression, simultaneously explaining the relevancy of the project for the Multimedia Telecommunications Department.

"MPEG-4 Structured Audio [13] standard of compression defines decoders for generating sound based on several kinds of "structured" inputs. Text input is converted to speech in the Text-To-Speech (TTS) decoder, while more general sounds including music may be normatively synthesized" [14]. Hence, a synthetic music may be transmitted at extremely low bitrates. The structured audio tools are able to decode music in a parameterized form (e.g. scores, MIDI) placed in the bit stream using special synthesis language called Structured Audio Orchestral Language.

The SAOL defines an orchestra made up of various instruments, which create and process a control data. The MPEG-4 does not standardize a single method of synthesis for this task, but rather a way to describe method of synthesis. Therefore any of future sound synthesis method could be used, including a physical modelling.

One of the biggest advantages of physical modelling to become a synthesis method of choice in an audio codec's industry, is its ability to realistically synthesize sound of acoustic instruments having a time-sequenced set of commands (score) and couple parameters describing an instrument model. Physically-based models are a highly structured representation of sound. Moreover, the control parameters have a direct physical interpretation, and therefore vary slowly enough to be used for efficient coding.

Naturally other methods should manage to perform the task as well, but for a cost of extra memory space in the decoder to keep samples or waveforms.

Summing up, the main advantage of physical modelling approach in compression is that ultralow bit-rate transmission can be achieved.

#### **1.4.2 Desired outcome**

Keeping in mind physical modelling properties in the context of audio compression and possible future research in this field, the desired project outcome could be a set of documented Matlab functions, able to generate realistic sound of a woodwind instrument.

#### **1.4.3 Limitations**

At the beginning, physical modelling seems to a be very complex and overwhelming topic. Exploration of numerous conference papers demands significant amount of knowledge from sciences like digital signal processing, acoustics, signals theory, even music. Before this project, author's experience in the field of music synthesis was rather analytical than design oriented. Regardless of intellectually exacting and time-consuming process of data collection and initial implementation problems, the project was a fascinating journey through various author's interest.

Implementation code was not optimized, therefore real-time processing is not possible. It is very difficult to compete alone with heavy experienced teams from CCRMA or Yamaha. Another factor was lack of a MIDI breath

controller (e.g. Akai EWI USB) [15], which could take advantage from real-time control functionality. Woodwind and brass virtual instruments possess a dedicated MIDI controller with a mouth pressure sensor and construction similar to woodwind instruments. Control buttons are placed along the bore simulating tone-holes and therefore allowing original fingering. Without no doubt such device would be a great help to obtain realistic input signal to feed later into a physical model.

## 2 Theory

### 2.1 Acoustic Waves

#### 2.1.1 Acoustic waves propagation in space

Wave equation governs the propagation of an acoustic wave through a material medium e.g. air and describes the evolution of acoustic pressure  $p$  and particle velocity  $u$  as a function of position  $\mathbf{r}$  and time  $t$ . The displacement vector  $\mathbf{r}$  is equals to  $\mathbf{r} = (x, y, z)$  for the most general three-dimensional case. A simplified form considering only one spatial dimension has a form:

$$\frac{\partial^2 p(t, x)}{\partial t^2} = \frac{K}{\rho} \frac{\partial^2 p(t, x)}{\partial x^2} \quad (2.1)$$

Here,  $K$  is a bulk modulus of a medium and  $\rho$  is a density of air. More popular form of the same equation is the one with the speed of wave:

$$\frac{\partial^2 p(t, x)}{\partial t^2} = c^2 \frac{\partial^2 p(t, x)}{\partial x^2} \quad (2.2)$$

From two above equation one can easily see that the speed of wave equals to:

$$c = \sqrt{\frac{K}{\rho}} \quad (2.3)$$

#### 2.1.2 D'Alembert Solution

The generalized solution of a one-dimensional wave equation is called D'Alembert's formula and has a form:

$$p(t, x) = p^+ \left( t - \frac{x}{c} \right) + p^- \left( t + \frac{x}{c} \right) \quad (2.4)$$

where  $p^+$  and  $p^-$  are any arbitrary functions representing two oppositely directed pressure waves travelling along the direction of propagation  $x$ . The plus (+) superscripts indicates travelling in the positive  $x$ -direction or to the right, while negative (-) superscripts indicate travel in the negative  $x$ -direction or to the left. "An important point to note about the travelling wave solution of the 1D wave equation is that a function of two

variables has been replaced by two functions of a single variable in time units. This leads to great reductions in computational complexity" [16]. Detailed derivation of the D'Alembert from a one-dimensional wave equation can be found in [16].

D'Alembert's solution serves as the theoretical foundation on which physical models for stringed and woodwind instruments are based upon. The superposition of two travelling waves yields the standing wave present in an actual instrument which is physically responsible for a sound generation.

### 2.1.3 Digital Waveguide

In order to digitally represent travelling waves from a D'Alembert solution, first they need to be sampled with some time period  $T$ .

$$x \rightarrow mX \tag{2.5}$$

$$t \rightarrow nT \tag{2.6}$$

$$y(n, m) = y_r(n - m) + y_l(n + m) \tag{2.7}$$

After that the propagation of a wave can be simulated using a simple digital delay line. Since there are two oppositely directed travelling waves in the solution, a second delay line is needed to perform a simulation of a standing wave in a flute bore.

This leads to the invention of a nifty structure called digital waveguide, which allows to perform digitalization along both temporal and spatial dimensions and may be defined as a bidirectional delay line with some impedance  $R$ .

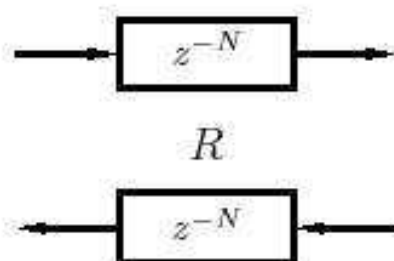
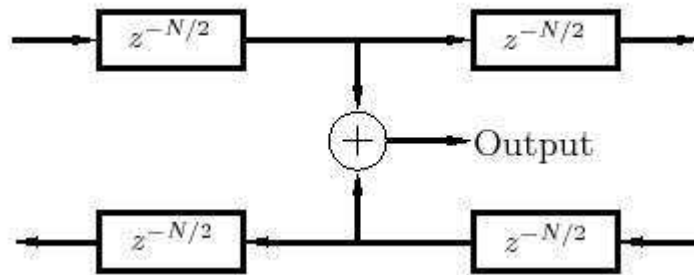


Figure 2.1: A  $N$  samples long digital waveguide at wave-impedance. (source: [37])

Each segment of digital waveguide corresponds not only to the time interval of  $T$  seconds, but also to the spatial interval of  $Tc$  meters. Wave impedance  $R$  is needed for e.g. in case of connecting two digital waveguides and calculating losses due to reflection at their coupling.

The physical standing wave vibration in the instrument is a sum of left and right travelling waves. Figure 2.2 shows an extraction of a physical signal from a middle of a digital waveguide using digital line taps.



**Figure 2.2: Extracting a physical signal using delay line taps from the middle of a digital waveguide. (source: [37])**

Delay lines may be tapped in any arbitrary place, so an acoustic vibration signal may be obtained from any section of the instrument resonant part in a form:

$$P = P^+ + P^- \tag{2.8}$$

Or using a digital waveguide model variables:

$$p(t_n, x_m) = p^+(n - m) + p^-(n + m) \tag{2.9}$$

## 2.2 Digital waveguide acoustic modelling

### 2.2.1 Lumped acoustic systems

“An acoustic system in which sound wave propagation is determined by solutions to the wave equation is referred as a *distributed* system” [6]. In such case wave variables are functions of both space and time. However sometimes it is convenient to determine a *lumped* input-output response of sound wave propagation through an acoustic system and ignore information about the exact behaviour everywhere within it. A good example of using a lumped-parameter system for convenience comes from a realm of an electromagnetism. Instead of considering distributed-parameter systems like electric transmission lines or optical waveguides, engineers take

advantage of ordinary RLC circuits. However one condition has to be met in order to ensure correct results – the oscillation wavelength has to be large relatively to the geometry of the physical component. So the lumped system is convenient during analysis of the behaviour of large wavelength sound waves within small structures. Operating in the *low-frequency* limit allows describing an acoustic system in terms of fundamental acoustic components analogous to masses, springs and dampers known from mechanical system analysis or inductors, capacitors and resistors in electrical circuit analysis.

### 2.2.2 Acoustic impedance, admittance and their electrical analogies

Lumped acoustic system input-output relation in a frequency domain may be described using an *admittance*  $\Gamma$  (velocity response of the system to an applied pressure input) or *impedance*  $Z$  (pressure response to an applied velocity input) as presented in figure 2.3. “Velocity can take form of either *particle velocity*  $V$  (in meters per second) for systems in open air or *volume velocity*  $U$  (in meters cubed per second) for enclosed structures” [6].

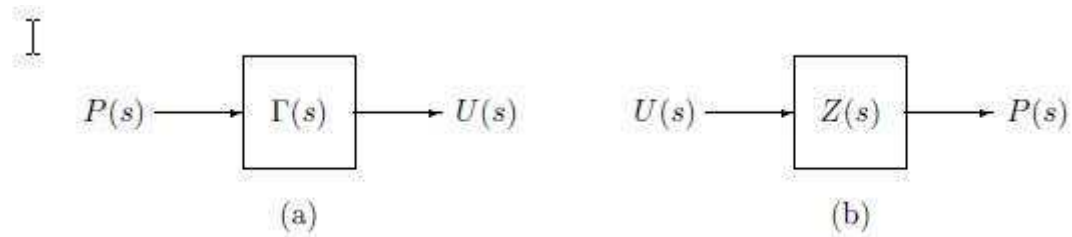


**Figure 2.3: Linear acoustic system block diagrams. (source: [6])**

*Wave impedance* referred also as the *characteristic impedance* in open air is the ratio of pressure  $P$  to particle velocity  $U$  in a sound wave travelling through air is given by:

$$Z_0 = \frac{P}{U} = \rho c \quad (2.10)$$

where  $\rho$  is the density of air and  $c$  is a speed of sound propagation.

The acoustic impedance of the open tube expressed in terms of the Laplace transform, for zero initial conditions has a form:

$$Z(s) = \frac{P(s)}{U(s)} = \left(\frac{\rho L}{S}\right) s \quad (2.11)$$

Where  $L$  is the length of the tube and  $S$  is its cross-section. In the low-frequency limit an acoustic impedance of an open tube is called an inductance or an *inertance* and it is analogous to the inductance and mass in an electrical and mechanical systems, respectively.

A cavity or a *tank* is the acoustic analogy of the electrical capacitor or the mechanical spring and is given by:

$$Z(s) = \frac{\rho c^2}{Q} \frac{1}{s} \tag{2.12}$$

where  $Q$  is the cavity volume.

To express losses in an acoustical system one may use frequency-independent real value resistive component with impedance:

$$Z(s) = R \tag{2.13}$$

An acoustic resistance equivalent in an electrical and mechanical realm are resistor and dashpot, respectively. In practice to represent viscous and thermal losses present in the tube, frequency-dependent parameters are used and will be described in more details in the next section.

A detailed derivation of presented formulas for an acoustic inertance, cavity and resistance can be found in [6 p. 7].

### 2.2.3 Wave propagation in cylindrical tubes

This section describes the behaviour of an acoustic wave propagating inside the cylindrical tube. Presented theory forms a basis for understanding processes in the cylindrical bores of the clarinet and flute. It is worth mentioning that this project does not deal with woodwind instruments having a conical, complex bores (e.g. trumpet, saxophone), because of their much more advanced acoustical description and bigger computational power requirements of their models.

In general a bore acts as a resonator whose first goal is to emphasize certain desirable frequencies. The second goal is to encourage production of sustained oscillations within a feedback system. Special finger holes are placed along the bore in order to allow effective length variations, thus to produce musically useful range of frequencies. A more detailed description of flute bore and tone holes is presented in sections 2.3.5 and 2.4.

An infinite cylindrical pipe, assuming its walls are rigid, perfectly smooth and thermally insulated, theoretically allows a lossless propagation of the plane wave along its main axis. However, in practice to make the pipe resemble a cylindrical bore, one should consider a confine, cylindrical pipe of radius  $r$  and length  $L$ . The axis of the pipe is coincident with the direction of wave propagation along the  $x$  axis.

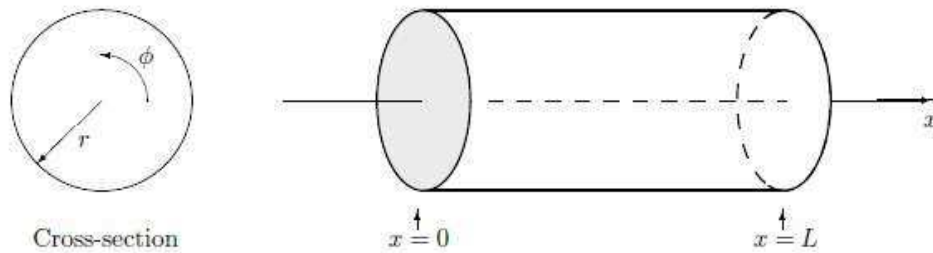


**Figure 2.4 A cylindrical pipe in cylindrical polar coordinates. (source: [6])**

Scavone in his work [6 p. 10] solves a three dimensional Helmholtz equation in cylindrical polar coordinates for such pipe and proves that “wave motion in cylindrical bores is primarily planar along the principal axis of the tube  $x$ ”.[6]

A sinusoidal time dependent planar wave motion equation in the tube has a form:

$$P(x, t) = C e^{j(\omega t - kx)} \tag{2.14}$$

where  $\omega$  is the angular velocity of the wave,  $k$  is the wave number equal to  $k = \frac{\omega}{c}$  and  $C$  is the amplitude of the wave.

Following [6] the volume flow for a cross-sectional area  $S$  is given by:

$$U(x, t) = \frac{S}{\rho c} C e^{j(\omega t - kx)} \tag{2.15}$$

Hence, the wave impedance is:

$$Z_0(x) = \frac{P(x)}{U(x)} = \frac{\rho c}{S} \tag{2.16}$$

In the previous section a digital waveguide with sampled travelling pressure waves components within was introduced. To calculate the value of propagating volume flow it is necessary to know the acoustic impedance of the pipe being modelled.

Knowing that the total pressure of two oppositely travelling pressure waves in the tapped digital waveguide is given by:

$$P = P^+ + P^- \quad (2.17)$$

Then the volume flow  $U$  has a form:

$$U = \frac{(P^+ - P^-)}{Z_0} \quad (2.18)$$

Relations between the pressure and volume velocity travelling wave components at any particular position in space  $x$  and time  $t$  are:

$$P^+ = Z_0 U^+ \quad (2.19)$$

And

$$P^- = -Z_0 U^- \quad (2.20)$$

The characteristic wave impedance  $Z_0$  is a frequency-domain parameter. Presented equations for pressure and volume velocity in-phase travelling-wave components are valid for both frequency- and time-domain analyses, because the wave impedance of sound plane wave is purely real and independent of position.

The analysis assumes a lossless wave propagation along the bore, by neglecting viscous and thermal effects near the pipe walls. In reality this is not a case. Scavone in [6 p. 23] meticulously described an impact of the boundary layer friction and thermal exchange with the environment.

Albeit, for the purposes of this study, theoretical description might be omitted. More interesting explanation of the actual influence of the visco-thermal layer can be done showing its implementation taken from the waveguide bore model.

In order to truly model a thermoviscous losses distributed along the pipe in a digital domain, low pass digital filter should be placed after each unit delay in a digital waveguide. To improve computational performance one can replace each unit delay with the digital filter designed to approximate the attenuation and phase delay incurred over the distance  $cT$  (spatial sampling interval).

The transfer function of the filter is given by:

$$H(z) = e^{-\alpha c T} z^{-c/v_p} \quad (2.21)$$

Where  $v_p$  is a phase velocity and  $\alpha$  is an attenuation coefficient per unit length [6]. Both parameters vary with the frequency and depend upon pipe radius.

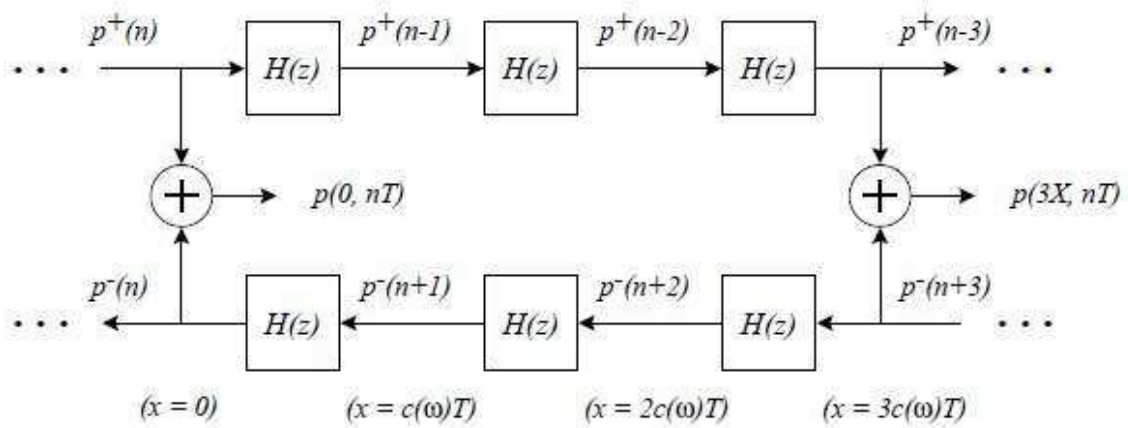


**Figure 2.5 Digital waveguide implementation of lossy plane-wave propagation in the air, with the unit delays incorporated into  $H(z)$ . (source: [6])**

Unfortunately, the solution presented in figure 2.5 significantly increase number of calculations in the system. Since the woodwind bore model is linear, the problem may be overcome by commuting or *lumping* filters together into one filter  $H_b^m$ , as long as the signal is not being observed:

$$H_b^m(z) = z^m H^m(z) \quad (2.22)$$

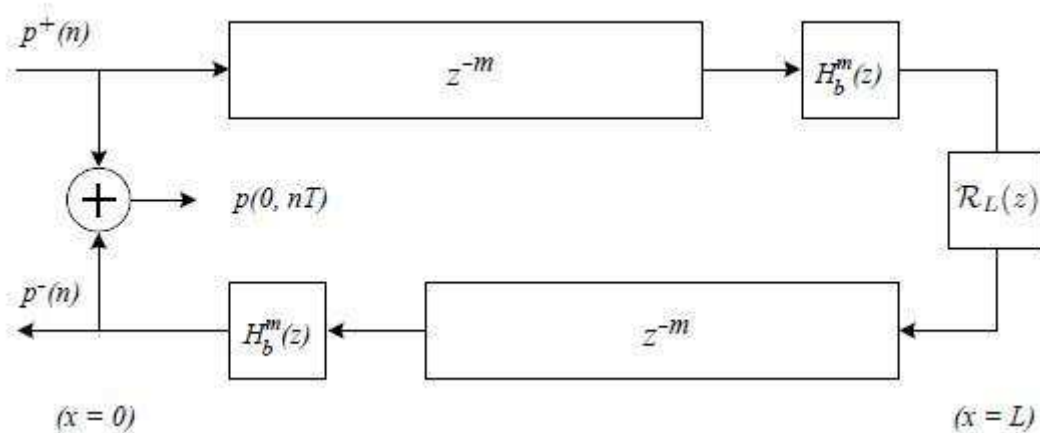


**Figure 2.6 Commuted thermoviscous losses in digital waveguide cylindrical air column implementation. (source: [6])**

The solution, as presented in the figure 2.6, allows for significant computational savings. It is possible to improve the bore model even further by incorporating thermoviscous losses into the transfer function of the reflection filter at the end of the bore.

Figure 2.7 presents the second order digital filter frequency response obtained using a least-square approximation with the *invfreqz* function in Matlab. Thermoviscous losses were calculated for an Irish flute bore of 12 mm diameter. Length of the bore is 25.6 cm equal to approximately 33 samples for the sampling frequency of 44.1 kHz and speed of sound 343 m/s. In order to increase an accuracy of approximation in the low frequency region, a weighting function  $\frac{1}{\omega^2}$  was applied to the approximation error during the optimization.

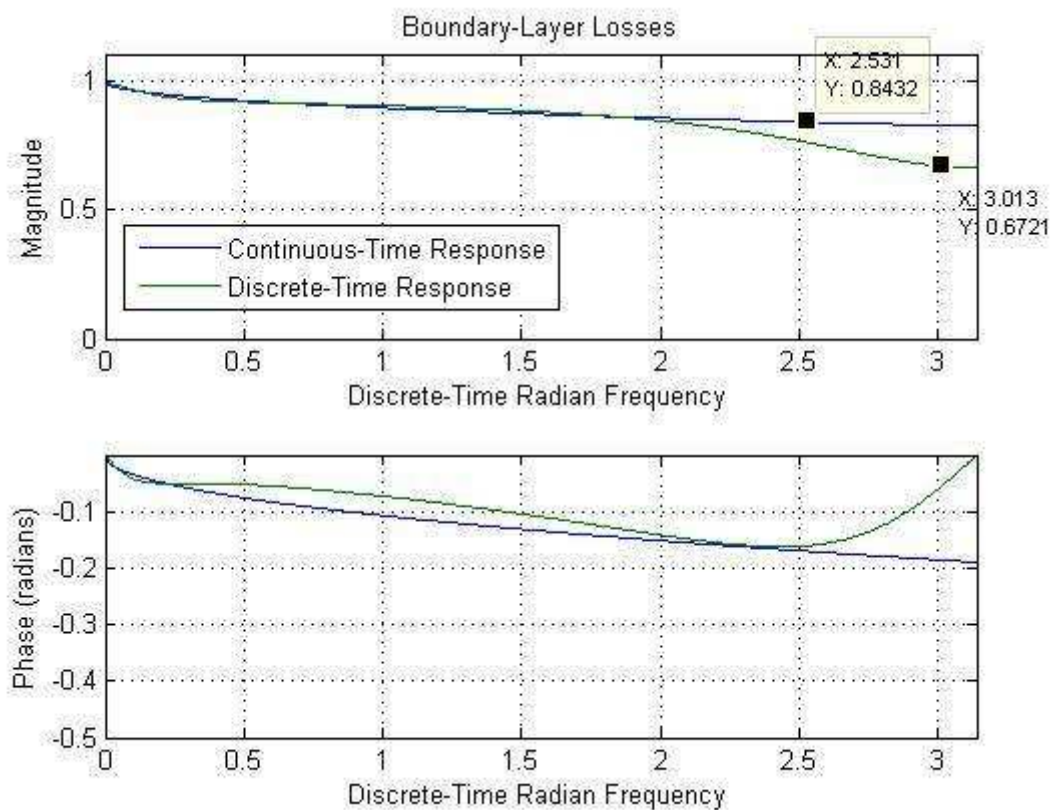


**Figure 2.7 Thermoviscous damping theoretical response (blue) and its digital filter approximation (green) for sampling frequency 44100 Hz, pipe radius of 6 mm and pipe length 25.6 cm.**

#### 2.2.4 Load Impedances and discontinuities

Similarly to the transmission line discontinuities known from electromagnetism, an acoustic wave passing between media characterised by different impedances produces a reflected wave and transmitted wave. Travelling pressure waves are typically reflected in a frequency dependent manner characterised by reflection coefficient, or *reflectance*. *Reflectance* is a frequency-dependent ratio between complex amplitudes of incident and reflected waves. For a pipe of characteristic impedance  $Z_0$  loaded at the end with the impedance  $Z_L$ , continuous time-domain pressure-wave reflectance is given by:

$$R(\omega) = e^{-j2kL} \left[ \frac{Z_L(\omega) - Z_0}{Z_L(\omega) + Z_0} \right] = \frac{Z_L(\omega) - Z_0}{Z_L(\omega) + Z_0} \quad (2.23)$$

Where  $Z_L$  is the load impedance at  $x=L$  and  $Z_0$  is the characteristic impedance of the cylindrical tube. Phase-shift term  $e^{-j2kL}$  comes from wave propagation from  $x=0$  to  $x=L$  and back and has a unity magnitude and can be ignored in case of plane waves.

Similarly as in the transmission line theory reflection coefficient comes in pair with transmission coefficient, representing the ratio of incident to transmitted complex amplitudes at a particular frequency.

$$T(\omega) = e^{-jkL} \left[ \frac{2Z_L(\omega)}{Z_L(\omega) + Z_0} \right] = \frac{2Z_L(\omega)}{Z_L(\omega) + Z_0} \quad (2.24)$$

For the low-frequency waves the end of the open tube may be approximated by  $Z_L = 0$ . Reflectance becomes negative, indicating that pressure travelling-wave components are reflected from the open end of a cylindrical tube with an inversion (or a  $180^\circ$  phase shift). For the rigidly terminated pipe at  $x=L$ ,  $Z_L$  is close to infinity, hence reflectance is equal to one and reflection occurs without attenuation and sign change.

Presented formulas are extensively used to model non-uniform bores by division into uniform cylindrical sections and calculating reflected and transmitted travelling waves components for every junction.

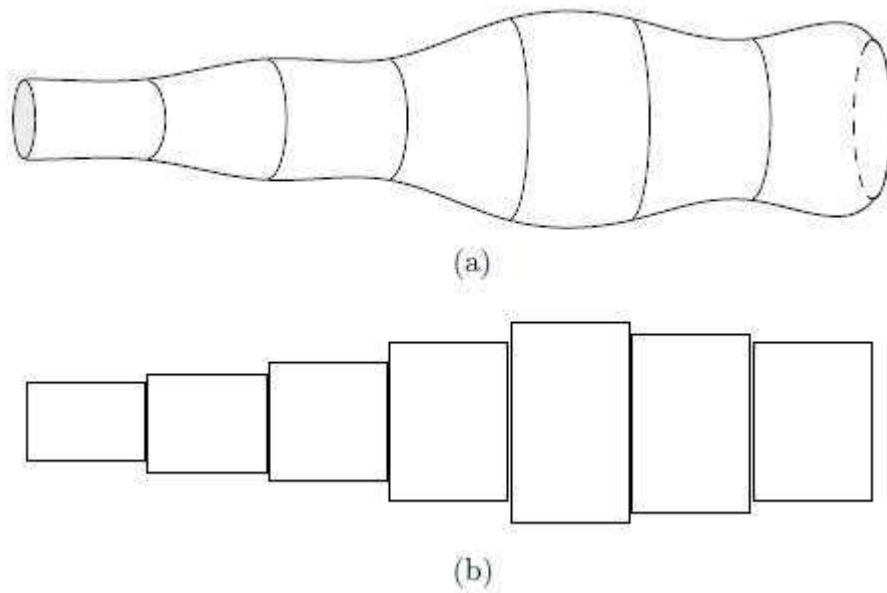


**Figure 2.8 A non-uniform bore (a) and its approximation by cylindrical sections (b) (source: [6])**

The actual load impedance of the unflanged cylindrical pipe of flute or organ pipe is complex and frequency dependent. The theoretical solution and its derivation obtained by Levine and Schwinger in 1947 is very complicated and can be found in [17].

However for the digital waveguide modelling purposes it is possible to design the digital filter, which accurately mimics continuous time characteristics mentioned above. Figure 2.9 presents a first order IIR filter designed using *invfreqz* method and its location at the termination of the bore model.

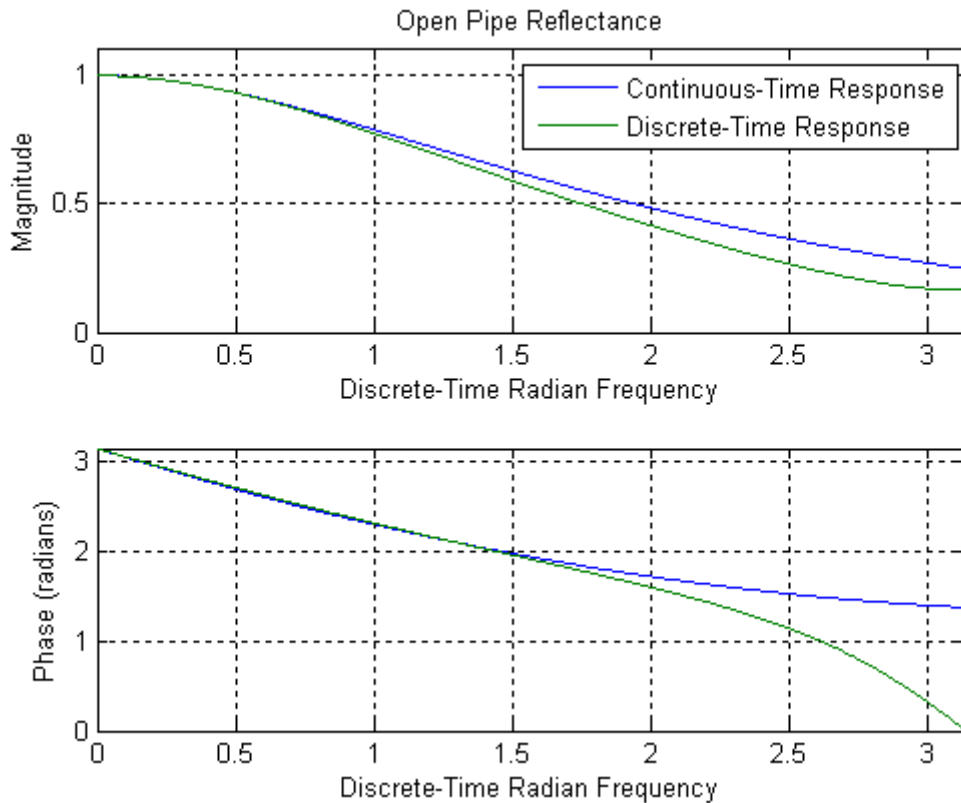


**Figure 2.9 Continuous-time and first order digital filter magnitude and phase response for the Levine and Schwinger reflectance in a cylindrical duct of radius 0.0061 meters. (source: [6])**

Figure 2.9 reveals a low-pass characteristics of the reflectance filter. The cut-off frequency depends on the radius of the bore. As expected from the previous idealized reflectance calculations ( $Z_L=0$ ), filter changes the polarity of the input signal, however mostly for low-frequencies (approx. 180 degrees phase response near DC).

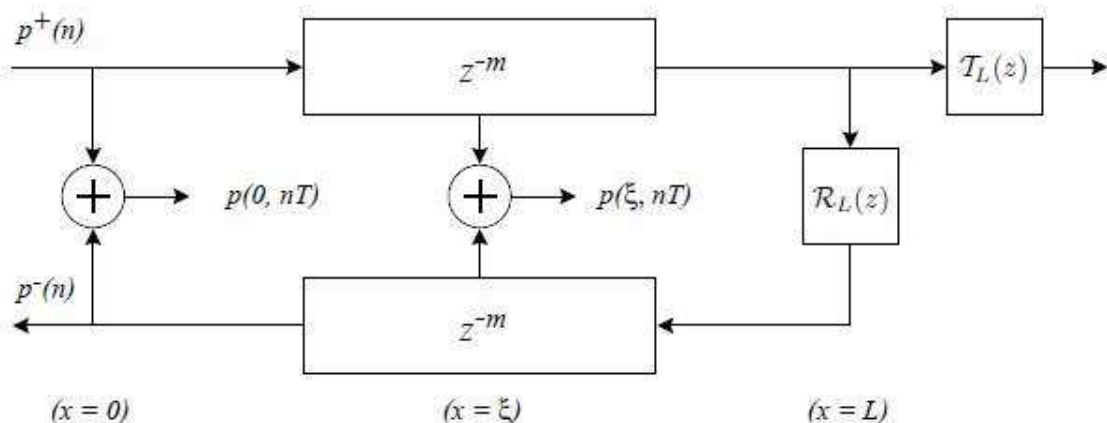


**Figure 2.10 Sound radiation filter implementation in a digital waveguide cylindrical duct model – complementary model with reflectance and transmittance filters. (source: [6])**

The output of top delay line in a digital waveguide bore model is fed through a filter modelling the reflection impedance. Its output is piped into the bottom, oppositely directed delay line. Optionally, the output of the top delay line may be filtered by the transmission filter of complementary, high-pass characteristics as illustrated in the figure 2.10.

### 2.2.5 Input impedance

In the electromagnetism realm transmission lines can be described in the frequency domain by the characteristic impedance, defined as the ratio of the amplitude of a single voltage to its current wave. Since both electromagnetic as acoustic ducts also transfer reflected waves, characteristic impedance differs from the impedance measured at the arbitrary place on the line.

The input impedance (at  $x=0$ )  $Z_{IN}$  of an acoustic cylindrical tube of length  $L$  terminated by a load impedance  $Z_L$  is given by:

$$Z_{IN} = Z_0 \left[ \frac{Z_L \cos(kL) + jZ_0 \sin(kL)}{jZ_L \sin(kL) + Z_0 \cos(kL)} \right] \quad (2.25)$$

Scavone in [6 p.14], using the above equation, derives formulas for resonant frequencies of the open-closed (o-c) pipe and open-open pipe (o-o), for  $n=1,2,\dots$  given by:

$$f^{(o-c)} = \frac{2(n-1)c}{4L} \quad (2.26)$$

$$f^{(o-o)} = \frac{nc}{2L} \quad (2.27)$$

respectively. Open-closed pipe fundamental wavelength is equal to four times its length, while higher harmonics appears at odd integer multiplies of the fundamental frequency. In the open-open case resonances occur at all integer multiplies of the fundamental frequency, which corresponds to the wavelength equal to pipe doubled length.

The input impedance of an acoustic structure provides a valuable information regarding its natural modes of vibration and effectively describes particular resonance properties. A method for measuring an input impedance of the non-uniformly distributed bore is shown in [6 p. 16].

In a digital domain one can find the input impedance using the impulse response  $h(n)$ . Cylindrical bore model with thermoviscous losses ignored and rigid termination at the entrance (e.g. clarinet) has a form of the open-closed pipe feedback system presented in the figure 2.11.

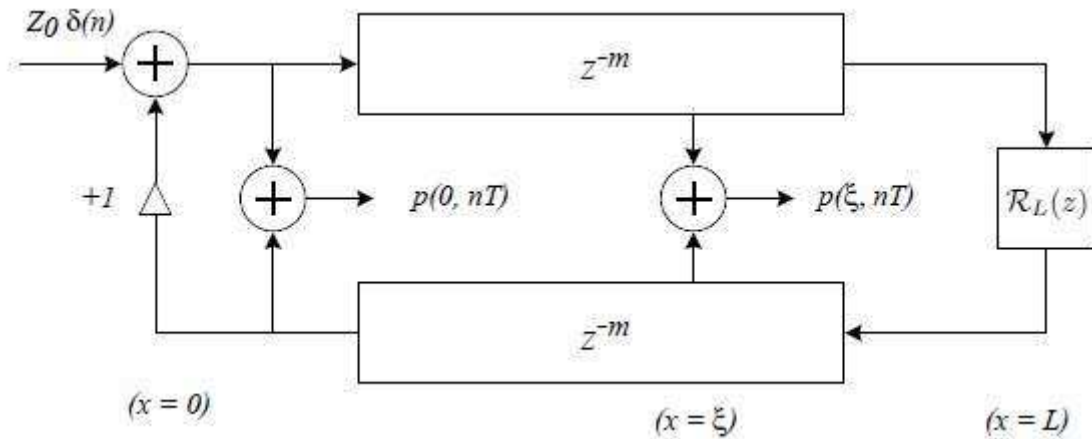


Figure 2.11 Digital waveguide model of closed-open cylindrical bore. (source: [6])

The first step of the analysis of a system impedance is to measure the impulse response  $h(n)$ . If the terminating reflectance is approximated by a simple polarity change, then the impulse response has a form of infinite length periodic impulse train. After that  $h(n)$  has to be transformed to the frequency domain using the discrete Fourier transform DFT, yielding to  $j \tan(kL)$ . One can quickly find obtained result correct, by substituting  $Z_L=0$  and founding the input impedance analytically from:

$$Z_{IN} = Z_0 \left[ \frac{Z_L \cos(kL) + jZ_0 \sin(kL)}{jZ_L \sin(kL) + Z_0 \cos(kL)} \right]$$

(2.28)

### 2.3 Tone holes and other practicalities

For a musical instrument to be of any particular use, certain requirements need to be met. Firstly it should be able to easily produce a variety of sounds of different pitches. Cylindrical bore of flute or clarinet is musically useful, because it supports the sound generation over a wide range of frequencies. This is done twofold – by encouraging sounding on higher harmonic normal modes and allowing the effective tube length to be variable. In order to preserve the timbre within full available frequency

range another conditions needs to be fulfilled, which is the constant ratio between the first and successive higher harmonics, regardless of the effective acoustical length of the tube.

Usually woodwind instruments are not able to produce all twelve semitones in an octave over several octaves in contrary to e.g. piano or guitar, which would allow musicians to play arbitrary scale in multiple registers. Available range of frequencies depends on the geometrical dimensions and number of tone holes. Unsophisticated woodwind instruments like an Irish flute are rather designed to allow comfortable work in a particular musical scale only. Adjustments of the instrument pitch are controlled by cylindrical holes placed strategically along the bore. Appropriate combination of open and closed holes changes the effective acoustic length of the bore according to musician desire.

Much of the acoustics behind woodwind tone holes is complicated and is generally beyond the scope of this work. However physical process behind the functioning of tone holes may be roughly explained within the description of implemented discrete-time models.

“One modelling approach would be to treat the tone hole as a small waveguide which connects to the main bore via one port on a three-port junction. However, since the tone hole length is small compared with the distance sound travels in one sampling instant  $cT$  it is more straightforward to treat the hole as a lumped load along the bore” [18]. This approach is taken by two-port model developed by Keefe and improved by Smith and Scavone [19]. Last type of the tone hole model implemented in this project relies on wave digital filters [20].

### **2.3.1 Two port junction model**

Very detailed description of the Keefe’s tone hole model in the four-filter form can be found in [6]. Single tone hole is represented by the two-port junction placed between particular bore sections and consists of two reflectance and two transmittance filters. Interaction between neighbouring holes is negligible.

Using travelling pressure waves variables, two-port model transmission matrix is given by:

$$\begin{bmatrix} P_1^- \\ P_2^+ \end{bmatrix} = \frac{1}{Z_a Z_s + 2Z_0 Z_s + Z_0^2} \begin{bmatrix} Z_a Z_s - Z_0^2 & 2Z_0(Z_s - Z_a) \\ 2Z_0 Z_s & Z_a Z_s - Z_0^2 \end{bmatrix} \begin{bmatrix} P_1^+ \\ P_2^- \end{bmatrix}$$

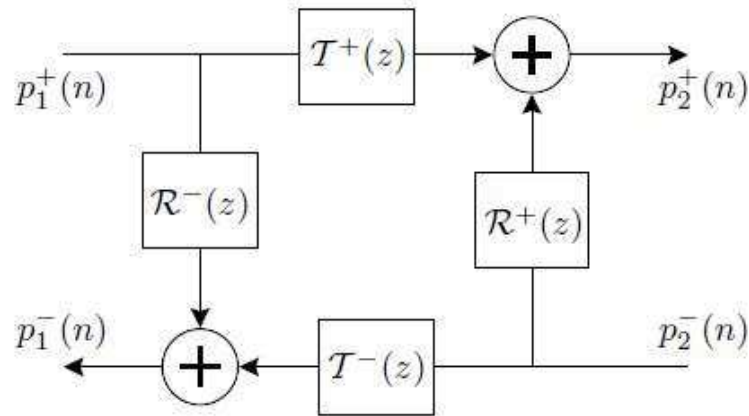


**Figure 2.12 A DWG two port scattering junction in four-filter form. (source: [6])**

Scavone describes all acoustical and physical parameters needed to calculate transmittance and reflectance of the junction. Second order digital filters responsible for filtering transmitted and reflected travelling waves are designed using the Matlab error-minimization method *invfreqz*.

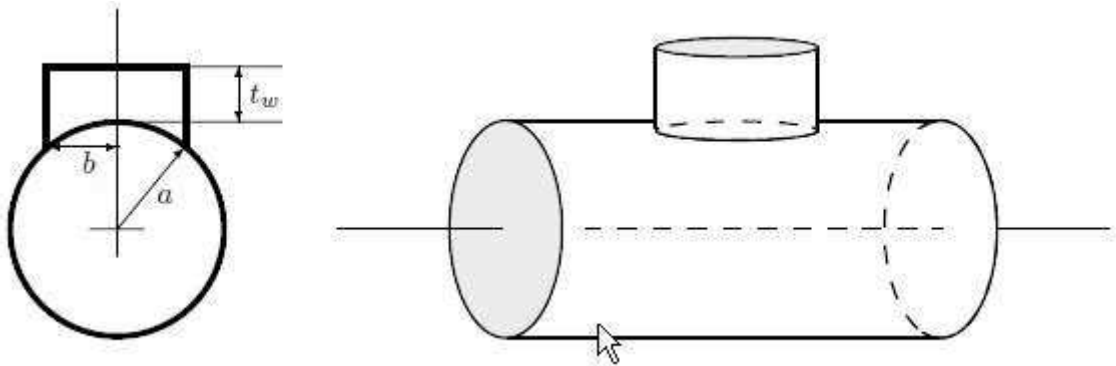


**Figure 2.13 Basic tone hole geometry (source: [6])**

Figures 2.14 and 2.15 present a theoretical reflectance and transmittance of an open tone hole calculated for clarinet's bore of radius  $a = 9.5$  mm, tone hole radius  $b = 4.75$  mm and its shortest height  $t_w = 3.4$  mm. Figures 2.16 and 2.17 show a reflectance and transmittance of a closed hole. Green curve represents a continuous time characteristics and blue one its second order digital filter least-square approximation.

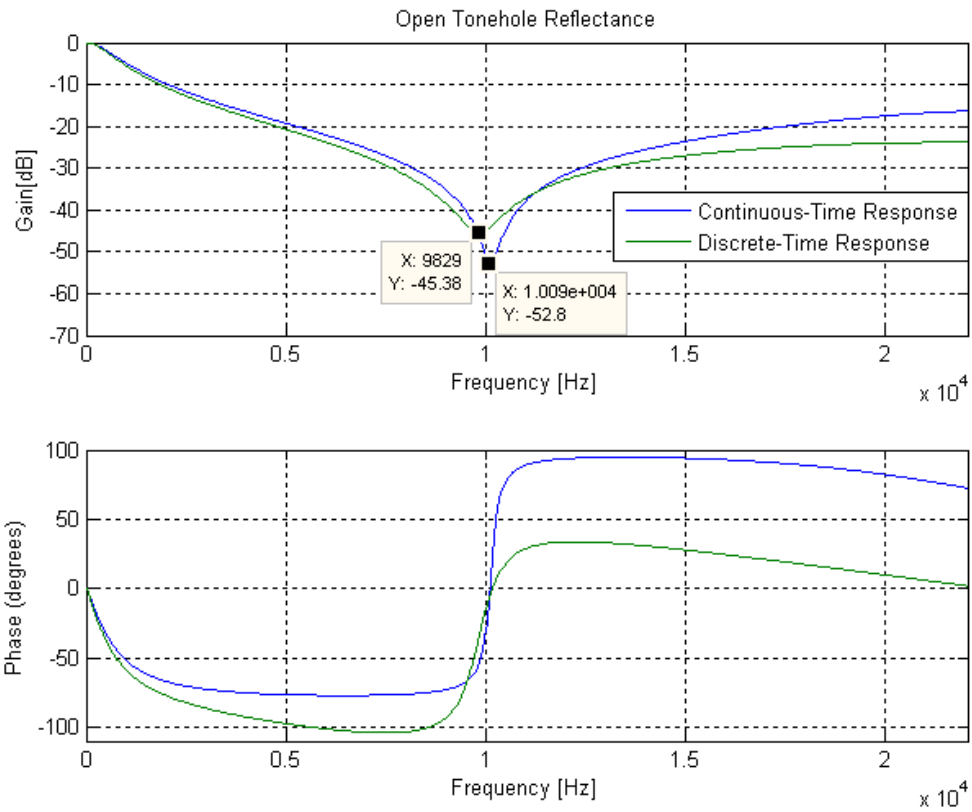


Figure 2.14 Open tone hole reflectance

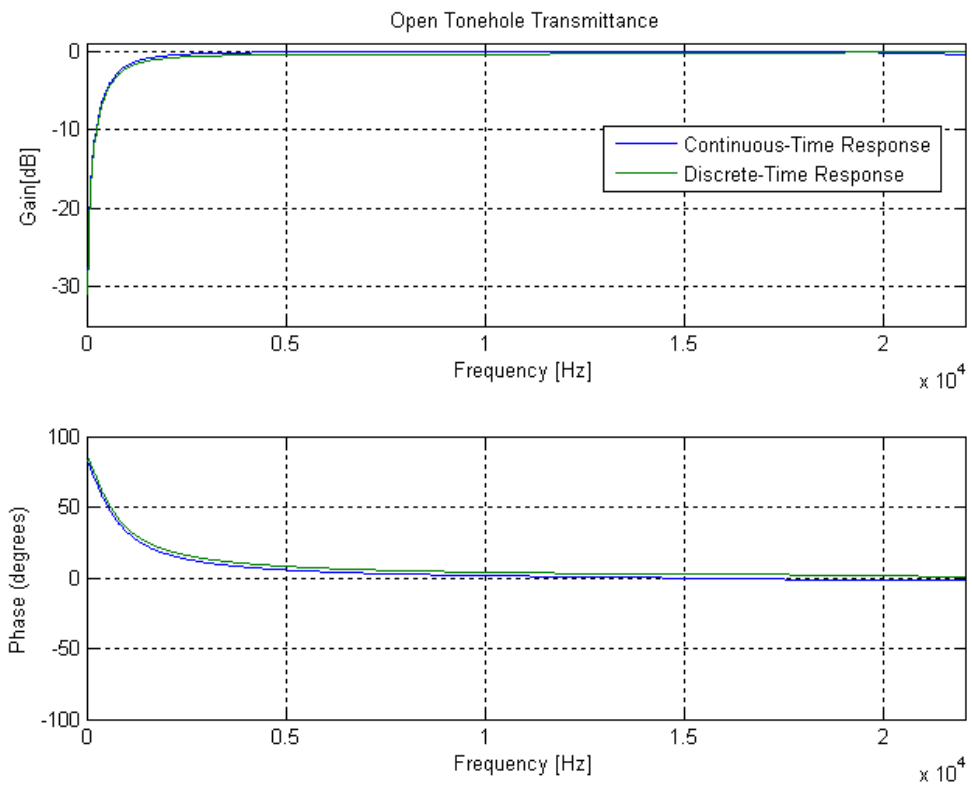


Figure 2.15 Open tone hole transmittance

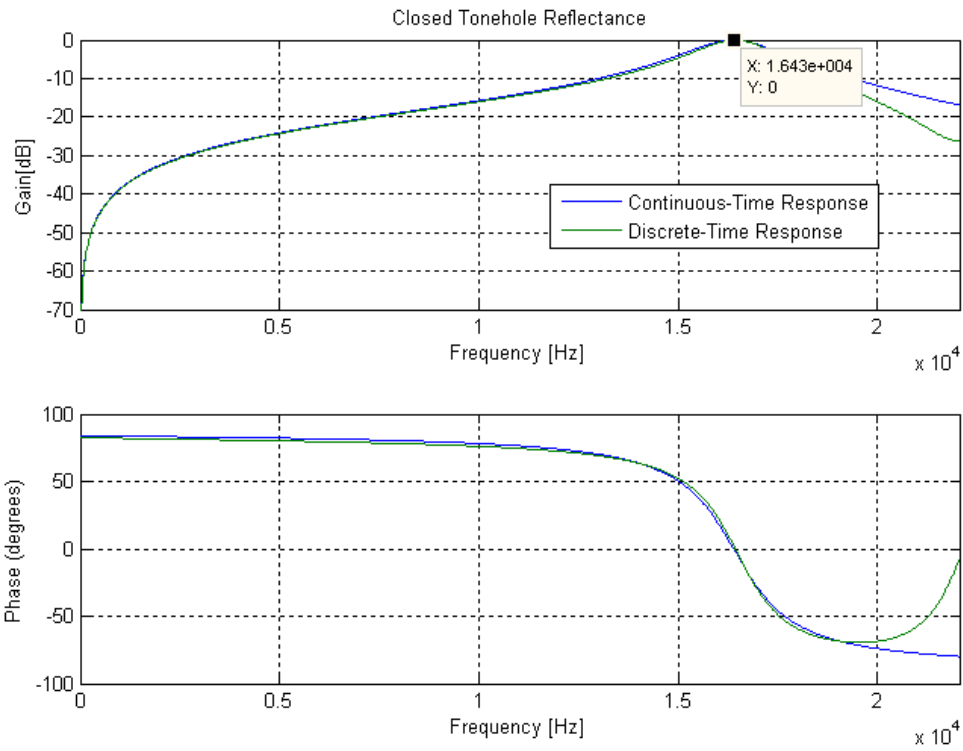


Figure 2.16 Closed tone hole reflectance

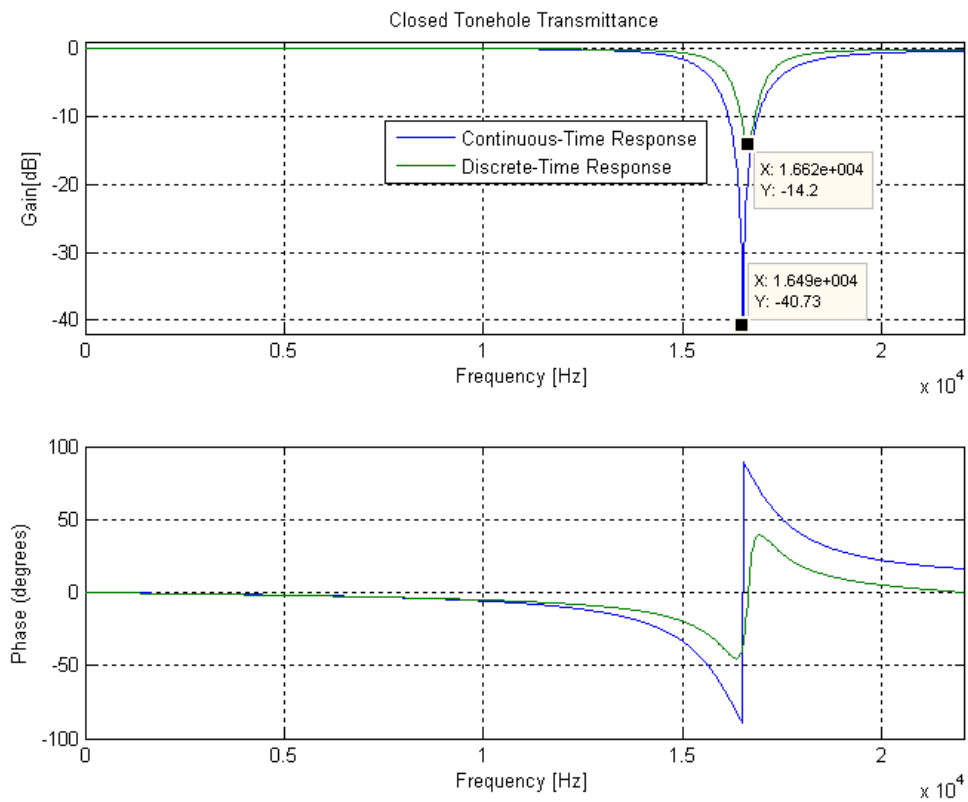
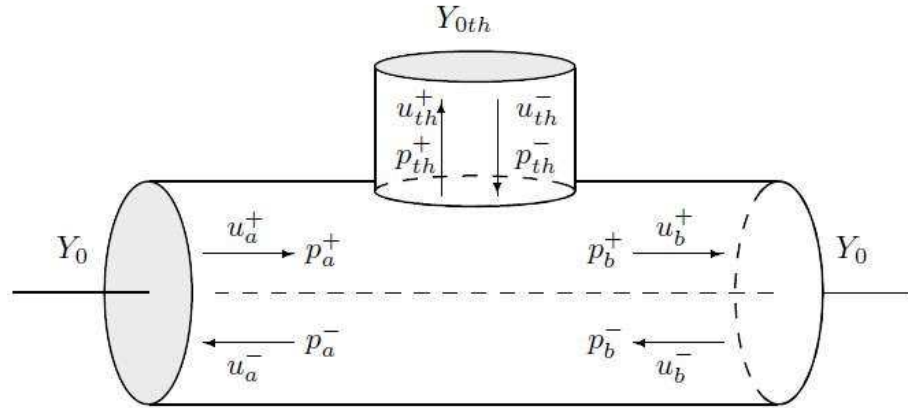


Figure 2.17 Closed tone hole transmittance

### 2.3.2 Three-port junction model

A more computationally efficient approach is to represent the tone hole as the junction of three pipes as presented in the figure 2.18:



**Figure 2.18** The three-port tone hole junction where a side branch is connected to a uniform cylindrical tube. (source: [6])

Scavone [6 p. 141] expands dynamic tone hole model proposed by Valimaki [22] and derives a one-multiply form of three-port scattering equations for pressure travelling waves components, allowing an efficient implementation within the physical model of the instrument.

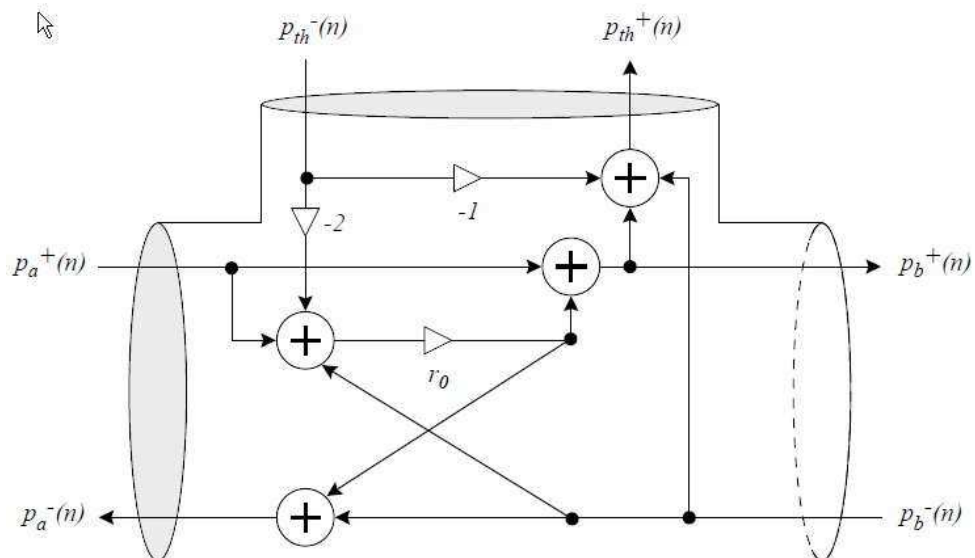


**Figure 2.19** Tone hole three-port scattering junction implementation in one-multiply form. (source: [6])

$$p_a^-(t) = p_b^-(t) + w \tag{2.29}$$

$$p_b^+(t) = p_a^+(t) + w \tag{2.30}$$

$$p_{th}^+(t) = p_a^+(t) + p_b^-(t) - p_{th}^-(t) + w \quad (2.31)$$

where

$$w = r_0[p_a^+(t) + p_b^-(t) - 2p_{th}^-(t)] \quad (2.32)$$

and

$$r_0 = r_a = r_b = \frac{-Z_0}{Z_0 + 2Z_{0th}} \quad (2.33)$$

Last thing to complete the digital waveguide three-port tone hole implementation is to find an appropriate model of the tone hole itself.

For the spatial interval  $cT = 7.87$  mm it may be modelled by a short delay followed by some sort of terminating reflectance filter  $R_s(z)$ . When the tone hole is completely closed incident pressure waves are ideally reflected without inversion. For the open state one can design reflectance filter based on the previously shown Levine-Schwinger unflanged pipe solution. Single first-order low-pass filter works perfectly, accounting for frequency dependent reflection, losses and propagation delay.

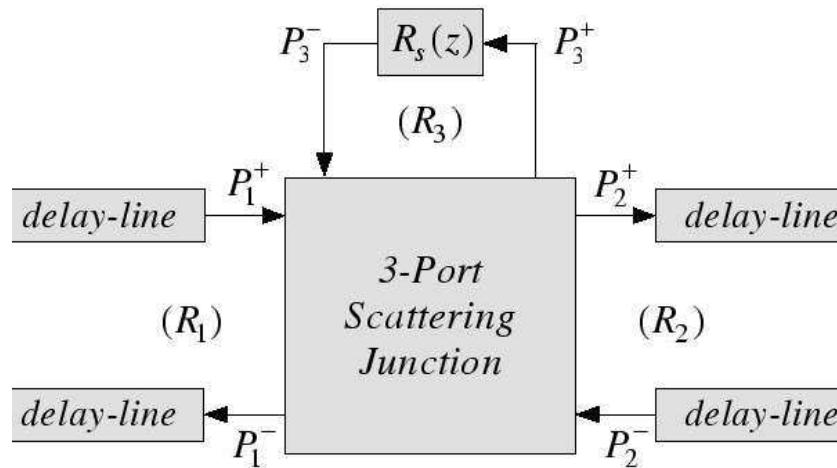


**Figure 2.20 Complete structure for discrete-time modelling of three-port tone hole model, including the reflectance filter  $R_s(z)$ . (source: [20])**

### 2.3.3 Dynamic three-port filter model

To simulate a more sophisticated behaviour of the hole by allowing it to dynamically change its state of openness, the reflectance filter characteristics has to become variable.

The input impedance of the open finger hole seen from the main bore, may be expressed as acoustic inertance:

$$Z_{th}(s) = \frac{\rho t}{S_{th}} s \quad (2.34)$$

Where  $t$  is the tone hole effective height,  $\rho$  is the density of air and  $S_{th}$  is the cross-sectional area of the hole.

The tone hole reflectance in terms of Laplace transform is then given by:

$$R_{th}(s) = \frac{Z_{th}(s) - Z_{0th}}{Z_{th}(s) + Z_{0th}} = \frac{t\alpha - c}{t\alpha + c} \quad (2.35)$$

Formula 2.35 may be transformed to a discrete-time filter using the bilinear transform:

$$R_{th}(z) = \frac{a_1 - z^{-1}}{1 - a_1 z^{-1}} \quad (2.36)$$

Where

$$a_1 = \frac{t\alpha - c}{t\alpha + c} \quad (2.37)$$

Alpha is a bilinear transform constant controlling the the non-uniform scaling of frequency called frequency warping. In case of the tone hole reflectance filter, alpha coefficient is set to  $2fs$  to ensure the best possible fit in the low-frequency region [6].

STK toolkit library instrument *Blowhole* models a dynamic register tone hole using varying all-pass filter. Reflectance characteristic mimics a reflection of the "mass-like" impedance. Filter phase response varies and is controlled by the measure of the hole openness  $g$  defined as the ratio between the open and total tone hole volume and radiation losses measure *gain*.

$$coeff = g(alpha - 0.995) + 0.995 \quad (2.38)$$

Differential equation describing a filter has a form:

$$y[n] = -coeff * y[n - 1] + gain * coeff * x[n] - gain * x[n - 1] \quad (2.39)$$

Figures 2.21 and 2.22 present phase responses of the reflectance filter calculated for  $gain=1$  and parameter  $g=0$  representing totally closed hole and  $g=1$  standing for fully opened hole.

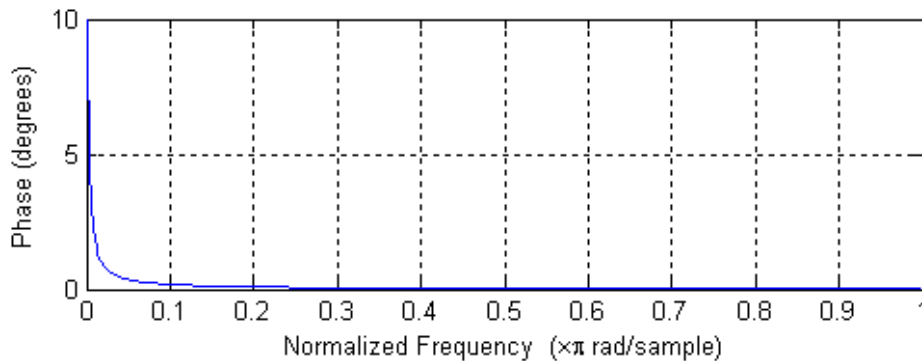


**Figure 2.21 Closed dynamic tone hole reflectance phase response.**

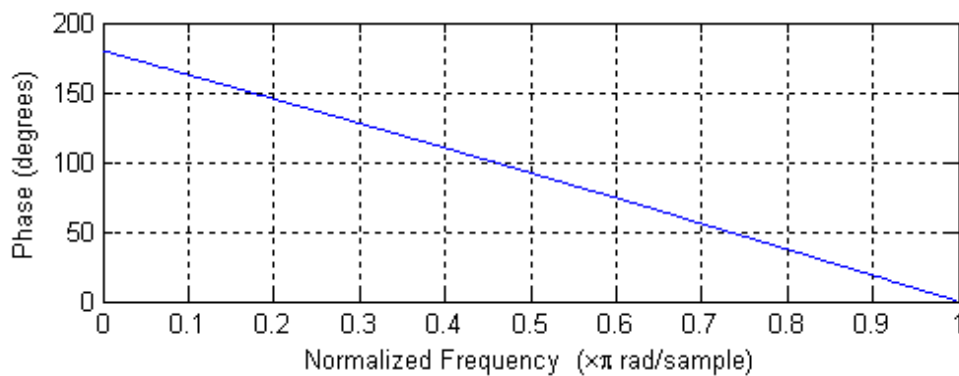


**Figure 2.22 Opened dynamic tone hole reflectance phase response.**

### 2.3.4 Wave digital filter model

Another efficient digital tone hole model with dynamically adjustable states is based on the wave digital filters (WDF). WDF are most often used for digital simulation of analogue RLC circuits and their common feature with digital waveguide modelling (DWM) techniques is a digitalization of continuous-time models using travelling wave variables.

Presented tone hole model is an example of the combined WDF and DWM approach, where lumped elements are represented using WDF and distributed elements are modelled using DWM techniques.

Figure 2.23 presents a cross-sectional view of a woodwind tone hole, whose dimensions are relatively small comparing to the acoustic wavelength. Therefore acoustic behaviour of the tone hole may be modelled using a lumped acoustic element.

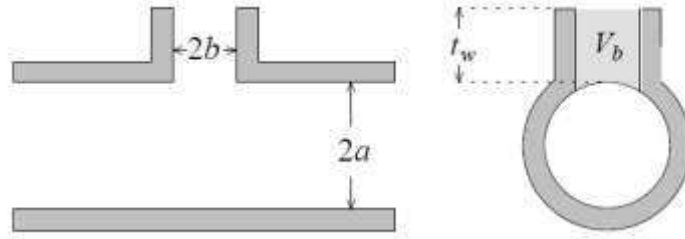


**Figure 2.23 Cross-sections of a woodwind tone hole. (source: [20])**

It was mentioned that an open tone hole behaviour is approximately that of pure inertance, while a closed state is very similar to a pure compliance. One may try to model an inter-state (partially open or half-hole) by dividing the tone hole volume  $V_b$  into an "open" and "closed" parts behaving as an inertance and compliance, respectively.

Such "half-hole" model can be equivalently represented using an electrical network:

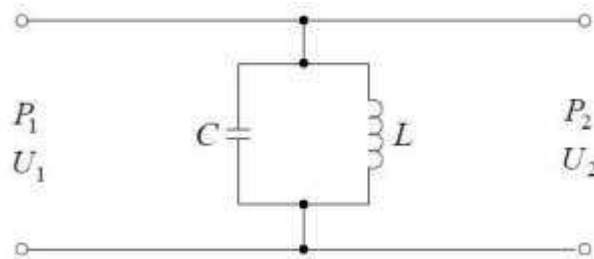


**Figure 2.24 Electrical network representation of the half-hole model.**

Formulas for an acoustical compliance and inertance, represented by a capacitor and an inductor, respectively can be found in [20].

Reflectance filter response is given by:

$$R_s(z) = -z^{-1} \left( \frac{\alpha_2 + z^{-1}}{1 + \alpha_2 z^{-1}} \right) \quad (2.40)$$

where

$$\alpha_2 = \frac{L^{-1} - \beta^2 C}{L^{-1} + \beta^2 C} \quad (2.41)$$

Hence proposed solution includes only one multiplication in the filter and one for a three-port scattering function.

In the previously presented dynamic hole model, a hole was represented by either a short digital waveguide followed by a filter or a terminating filter

only modelling both propagation and reflectance characteristics. In order for the model to work properly, a tone hole minimal height is constrained to the value corresponding to at least one-sample delay introduced by the reflectance filter or waveguide. Spatial sampling interval for sampling frequency 44100 Hz is  $t = cT/2 = 343/882000 = 3.8$  mm. It is possible to model smaller tone hole heights by increasing the sampling frequency, which is computationally expensive. On the contrary, a WDF model is able to perform simulations of finger holes of an arbitrary height, without a need of using costly fractional interpolation techniques.

## 2.4 Interpolation

The appropriate effect of a given tone hole or tone hole network strongly depends on its placement. Therefore it is important for digital waveguide models to make available any arbitrary location along the bore. It would be very problematic e.g. to express the exact length of the bore section using only fixed number of discrete positions corresponding to the sampling frequency. Increasing accuracy by decreasing the sampling time interval leads to the growth of the computational cost.

Inaccuracies between lengths of particular digital waveguide sections and real instrument geometrical dimensions lead to problems with tuning. That is why special interpolation techniques are used, allowing representation of fractional delay lengths. Most popular methods in the context of digital waveguide modelling are Lagrange interpolators (introducing amplitude error) and All-pass filters (introducing phase error), described in details in [6 p.124].

This project takes advantage of the first order Lagrange interpolation referred also as linear interpolation. Lagrange interpolator is typically implemented as a FIR filter of coefficients given by general formula:

$$h_{\Delta}(n) = \prod_{k=0, k \neq n}^N \frac{\Delta - k}{n - k}$$

where  $n=0,1,2\dots N$ ,  $N$  is the order of the filter and  $\Delta$  is the fractional delay of the interpolator. Sum of the coefficients must be equal to one in order to preserve a unity gain at DC. Additionally, the delay  $\Delta$  should fall in range  $\frac{(N-1)}{2} < \Delta < \frac{(N+1)}{2}$  to keep the filter gains at or below unity over all frequencies

[22]. Table 2.1 presents specific values of the filter impulse response for orders 1, 2 and 3.

**Table 2.1 Interpolator coefficients for filter orders 1,2 and 3. (source: [21])**

$h_{\Delta}$ Order	$h_{\Delta}(0)$	$h_{\Delta}(1)$	$h_{\Delta}(2)$	$h_{\Delta}(3)$
$N = 1$	$1 - \Delta$	$\Delta$	0	0
$N = 2$	$\frac{(\Delta-1)(\Delta-2)}{2}$	$-\Delta(\Delta-2)$	$\frac{\Delta(\Delta-1)}{2}$	0
$N = 3$	$-\frac{(\Delta-1)(\Delta-2)(\Delta-3)}{6}$	$\frac{\Delta(\Delta-2)(\Delta-3)}{2}$	$-\frac{\Delta(\Delta-1)(\Delta-3)}{2}$	$\frac{\Delta(\Delta-1)(\Delta-2)}{6}$

## 2.5 Excitation models

A very important paper in the history of physical modelling by McIntyre, Schumacher and Woodhouse [23] noted that many musical instruments can be characterized as linear resonators, modelled by filters such as all-pole resonators or waveguides, and a single nonlinear oscillator like the reed of the clarinet, the bow-string friction of the violin or the jet of the flute [7].

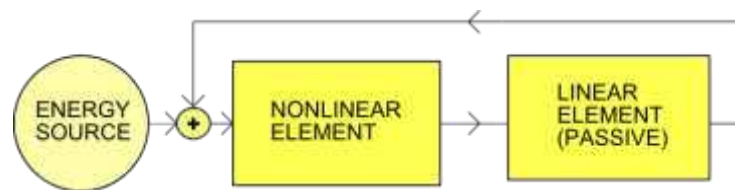


**Figure 2.25 Block diagram of a general musical oscillator, idealized as energetically active non-linear element coupled to an energetically passive linear element. (after: [23])**

The crucial element providing the energy and assisting in the production of stable oscillations within instrument resonator is called the excitation source.

This section covers a general description of the sound production mechanism in three woodwind family instruments – clarinet, transverse flute and recorder. Simple, one-dimensional models of the clarinet and transverse flute excitation sources are briefly described based on the Scavone’s and Cook’s STK physical models. Finally, more detailed description of the recorder sound generation process is carried out, which closely corresponds to the sound production of the project’s main instrument of choice - Tin Whistle.

### 2.5.1 Clarinet nonlinear excitation mechanism

Figure 2.26 presents the cross-section of a single-reed instrument mouthpiece (e.g. clarinet or saxophone).

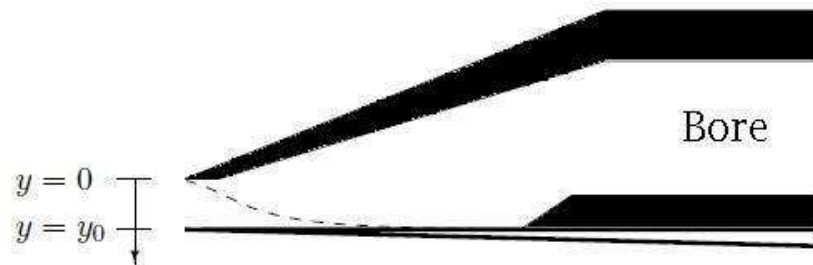


**Figure 2.26 A single-reed woodwind mouthpiece. (source: [6])**

The reed is springy and can bend upwards following the dashpot curve on the figure. The mouthpiece and reed act as pressure-controlled valve, which “allows the energy into the instrument for the initialization and maintenance of oscillations in the acoustic resonator” [6]. Player provides a flow of air at pressure above atmospheric, which is more or less steady source of energy. One can use an electrical analogy treating musician’s mouth pressure as the DC acoustic power.

Therefore reed and mouthpiece characteristics has to be nonlinear to be capable of converting the DC input power into the AC oscillating air flow producing a sound in the resonator. The single-reed mechanism in a mouthpiece also restores the energy lost in the instrument bore due to radiation and thermoviscous losses.

Common simplification for woodwind instruments is to neglect the reed mass, hence treating the reed nonlinearity behaviour as memory-less [23]. Assuming that force acting on the reed is equal to  $S_r \Delta p$ , where  $S_r$  is the reed effective surface area and  $\Delta p$  is the difference between the pressure inside the bore and the input mouth pressure, one can calculate the reed opening position from its spring time constant  $k$  using Hooke’s Law:

$$y = y_0 - \frac{S_r \Delta p}{k} \tag{2.42}$$

The reed movement controls the volume flow through the reed channel and into the mouthpiece. Many acoustic papers take advantage of the reed movement formula to find a relation between the volume flow through the reed channel by using the Bernoulli equation for a steady flow.

$$u_r = w y \sqrt{\frac{2\Delta p}{\rho}} \text{sgn}(\Delta p)$$

(2.43)

where  $w$  and  $y$  are the width and height of the reed channel, respectively, and  $\rho$  is the density of air.

Scavone in [6 p.50-51] presents specific formulas describing a volume flow through the reed channel for both dynamic and steady flow case. Starting with combining the reed opening formula with the Bernoulli equation:

$$u_r = w y_0 \left(1 - \frac{\Delta p}{p_c}\right) \sqrt{\frac{2\Delta p}{\rho}} \text{sgn}(\Delta p)$$

(2.44)

Where  $p_c = k y_0 / S_r$  is pressure necessary to push the reed against the mouthpiece facing and completely close the reed channel.

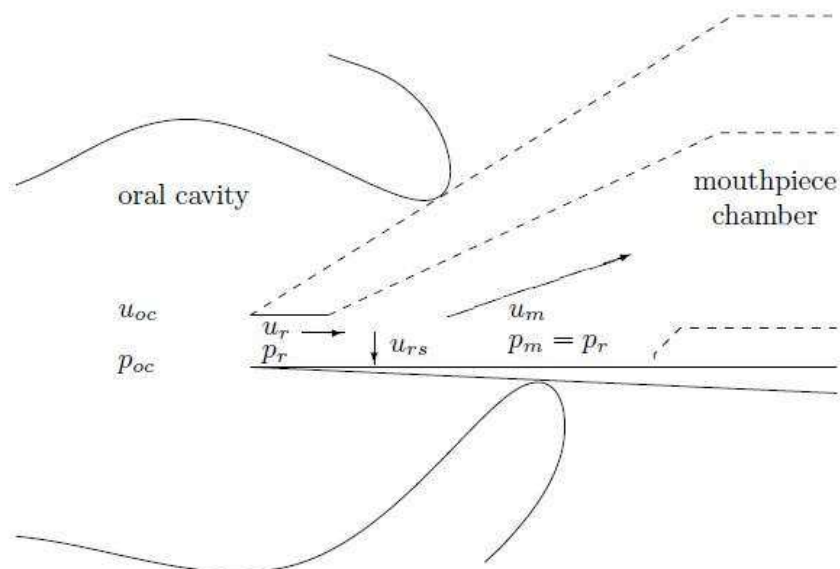


**Figure 2.27 The volume flow and pressure relationships for a single-reed oral cavity/mouthpiece. (source: [6])**

When the player starts blowing into the instrument, the initial reed pressure is equal to zero and the term  $\Delta p$  may be approximated by  $p_{oc}$ . Figure 2.28 illustrates the formula for the nonlinear static volume flow  $u_{r0}$  in the non-oscillating regime for  $0 < p_{oc} < p_c$

$$u_{r0} = w y_0 \left(1 - \frac{p_{oc}}{p_c}\right) \sqrt{\frac{2p_{oc}}{\rho}}$$

(2.45)

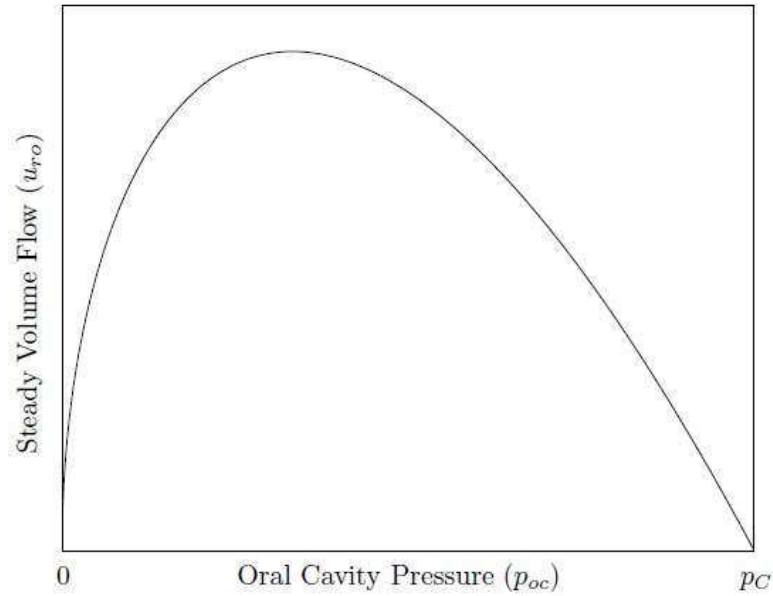


**Figure 2.28 Steady flow ( $u_{r0}$ ) through a pressure controlled valve blown closed. (source: [6])**

One can see that initial increase in the oral cavity pressure results in a rapid increase in static volume flow. However, continuous increase of the oral cavity pressure leads to forcing the reed toward the mouthpiece facing and decrease in the volume flow. When oral cavity reaches  $p_C$  the reed becomes completely shut and volume flow is equal to zero. The region of the curve in which flow decreases with increasing pressure is a region of a dynamic negative resistance. Whereas positive resistance takes energy out of the circuit, a negative one puts energy into the system. This particular region downward the sloping curve is the actual operating (active) regime of the clarinet during playing.

After the reed is biased in the negative regime, we can consider the dynamic flow through the mouthpiece. In such case, the pressure difference becomes a function of both oral cavity pressure and reed pressure and dynamic flow behaviour can be described using equations provided by Hirschberg:

$$u_r = u_{r0} \left( 1 + \frac{p_r}{p_C - p_{oc}} \right) \sqrt{1 - \frac{p_r}{p_{oc}}} \quad \text{if } p_{oc} > p_r > p_{oc} - p_C \quad (2.46)$$

$$u_r = 0 \quad \text{if } p_r \leq p_{oc} - p_C \quad (2.47)$$

$$u_r = -u_{r0} \left( 1 + \frac{p_r}{p_c - p_{oc}} \right) \sqrt{\frac{p_r}{p_{oc}} - 1} \quad \text{if } p_r \geq p_{oc} \quad (2.48)$$

Figure 2.29 depicts the nonlinear dynamic volume flow characteristics for constant oral cavity  $\frac{p_{oc}}{p_c} = 0.4$ , which pushed the reed by some constant distance  $y$  toward the mouthpiece facing, resulting in production of some static volume flow  $u_{r0}$ . Then the dynamic flow changes according to the varying reed channel pressure.

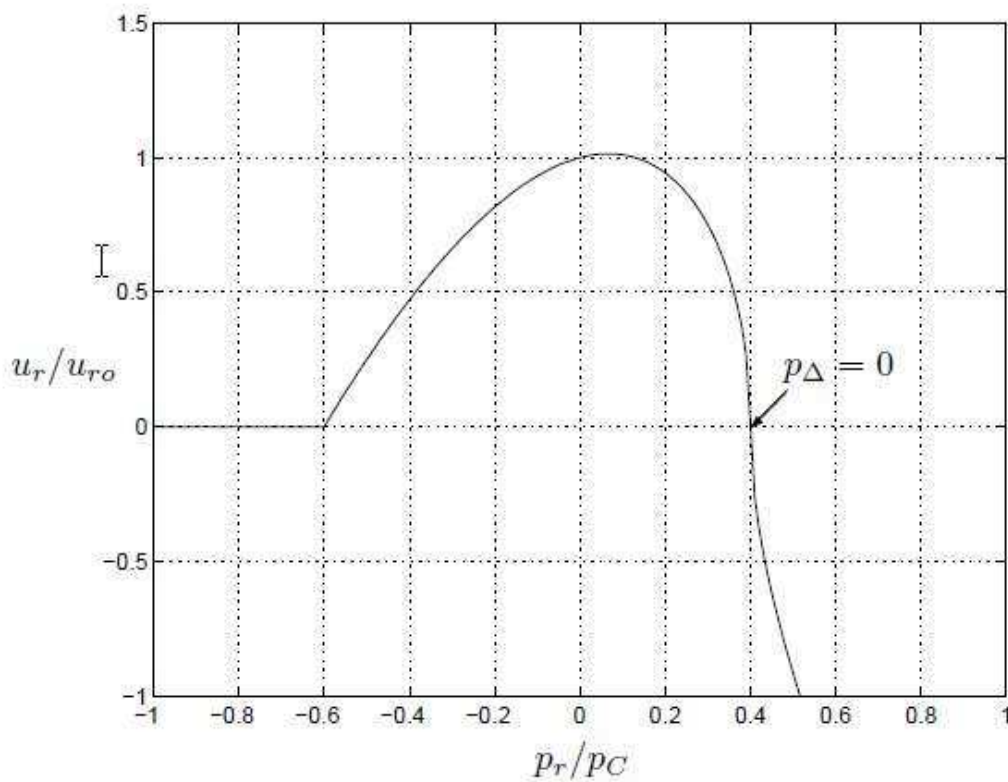


**Figure 2.29 Dynamic flow through a pressure controlled valve blown closed for  $p_{oc}/p_c=0.4$  (source: [6])**

In the first region when  $p_r \leq p_{oc} - p_c$  the volume flow is equal to zero, because the negative pressure inside the mouthpiece pulls the reed against the mouthpiece facing and stop any volume flow. The next region is characterised by increased rapid volume flow which reach a top for reed channel pressure equal to 0 which in turn is the point of undisturbed flow of static volume flow  $u_r$  resulting from  $p_{oc}$ . When  $p_{oc}=p_r$ , the volume flow stops, because  $\Delta p=0$ . Finally, when reed channel pressure becomes bigger than oral cavity, the negative flow into the mouth cavity occurs.

### 2.5.2 Models of clarinet excitation mechanism

In 1986 Smith [24] proposed the processing of reed/bore boundary using memory-less reflection coefficient, dependent on the difference between oral cavity pressure  $p_{oc}$  and bore pressures  $p_b$ . His idea was to present the reed system in a form of lumped varying acoustic impedance  $Z_r(\Delta p)$ , dependent on the pressure difference  $\Delta p$ . He also assumed the continuity of the flow in the bore and the through the reed opening. Using travelling pressure waves variables, the equation assuming the conservation of flow between the bore and reed has a form:

$$u_r(\Delta p) = \frac{\Delta p}{Z_r(\Delta p)} = u_b = \frac{p_b^+ + p_b^-}{Z_{ob}} \quad (2.49)$$

Where  $Z_{ob}$  is the characteristic impedance of the bore,  $u_r$  is the volume flow in the reed channel,  $u_b$  is the volume flow in the bore and  $p_b^+$  and  $p_b^-$  is right (outgoing) and left (incoming) travelling pressure waves components, respectively. Full derivation can be found in [6 p.148]. Finally an expression to calculate the value of the right travelling pressure wave using only left travelling wave and input oral cavity pressure is found:

$$p_b^+ = r(\Delta p) \left[ p_b^- - \frac{p_{oc}}{2} \right] + \frac{p_{oc}}{2} \quad (2.50)$$

Substituting  $p_b^+ = \frac{p_{oc}}{2} - p_b^-$  yields:

$$p_b^+ = -\hat{r}(p_b^-) p_b^- + \frac{p_{oc}}{2} \quad (2.51)$$

The presented equation may be easily incorporated into the digital waveguide physical model of clarinet in a form as in the figure 2.30. Signal dependent reflection coefficient is calculated as:

$$r(p\Delta^+) = \begin{cases} 1 + m(p\Delta^+ - p_c) & \text{if } p\Delta^+ < p_c \\ 1 & \text{if } p\Delta^+ \geq p_c \end{cases} \quad (2.52)$$

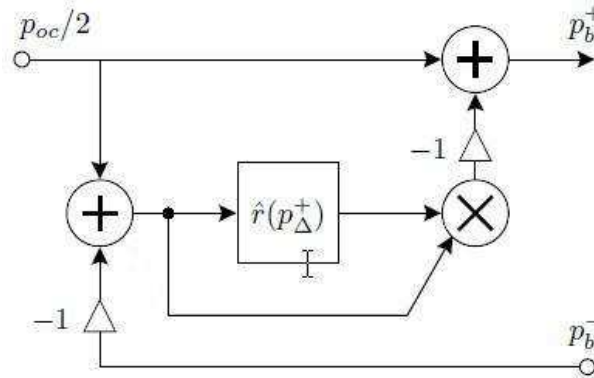


Figure 2.30 The pressure-dependent reflection coefficient digital waveguide implementation. (after: [6])

The model behaviour can be controlled using the slope parameter  $m$  and closing reed pressure (also referred as offset)  $p_c$ . The former models the reed stiffness, which may vary depending on the material it was made. The latter roughly mimics musician embouchure.

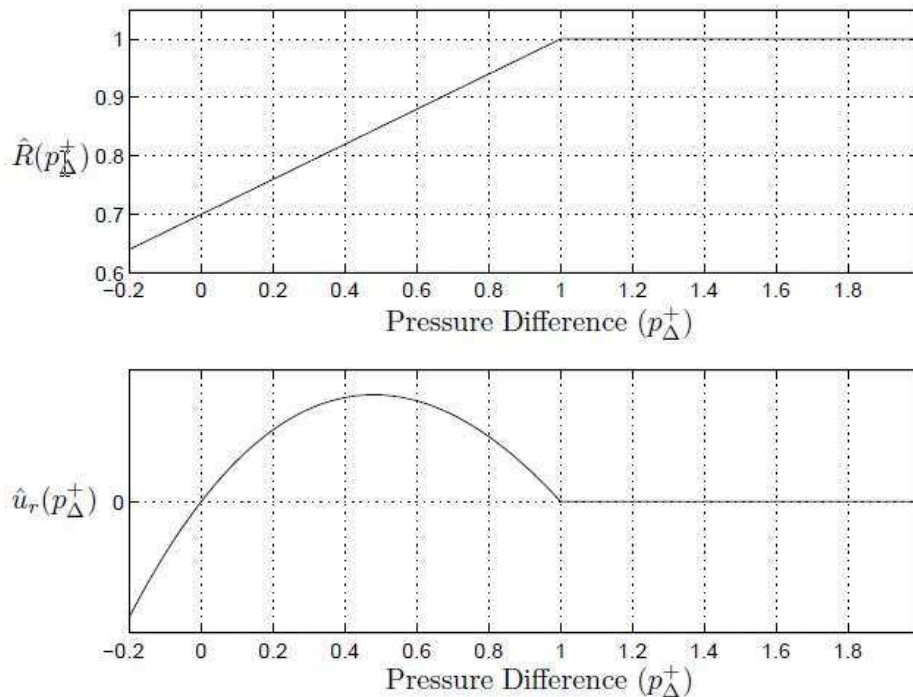
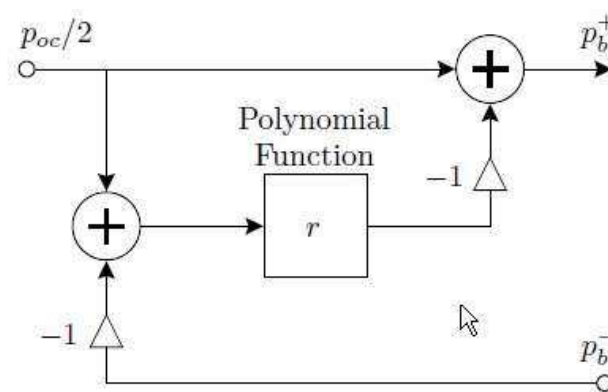


Figure 2.31 An example reflection coefficient  $r(p\Delta^+)$  (top), and the corresponding reed volume flow  $u_r(p\Delta^+)$  (bottom). (source: [6])

Figure 2.31 displays a sample reflection coefficient and corresponding volume flow. These values are normalized with respect to oral cavity pressure. The pressure necessary to close the reed channel is equal to 1. When  $p\Delta^+$  exceeds  $p_{oc}$ , the reed starts to beat against mouthpiece and completely close the reed channel. Hence the reflection coefficient is equal to 1 and all incoming pressure from the instrument is reflected. If differential pressure is smaller than one incoming pressure reflects partially and oral cavity pressure is partially transmitted inside the bore. When  $p_b^-$  is greater than  $p_{oc}$  the negative flow through the reed channel occurs as expected. In the above table the desired negative resistance region occurs for  $0.5 < p\Delta^+ < 1$ .

It is also possible to model the reed using a reflection polynomial method, which has much in common with the signal dependent reflection coefficient approach. Both methods were successfully implemented in the course of this project



**Figure 2.32 The implementation of pressure-dependent reflection coefficient polynomial. (source: [6])**

Almost twenty years have passed since the development of simple linear reed models described in this section. One can find more advanced dynamic model in [6 p. 152], which represents the reed by a linear mass-spring-damper system with memory; hence more accurately simulate reed beating against the mouthpiece. Further improvements can be found in [25], [26] and [27]. More advanced single-reed excitation models weren't investigated during this study, because the project scope has turned to the recorder/Irish flute modelling.

### 2.5.3 Excitation mechanism of transverse flute and recorder

Likewise to the clarinet, flute and recorder are also separable instruments, so one can divide them into the nonlinear excitation source and linear resonator.

Flutes, recorders and organ pipes share a common sound production mechanism which employs an airstream directed at a sharp edge. An airstream can be formed by either musician's lips (transverse flute) or special windway duct ended with a flue as in the case of recorder. Sound generation process referred as "air jet" or "air reed" can be described as the "flow-controlled valve" or "flow-controlled oscillator", which has much in common with tone producing air oscillations in a bottle, if one blows across the opening of the neck.

Tone generation process in a bottle consist of two complementary stages – "when the air is flowing out of the bottle, it directs the airstream outward, and when the airflow associated with the resonant vibration is inward, it directs the airstream inward to provide energy to sustain the oscillation" [28]. Blowing across the opening actually decrease the pressure inside the bottle, because of the conservation energy in fluids. According to Bernoulli's Law, if the velocity of the air goes up (kinetic energy), the pressure must goes down (potential energy). So the increased velocity of the flow across the bottle causes the pressure to drop and in result pulls out some air from the neck. However there's no equilibrium in the system, because perturbations in the air jet cause fluctuations of the air piston inside the bottle neck, producing a steady state oscillation.

This most basic cavity resonator is called the "Helmholtz resonator", having an oscillation frequency equal to [7]:

$$f = \frac{cr}{2\pi} \sqrt{\frac{\pi}{VL}}$$

(2.53)

Where  $c$  is the speed of sound,  $r$  and  $L$  are bottle's neck radius and height, respectively and  $V$  is the total volume of the cavity.

Similar mechanism involving an oscillating jet appears in flute and recorder instruments. The frequency of jet fluctuations corresponds to the resonant characteristics of the instrument bore. The theory of jet driven acoustic systems is fairly well understood and has been presented in details in the

literature: [23], [29], [30] and [31]. Analysis of the jet-drive system operation involves various research fields including fluid dynamics, aeroacoustics, and physics. Very advanced description of jet behaviour in flute-like instruments can be found in [31], including the time-domain physical model being a fruit of the research on extraction of quantitative information from jet images using image detection algorithms.

Figure 2.33 presents a cross-section of a typical organ pipe. Its construction is very similar to the recorder, therefore one can use as the illustration of an air jet sound generation process.

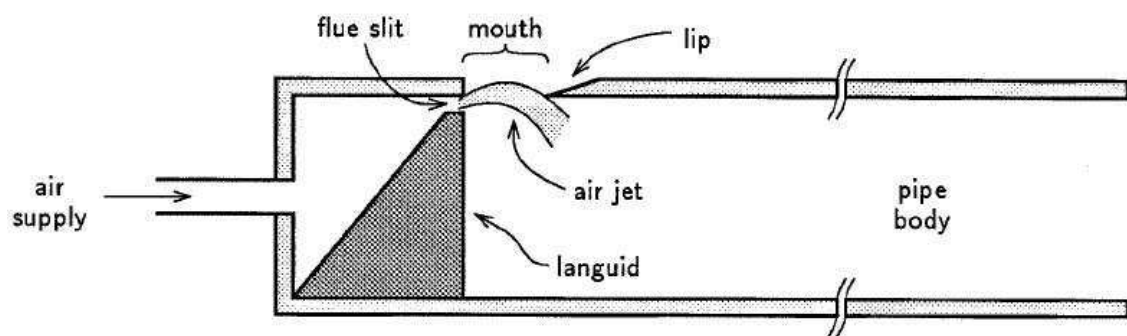


**Figure 2.33 Organ pipe. (source: [32])**

In the organ pipe and the recorder the air is forced through the flue slit, across the mouth of the pipe where it hits a hard, bladed edge called the labium lip. In the transverse flute the role of the flue slit is played by the appropriately shaped mouth and lips of the musician, which forms the air jet. Air forced through the flue interacts with the air within the bore such as to generate sustained oscillations. Likewise as in the clarinet reed model, crucial factor of the system for sustaining oscillations is a negative resistance characteristic of the excitation source.

The air supply is forced out of the slit across the mouth of the pipe and forms a turbulent jet, that reacts to the acoustical vibrations of the air within the pipe analogically as clarinet's reed. Wawrzynek in [32] points out that, if the jet were simply allowed to move in and out with the air in the pipe, the oscillations would be cancelled out, because increased pressure inside the pipe would instantaneously force the jet out of the pipe and therefore decrease the pressure in the pipe (similarly for the low pressure inside the tube). However the jet does not travel as a flat sheet, but it interacts with acoustical vibrations in the pipe. As a result transverse waves are induced in the jet. The distance between the flue slit and the labium lip

is carefully designed to correspond to one-half wavelength of the induced transverse wave. The delay along the distance from the flue to the lip results in the jet's alternatively blowing in and out of the pipe one-half cycle out of phase with the acoustic displacement out of the mouth pipe due to vibration of the air column. This one-half cycle delay is the source of the negative resistance [32].

The mathematical description of this phenomenon can be found at [23], [29], [30] and [31]. For purposes of this study, the complicated derivations and equations can be omitted, only essential information will be provided instead.

It is common to present the air jet behaviour in the flute-like instruments as the relation between the volume flow inside the pipe and the jet deflection.

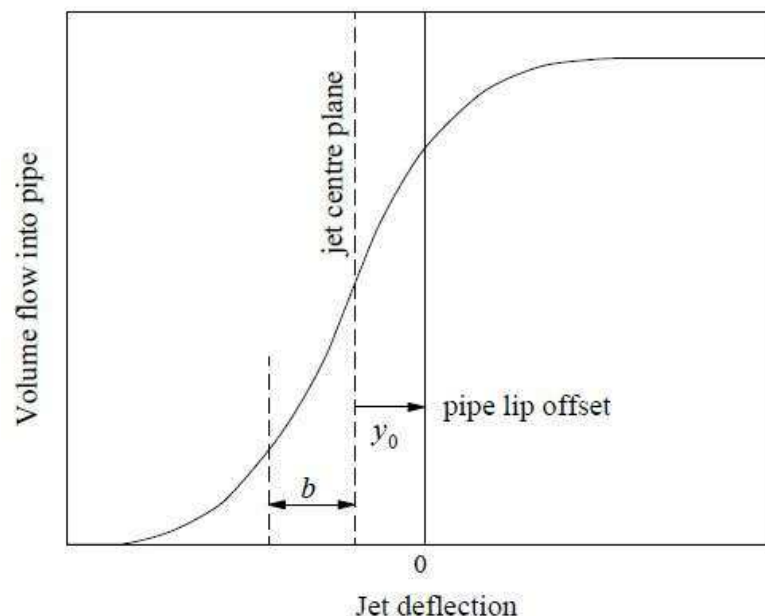


**Figure 2.34 Jet volume flow into a pipe past a lip with offset  $y_0$ . (source: [30])**

It is interesting to recognize, that the jet flow saturates once is it blowing completely into the pipe and similarly when is blowing completely out of the pipe. This saturation result in an hyperbolic tangent like function presented in the figure 2.34. Saturation distortion inserts odd-numbered harmonics into the pipe along with the fundamental frequency of the deflection. However the complete system will resonate at frequencies resulting from the resonant modes of the body pipe. Harmonic content can be controlled by changing the vertical position of labium lip, which in result offset the deflection vs. flow curve along the x-axis, making it asymmetric and

inducing production of even harmonics. Altering the position of interaction between the jet and labium lip is a common practice of organ designers and transverse flute players to increase even harmonics in the produced sound. In recorders the pipe lip is placed at approximately the same height as the flue, therefore mostly odd harmonics are created.

Our environment is filled with sounds resulting from directing the air flow at sharp edges of objects which are not coupled with any resonant cavity e.g. tightly stretched electric wires in the wind or stretched grass cane placed between the thumbs.

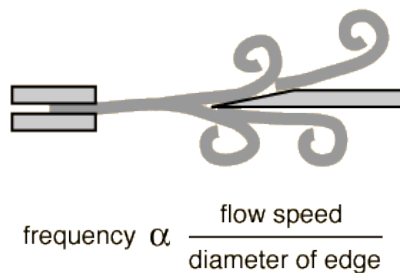


**Figure 2.35 Edge tone generation. (source: [28])**

Instead of the smooth and even flow division of the jet at the obstacle, one may observe oscillation of the flow back and forth across the edge. The reason for that is the formation of swirls and vortices in the flow. The frequency of obtained tone is proportional to the flow speed and reciprocal to the diameter of edge. Edge-tone instability producing vortex shedding happens only for a specified oscillation flow conditions, which can be conveniently described using a Strouhal number:

$$St = \frac{fL}{V}$$

**(2.54)**

Where  $f$  is the frequency of vortex shedding,  $L$  is the characteristic length and  $V$  is the velocity of fluid.

Vortex shedding is responsible for *overblowing* phenomena, which is another way of controlling the pitch by musicians. Apart from using tone holes to adjust the effective length of the pipe, musicians, especially those playing a transverse flute, are able to control a pitch by adjusting the length and speed of the air jet across the embouchure hole.

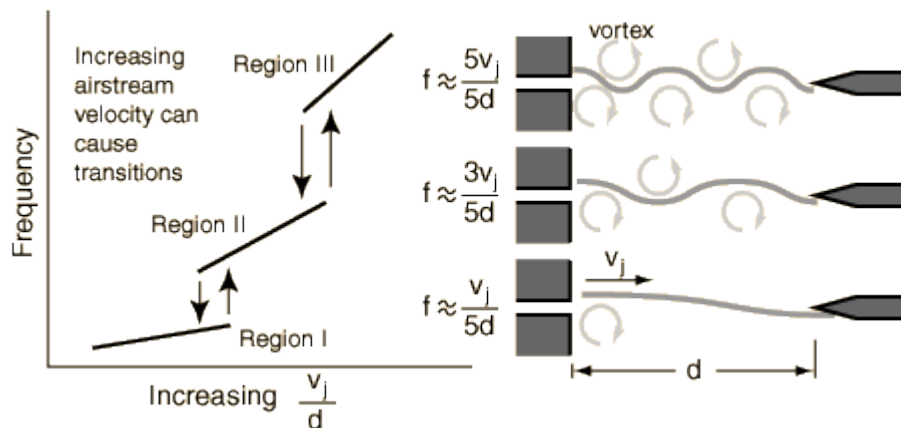


**Figure 2.36 Overblowing mechanism. (source: [28])**

In the figure 2.36 different edge tone regimes with patterns of vortex formation of some air-reed instrument are presented. As expected increasing the velocity of the jet or decreasing the distance from the flue to the edge raises the frequency of the produced sound. In contrary to edge tone generation in a free-space, where frequency increase is linear in full range, one can see that in this case the frequency increase is linear only in particular regions, which correspond to the propagating modes of the resonance cavity. Hence, to achieve higher notes one may force the air column to sound its second harmonic, up an octave from the fundamental. In case of the transverse flute both increasing the velocity and decreasing the distance (rolling-in) methods are used. In case of recorder it is possible to only increase the velocity by blowing harder into the mouthpiece. However overblowing in recorders is not so easy to achieve, because of the impact of a windway forming a jet. Perhaps this relative easiness of control and low price made it so popular classroom instrument in schools.

#### **2.5.4 Perry's Cook STK flute excitation model**

Most basic excitation source model was developed by Perry Cook and can be found in his book concerning sound synthesis [7] and STK synthesis toolkit [5]. The basic idea behind the model is similar to the reflection function of clarinet's reed presented in the previous section.

Cook proposed a model consisting of a simple, nonlinear polynomial function and a delay line. Nonlinear function mimics the tendency of the air to flow into or out of the mouth of the instrument as a function of

differential pressure between the incoming mouth pressure and bore pressure. Very often the nonlinearity has a hyperbolic tangent shape with apparent saturation characteristics which simulates the flow limiting of the jet as it deflects fully into and out of the pipe. Delay line is responsible for simulation of the jet propagation from the flue to the labium lip.

One can see an analogy between the nonlinear function modelling the excitation source and the classic waveshaping technique [33], which changes an original waveform by responding to its amplitude in a non-linear fashion. Waveshaping is a popular method to digitally simulate distortion introduced by analog amplifiers.

Cook proposed a nonlinearity defined as:

$$f(x) = \begin{cases} -1 & \text{if } x \leq -1.325 \\ x^3 - x & \text{if } -1.325 < x < 1.325 \\ 1 & \text{if } x \geq 1.325 \end{cases}$$

Figure 2.37 presents the waveshaping function response for the linear function from  $\langle -2, 2 \rangle$  range.

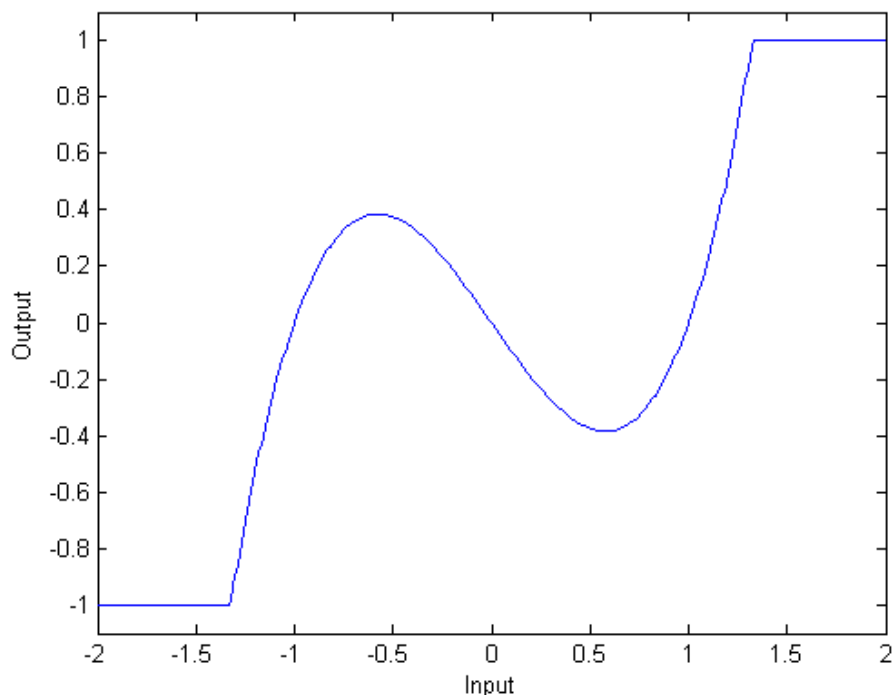


**Figure 2.37 Nonlinear waveshaping function  $x^3-x$ .**

If the input signal does not go beyond  $\langle -1.325, 1.325 \rangle$  range the waveshaper inverts the phase of the input signal and introduces the third harmonic. Once the limit is exceeded hard limiting occurs and inserts a

series of odd harmonics resulting from clipping. Figures 2.38 and 2.39 present the spectrum of the nonlinear function output fed with sinusoidal 100 Hz signal. Amplitude of the signal on the left equals 1.3, while on the right 1.5.

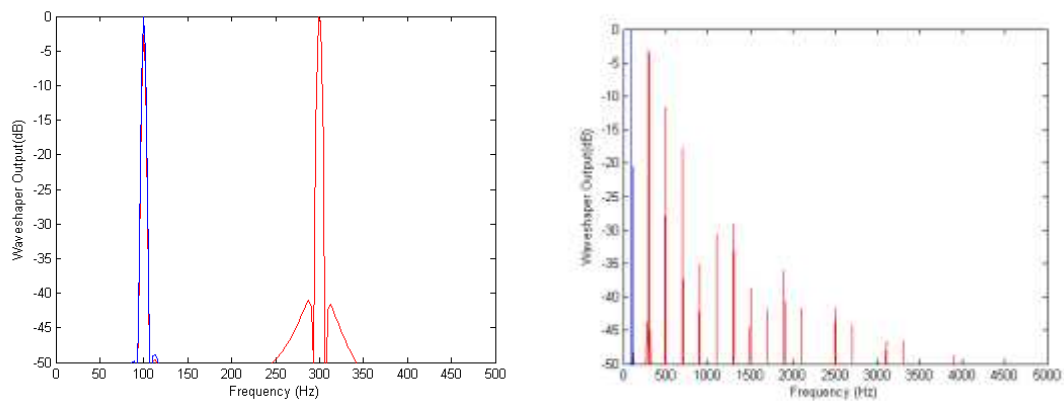


**Figure 2.38 and 2.39 Spectrum of the waveshaper output fed with sinusoidal 100 Hz signal of amplitude 1.3 (left) and 1.5 (right).**

Asymmetric nonlinear functions (as in case of organ pipe or transverse flute) introduce significant amount of DC error. In a complete physical model of a flute the nonlinear function can be followed by a DC blocking filter. A 2<sup>nd</sup> order high-pass filter was proposed, tuned at 20 Hz, In order to obtain the fundamental tone, jet length has to be two times smaller than the length of the bore. Overblowing is possible by manipulating the jet's length e.g. double reduction of length results in the production of second harmonic.

Unfortunately, the control parameters of the described Cook's model are not determined from the physical dimensions and properties of the actual instrument. Verge in his advanced work [2] proposes a one-dimensional model of the recorder air-jet mechanism, which accounts for vortex shedding, turbulences and other effects that their research group had examined experimentally in great detail. Parameters of the model are determined by a measurement of real instrument physical dimensions. Even more advanced time-domain physical model can be found in [31] which incorporates research concerning extraction of quantitative information from jet images using image detection algorithms. Both models were not implemented during the project, because of the complexity of presented acoustics and significant effort invested in getting simpler model to work properly.

### 2.5.5 Chris's Chafe vortex noise model

Breath noise in wind instruments exhibits pitch-synchronous spectral features and has a more constant amplitude contour, compared to the pitch synchronous pulsed noise in other musical oscillator e.g. cello or violin [34]. The formation of vortices and modulation of fricative noise depends on the air column oscillation.

Detailed three-dimensional modelling of vortex formation is a very challenging problem. Moreover, the most woodwind excitation source models are one-dimensional like Cook's nonlinear polynomial. Attached simple breath noise component being a mixture of the random number generator output with the incoming pressure sounds unnatural, because there is no interaction with the standing wave in the air column.

Chafe proposed an efficient vortex-noise circuit extension, which can be incorporated into current physical models. Figure 2.40 presents the block diagram of the complete woodwind physical model. Elements being an inessential for the noise and edge tone generation were omitted and grouped in the resonator block.

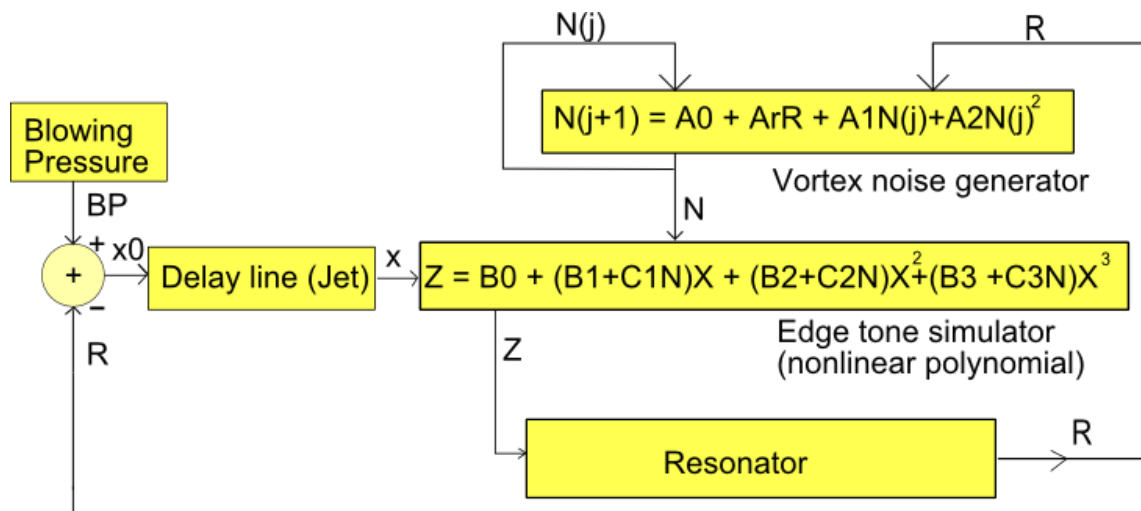


Figure 2.40 Block diagram of the pitch-synchronous noise model proposed by Chafe.

The proposed vortex-noise generator has a form of deterministic chaos produced by an iterative quadratic mapping function, whose primary input is the noise value in the previous computation cycle.

$$n(j + 1) = a_0 + a_r R + a_1 n(j) + a_2 n(j)^2$$

(2.55)

The second input is the feedback signal  $R$  from the resonator, whose amount is regulated using coefficient  $a_r$ . Coefficients  $a_0$ ,  $a_1$  and  $a_2$  control the character of produced noise for different values of  $R$ . Produced fluctuations can be more or less chaotic and oscillate over varying ranges, according to the reflected feedback signal  $R$ , hence having a spectral content modulated in a pitch synchronous manner to the output signal. Another improvement compared to Cook's model is a modulation of nonlinear function coefficients using an obtained noise signal. The general form of a waveshaping edge-tone function can be presented as:

$$Z = \sum_{i=0}^M (b_i + c_i n) x^i \quad (2.56)$$

Where  $x$  is the input differential pressure,  $n$  is the noise signal from the vortex-noise generator,  $M$  is an order of the polynomial,  $b_i$  are edge-tone polynomial coefficients and  $c_i$  are modulation coefficients.

An operating point of the nonlinearity is modulated by the noise signal  $n$ , which depends on the reflected signal  $R$ . Therefore a transfer function of the edge-tone generator is modulated in the pitch synchronous manner, resulting in the a natural sound.

## 2.6 Clarinet and flute physical models

During the initial stage of the project physical models of clarinet and flute were implemented in order to practically verify the theory presented in papers on digital waveguide modelling. The implemented clarinet waveguide model is well-documented in many publications by Julius O. Smith [4] and Scavone [6], as well as Cook's simple flute model [7]. Examination of both instrument models source code from Synthesis ToolKit [5] allowed an implementation in Matlab.

Clarinet and flute are examples of a closed pipe and an open pipe wind instruments, respectively. Formulas for calculating resonant frequencies in both types of pipes, as well as the theory concerning sound generation mechanisms and its models can be found in previous chapters.

Figure 2.41 presents a complete system of the clarinet DWG implementation from the STK library. The model consists of a nonlinear

excitation mechanism, two digital delay lines joined with a low-pass reflection filter.

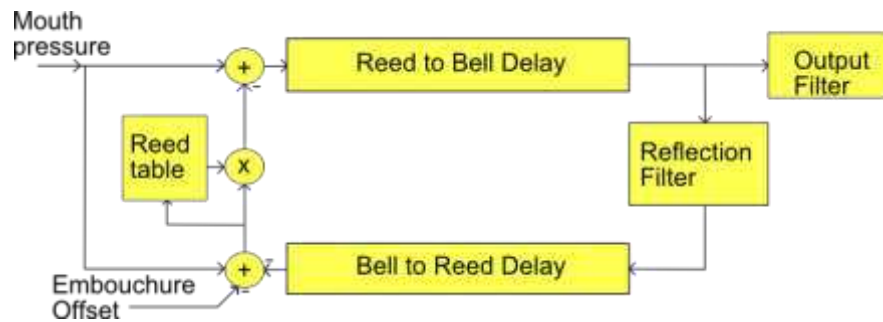


**Figure 2.41 Waveguide model of a single-reed, cylindrical-bore woodwind, such as a clarinet (after: [7])**

In [6] the bore is additionally divided into couple of sections interconnected by tone hole junctions, hence allowing pitch control in terms of various fingering configurations instead of changing the length of delay lines. However existing model implemented only three finger holes, therefore realistic pitch changes corresponding to the real-world clarinet behaviour were not possible.

Following implementation of flute was build upon MATLAB structures and functions developed for clarinet model. Cook's excitation source using nonlinearity and jet delay line were described in details in the previous chapter. One should notice that here the output from the main delay line is fed into the system in two places, multiplied by appropriate constant depending on the feedback node.

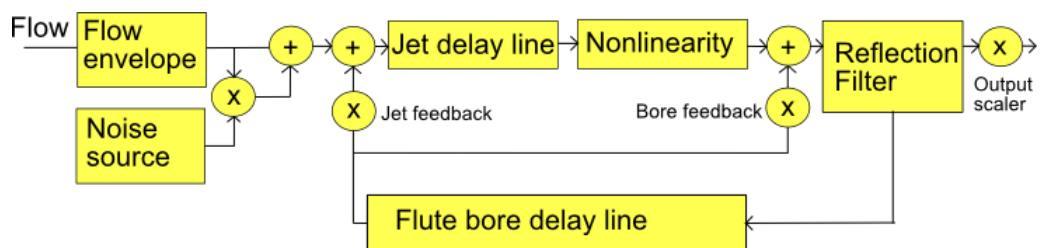


**Figure 2.42 Block diagram of Cook's slide flute physical model (after: [7])**

Flute and clarinet family instruments possess about ten finger holes and additional register holes. However doubts about future control and CPU performance of such complex models emerged. Furthermore during the evaluation phase, the author would be limited to perform comparison tests

using previously recorded sound samples only or find a professional musicians to record unique ones.

Instead of above, the decision was made to simulate an instrument, which is more easy to acquire and play – Irish tin whistle. So instead of extending described STK implementations with tone hole lattice models, new physical model being a fusion of already working components was built.

## 3 Implementation of an Irish flute physical model

### 3.1 Introduction

The Irish whistle is an instrument most often associated with an Irish folk music. What makes this particular instrument interesting is the fact that many professional whistle players prefer to play inexpensive whistles, founding their tone closer to the “heart” of the traditional Irish music, than more expensive varieties. Low cost of the real instrument was one of the factors behind the decision of choosing the tin whistle for the most detailed implementation and evaluation.

This chapter describes an Irish flute physical model implementation. In the first section the programming environment is introduced. Afterwards the block diagram of the model and principal rules of operation are presented. Next section covers an application user interface, with a short description of available model parameters. Section 3.4 describes most significant parameters and their impact on the stability of the model and timbre of generated sound. Finally the last section presents the methodology of test sound samples generation.

### 3.2 Irish tin whistle construction and acoustic properties



**Figure 3.1 Tin whistle In D scale. (source: [www.google.com](http://www.google.com))**

The whistle consist of approx. 26 cm long (usually metal) tube which is in most cases cylindrical, sometimes conical. Six tone holes of different radii are placed along the bore. A whistle is attached to one end of the instrument. Basic principles of operation are the same as in case of recorder, transverse flute or organ pipe and were described in details in section 2.5.3.

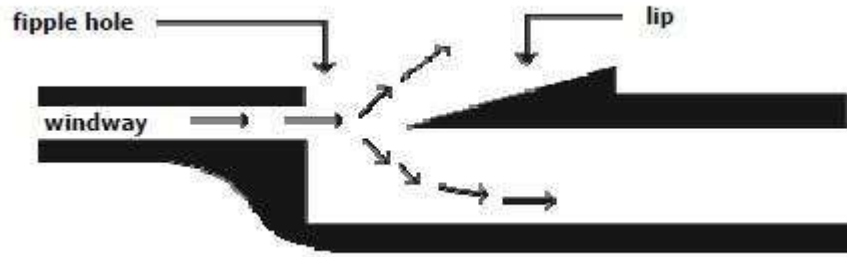


**Figure 3.2 Air jet hitting the fipple hole of a tin whistle. (source: [35])**

Shortly, the air jet formed in the flue channel hits the sharp edge called labium lip and rapidly switches between propagating either through the instrument bore or passing out the atmosphere, hence setting up acoustic oscillations in a pipe accordingly to its resonant frequency.

Different sounds can be obtained by changing the effective length of the resonance pipe while selecting different fingers patterns on the six finger holes.

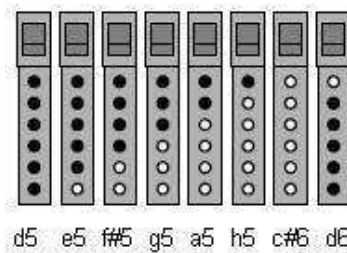


**Figure 3.3 Fingering positions for the tin whistle. (after: [35])**

The most common whistle type is in the key of D, which is also the key of the Irish folk music. Picture above presents fingering positions allowing playing in the D major scale. The black dots indicate closed finger hole, while the white dots indicate open finger holes. When all holes are closed instrument produces the D5 sound in a lower register (on the left hand side on the picture). Configuration on the right hand side, with only top hole open, produces the D6 sound in an upper register.

The tin whistle generates only small number of distinct harmonics comparing to other instruments. Most energy is concentrated at first harmonic, which is followed by a series of harmonics that roll-off at approximately 8 dB/octave. Spectral characteristics may vary depending on the played note, instrument manufacturer and embouchure character.

### 3.3 Block diagram of the Tin Whistle physical model

Physical model developed during the course of the project has its origins in two different physical models described in the previous chapter – STK flute and Scavone’s clarinet. Figure 3.4 depicts the block diagram of the Irish tin whistle:

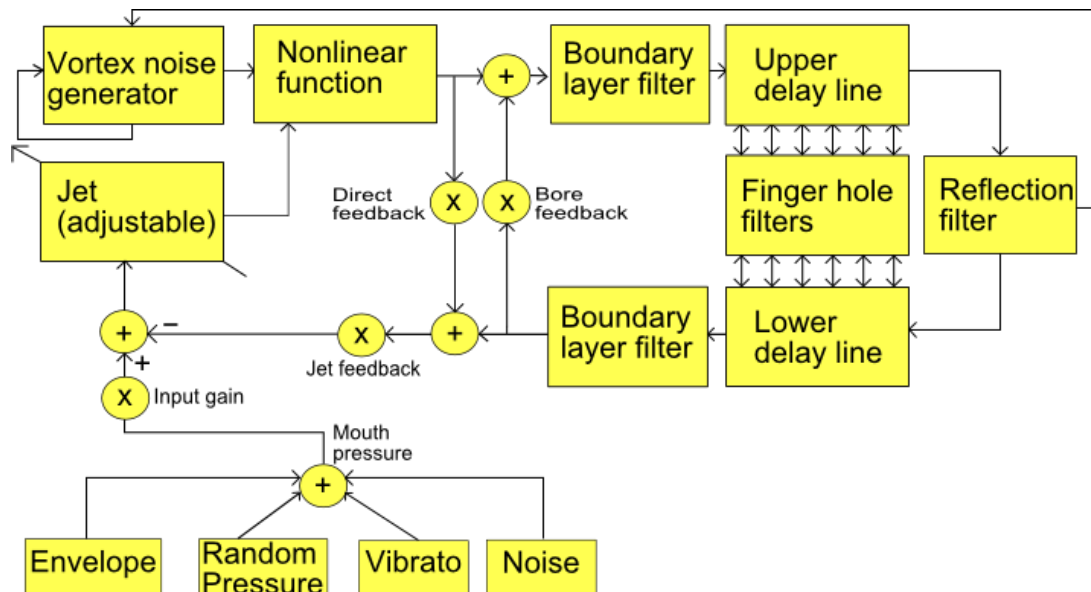


Figure 3.4 Block diagram of the Irish tin whistle physical model

Bottom part of the system is responsible for the input mouth signal generation and was inspired by the STK flute model [5]. Left hand side of the model acts as the excitation source, forming a jet and generating harmonics using wave shaping nonlinear function, pretty much alike as the one from the STK model. However nonlinear polynomial coefficients are now modulated using the period-synchronous noise signal generated in a similar manner as described in the work of Chafe [34]. Right hand side of the system models an open-ended bore with six tone holes and was inspired by the clarinet bore model in the work of Scavone [6].

Pressure signal coming from the player’s mouth is modelled as the sum of an envelope, random pressure, vibrato and noise signals. Afterwards the differential pressure signal is calculated as the difference between the input pressure and the pressure incoming from the bore. Subsequently differential pressure enters the delay line, which simulates the jet propagation delay. The length of the jet delay line is adjustable and may be altered in order to enable overblowing. The nonlinear waveshaping function has two inputs, first one is the jet output and second one is the output of

the vortex noise generator. The result of the nonlinear equation is summed with the scaled incoming bore pressure and enters the boundary layer filter responsible for the simulation of thermoviscous losses. The bore is modelled using seven tone hole segments, each one consisting of the tone hole junction and portions of delay lines on each side of the junction. The model uses the wave digital filter tone hole model described in [20]. Last segment output enters the reflectance filter, which simulates the acoustical reflection from the open end of the tube. Afterwards the pressure sample travels the similar path through seven tone hole segments and the boundary loss filter at the bottom of the system, finally reaching the junction between the jet and the resonator

- Envelope generator:

Envelope generator controls the amplitude contour of the generated input signal and has a very common form in the music synthesis world - ADSR. To control the shape of generated signal user may set four distinct times and amplitudes.

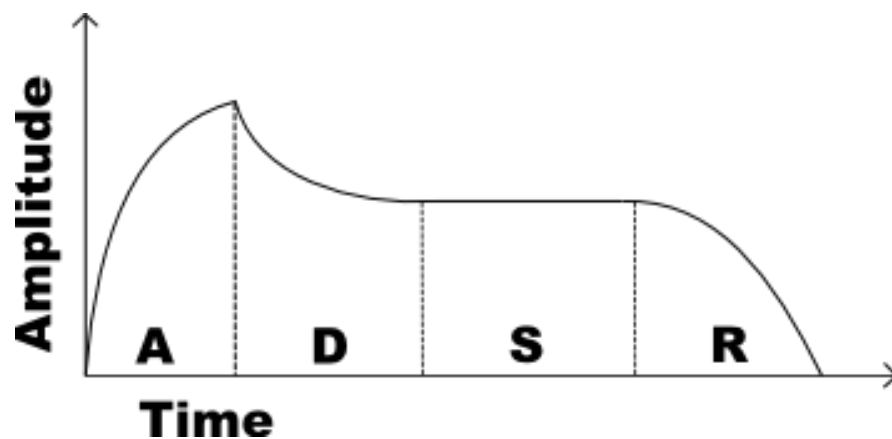


**Figure 3.5 Example of the ADSR envelope.**

Attack time is the time taken for initial run-up from zero to peak. Decay time is the time taken for the subsequent run down from the attack level to the designated sustain level. Sustain level is the level during the main sequence of the sound's duration. Release time is the time taken for the level to decay from the sustain level to zero.

The user sets the lengths of envelope sections as the factor of global number of samples  $N$ . E.g. if generated sound is 1 second long, for sampling frequency of 44100 kHz it means that the sequence is 44100

samples long ( $N=44100$ ). To obtain the attack time equal to 441 samples, attack time in the application should be set to 0.1.

- Random pressure generator

Random pressure generator is a simple module, which roughly simulates the random fluctuations of a pressure incoming from the musician's mouth. The user defines the standard deviation of the random signal, its amplitude, duration of the single section of constant amplitude and speed of the transition between sections. Duration and transition parameters are measured in number of samples and as previously user enters them as the factor of global number of samples.

- Vibrato module

Vibrato signal is a product of the FM modulation of sinusoid of few Hertz using the random signal.

- Noise module

Produces white noise signal of mean 0 and standard deviation defined by the user to simulate very small turbulences in the mouth pressure. Implementation derives from the Cook's STK breath noise model by simply adding the envelope multiplied white noise to the input signal. However in the Irish tin whistle model an input noise module has a secondary importance role, as the more advanced Chafe's noise model is used.

- Jet delay line

Length of the delay line is calculated in a similar manner as in the STK flute model:

$$Jet_{length} = Bore_{length} Jet_{ratio}$$

Complete length of the bore delay line is a sum of all its segments minus the delay introduced by the lumped elements e.g. the reflectance and boundary filters. Default  $Jet_{ratio}$  value is 0,33.

- Vortex noise generator

The vortex-noise generator iterative mapping function equation has a form:

$$n(j + 1) = a_0 + a_r R + a_1 n(j) + a_2 n(j)^2$$

(3.1)

where  $n(j)$  is the noise value in the previous computation cycle and  $R$  is the reflected signal incoming from the bore.

Coefficients ensuring chaotic behaviour of the quadratic map comes from the work of Chafe:

**Table 3.1 Coefficients of vortex-noise iterative map generator.**

Coefficient	Value
$a_r$	0.1
$a_0$	-0.6
$a_1$	-0.6
$a_2$	2

- Nonlinearity

General form of the waveshaping edge-tone function is given by:

$$Z = \sum_{i=0}^M (b_i + c_i n) x^i$$

(3.2)

where  $x$  is the input differential pressure,  $n$  is the noise signal from the vortex-noise generator,  $M$  is an order of the polynomial,  $b_i$  are edge-tone polynomial coefficients and  $c_i$  are modulation coefficients.

In the tin whistle model polynomial has an order of  $M=3$ . Values of  $b_i$  coefficients are the same as in the Cook's model. Values of the modulation coefficients  $c_i$  were adjusted empirically during the generation of the reference sound samples.

**Table 3.2 Coefficients of waveshaping nonlinear function.**

Coefficient	Value
$b_0$	0
$c_0$	0
$b_1$	-1
$c_1$	-0.015
$b_2$	0
$c_2$	0
$b_3$	1
$c_3$	0.015

- Boundary layer filter

Thermoviscous losses are simulated using two second-order digital filters placed at the input and output of the junction between the bore and the excitation source. Filter responses were calculated using Matlab *invfreqz* function by the *boundary.m* m-function provided by Scavone [6]. The amount of the high frequencies attenuation introduced by the filters depends on the radius of the pipe and its length.

- Tone hole segment

The bore is modelled using a digital waveguide technique described in [6] The model can be divided into the tone hole segments with two additional

segments at the beginning of the bore and at its end being responsible for an excitation and open-ended reflection, respectively.

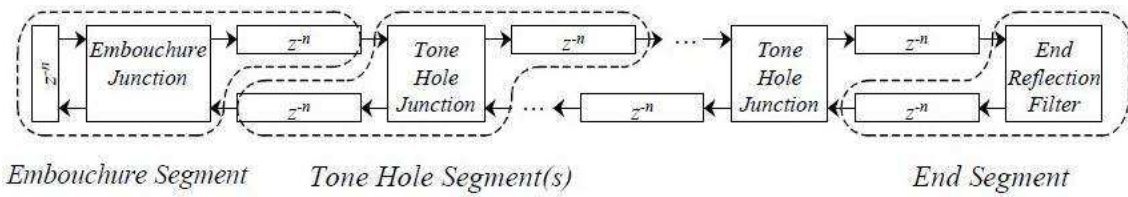


**Figure 3.6 Overall structure of the bore model. (source: [37])**

Each tone hole segment is represented by a three-port tone hole junction and two delay lines coupled to the junction outputs. The preferred tone hole model used for reference samples generation is the wave digital filter model described in [20], because it does not limit the minimal geometrical length of the hole and enable smooth transitions between the fully open and fully closed state. The user may also choose between the dynamic tone hole model described in [6] and less advanced, discrete three-port model developed by Scavone and Smith [19]

To preserve the stability of the model, hole models were extended by an additional gain control which simulates losses during the radiation and eliminates lossless reflection. Both finger hole model parameters and lengths of delay lines are calculated using the real instrument geometrical dimensions.

- Reflection filter

The characteristics of the reflection filter depend on the geometrical dimensions of the bore. Irish whistle bore radius is equal to 7,5 mm. Scavone in [6] provides a function which takes the pipe radius and calculates coefficients of an arbitrary order digital filter using the *invfreqz* function. Figure 3.7 presents the transmittance of the second-order digital filter corresponding to the Levine-Schwinger solution for an unflanged cylindrical pipe of radius 7,5 mm.

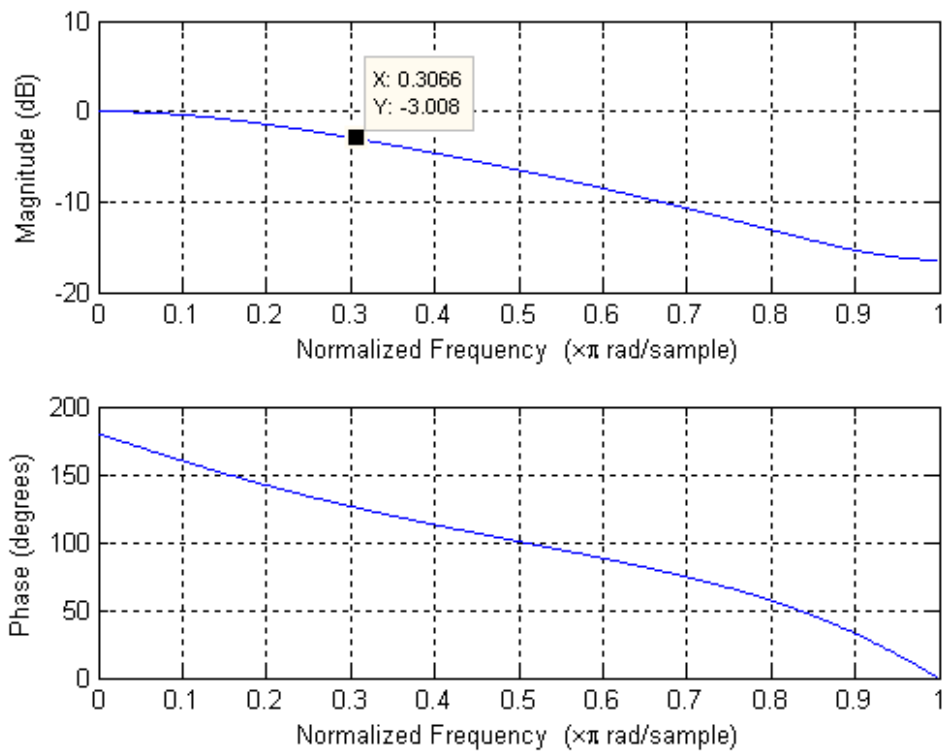


**Figure 3.7 Reflection filter calculated using `openpipe.m` function for pipe radius  $r = 7.5$  mm and sampling frequency  $f_s = 44100$  Hz.**

The filter has a low-pass characteristic with the cut-off frequency equal to 6 kHz and slope equal to 1.5 dB/octave. Low frequencies experience an almost 180 degrees phase-shift. The amount of phase shift decreases as the frequency is increased.

### 3.4 Graphical user interface

In order to make the painstaking tuning process more convenient, the graphical user interface was created using tools provided with the Matlab. Figure 3.8 presents the main window of the Irish tin whistle application.

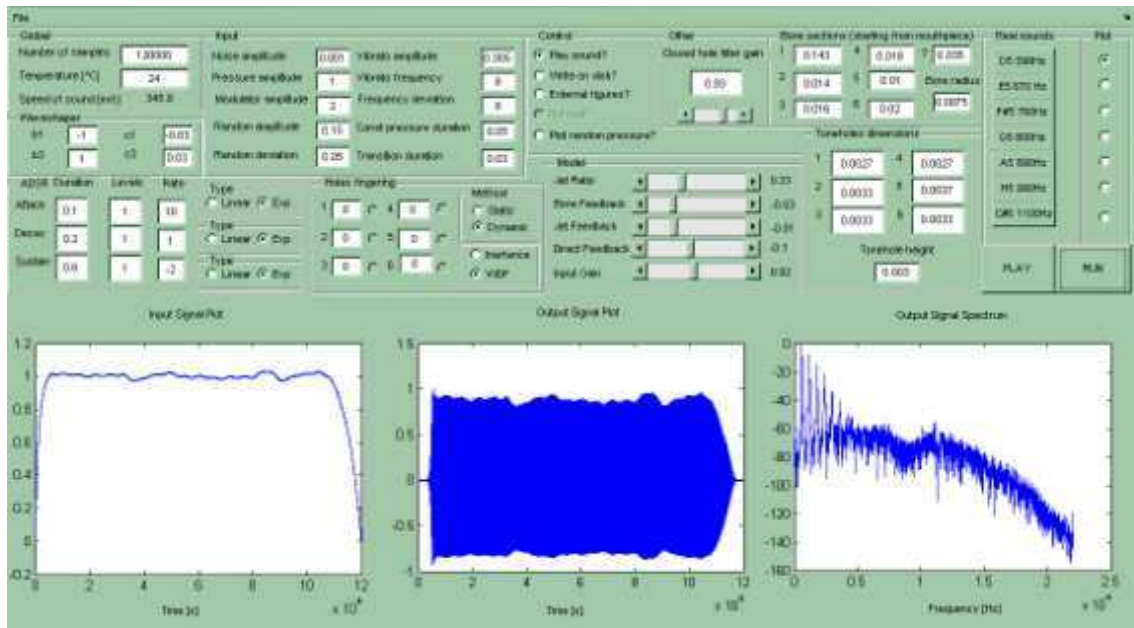


**Figure 3.8 Main window of the Irish flute model application.**

Bottom part of the application window contains graphs of the input mouth pressure signal and output of the system in time and frequency domain. Rest of the interface is designed to control the model, musician interaction and display options.

### 3.4.1 Global parameters and display properties

- Global panel

Sets the length of a generated sound by specifying the number of samples  $N$ . Another parameter to control is the air temperature measured in Celsius, which implies the speed of sound.

- Control panel

Top two buttons switch on the sound playback and write to disk functionalities. If the “external figures” button is enabled, the program shows three additional windows containing the output spectrum and its spectrogram and an output vs. input waveform. “Plot real” button allows a comparison between the real and synthesized signals, by plotting additional spectrogram of the recorded sound and recorded vs. synthesized spectrum. Last option enables visualization of the random pressure component of the input signal.

- Real sounds panel

Pressing an appropriate labelled button playbacks a sound of a recorded tin whistle, therefore allowing convenient comparison with a sound generated

by the model during the tuning process. Right hand side of the panel defines which note is displayed, if user decided to plot both recorded and synthesized signals using “plot real” button.

### 3.4.2 Input signal parameters

- Input panel

Controls the amplitudes and various parameters of vibrato, random pressure and noise signals, which form the mouth pressure signal.

- ADSR panel

ADSR panel is responsible for setting various envelope parameters like duration, amplitude and linear or exponential shape of the particular sections.

### 3.4.3 Physical model parameters

- Bore sections

Contains fields storing the lengths of seven bore sections and radius of the pipe measured in meters.

- Tone holes dimensions

Stores geometrical widths of six instrument tone holes and uniform height measured in meters. Similarly to the *bore sections* panel, tone hole numbering starts from a whistle mouthpiece.

- Model panel

Consists of four sliders representing physical model parameters controlling the amount of direct, jet and bore feedback. Jet ratio slider adjust the length of a jet and input gain regulates how much of an input mouth pressure signal is allowed into a system.

- Holes fingering

In this section user switches between the static and dynamic tone holes modelling method described in section 2.3 Static method is the three-port tone hole junction described by Scavone and Smith. If dynamic field is selected, the user may choose between the dynamic three-port junction (Inertance) or wave digital filter modelling (WDF). Depending on the selected option control over finger hole state is either two-state only or smooth. In the former case, enabled and disabled radio button represents fully closed tone and fully open hole, respectively. In the latter case, hole state ranges from 0 when fully opened and 1 when fully closed.

- Other controls

Stability of the model may be increased using the hole filter gain parameter, which simulates losses due to opened hole sound radiation and closed hole friction .

## 4 Evaluation of the Irish tin whistle physical model

### 4.1 Introduction

In general "sound quality is a fundamentally subjective (perceptual) concept, but it can be approximated by objective and computational criteria" [38]. In an audio realm primordial testing methods are comparative subjective listening experiments based on the Mean Opinion Score (MOS) given by a representative group of volunteers or experts. Depending on the type of a tested device/algorithm and character of an input sound (e.g. speech, music) various aesthetic and quality features may be examined like speech intelligibility, resemblance to the original, clarity of a concert hall or level of a degradation introduced by an encoding and decoding processes. Subjective MOS tests have proven to be sufficiently accurate, but they are generally expensive and time-consuming.

Before Wood's research concerning objective test methods for a waveguide audio synthesis [36], there have not been any studies conducted for objective testing methods for any form of audio synthesis. Calibration and testing of a music synthesizer consists of multiple interactions between programmers, sound designers, testers and other specialists involved in the design process. First of all sound synthesizers are musical instruments, and music itself is a completely subjective phenomenon. There are plenty examples of musically useful distortions and aesthetically pleasant sounds having an overdriven, noisy or just very specific character. Both musicians and sound engineers seek for a unique, warm sound, which is very often non-measurable by objective means.

In case of synthesizers using physical modeling technique, performing comparison tests between the real instrument and its digital counterpart seems to be a natural choice. Listening MOS tests and evaluation conducted by professional musicians can be very useful at the stage of interface design and model calibration. One may also conclude comparison tests concerning e.g. specific acoustical properties, behavior during playing or impact of various model parameters.

## 4.2 Evaluation methodology

This project in its initial stage assumed using both objective and subjective methods to evaluate how well designed model approaches the sound of the real tin whistle instrument. Subjective tests on the group of listeners have been considered to be the fundamental form of a model evaluation. Additional PAQM (Perceptual Audio Quality Measure) and NMR (Noise-to-Mask Ratio) test scores could be performed as supplementary objective tests. However Wood's work showed that in some cases both PAQM and NMR methods fail as the objective test method for the waveguide synthesis [36]. Both methods did not manage to correctly classify samples of a plucked string produced by leading synthesizers on the market. Even worse classification results are expected, when comparing woodwind instruments sounds, because of their chaotic, peculiar character.

Furthermore, test samples generation process revealed notable timbre discrepancies between recorded and synthesized sounds. This fact confirmed previous expectations that objective evaluation methods would probably give very poor results and therefore should be abandoned.

Subjective group listening tests were not performed either, mostly due to limited amount of time dedicated for this project. The second reason was an identification of audible differences between real instrument and synthesized sounds. Nevertheless, resignation from the timbre resemblance listening tests does not mean improper evaluation; there is still plenty of interesting model features worth investigating.

The first part of conducted evaluation includes a detailed description of most interesting control parameters affecting the timbre and stability of the implemented model. The following section presents results of a comparison between a real tin whistle and its digital simulation by a pitch control, timbre features and responses for different excitation signals. Finally the last section shows some simplifications and inaccuracies of the model responsible for discrepancies between an Irish tin whistle and proposed simulation.

## 4.3 Most interesting control parameters

### 4.3.1 Model adjustments

The scope of the tuning process was to find a best available model setup matching the timbre and envelope characteristics of collected real instrument sounds. A professional Shure KSM27 microphone and Digidesign Pro Tools system was used in the recording process. Each recorded sample consists of a approximately three seconds long sound of a single note played by the author on the Feadog [39] Irish whistle in key D.

The ideal outcome of the tuning process would be finding a single set of parameters describing a model and an input signal valid for all possible fingerings. However, due to the impact of a tone hole lattice, varying character of the player's mouth pressure signal entering the instrument and simplifications present in the model, the task of finding such universal configuration was not accomplished.

Table 4.1 shows values of selected parameters resulting from model adjustments. The table does not include parameters, which remain constant for all fingerings or are responsible for an input mouth pressure signal generation. Complete application setup files for particular fingers positions can be found on the attached CD, alongside with resulting sounds from the model and reference sound samples of the real instrument.

**Table 4.1 Selected parameters from the configuration file.**

Parameter	Bore Feedback	Jet Feedback	Input Gain	Tone hole Filter Gain	C1 noise	C3 noise
D5	-0,530	-0,510	0,920	0,930	-0,030	0,030
E5	-0,730	-0,630	0,950	0,920	-0,015	0,015
F#5	-0,680	-0,610	0,950	0,935	-0,015	0,015
G5	-0,500	-0,500	0,920	0,970	-0,015	0,015
A5	-0,520	-0,500	0,940	0,970	-0,015	0,015
H5	-0,480	-0,480	0,920	0,970	-0,015	0,015
C#6	-0,480	-0,480	0,900	0,960	-0,010	0,010
Average	-0,560	-0,530	0,929	0,951	-0,016	0,016
Min	-0,730	-0,630	0,900	0,920	-0,030	0,010
Max	-0,480	-0,480	0,950	0,970	-0,010	0,030

From the table 4.1 one can see that finding one common set of parameters ensuring close reproduction of the tin whistle sound is a non trivial task. Problems are caused mostly due to the presence of the tone hole lattice

producing multiple reflections along the signal propagation path. The model behaves differently, depending on the configuration of opened and closed tone holes. Obtaining a whistle like sound for majority of fingerings was relatively simple; only slight parameter corrections were needed to increase the level of resemblance between synthesized and recorded sounds. However, for notes E5 or F#5, production of any sound while preserving the stability demanded significant increase of jet and bore feedbacks and simultaneous decrease of the tone hole radiation filter gain.

### 4.3.2 Stability control

The tone hole filter gain parameter is the main tool provided by the model ensuring its stable behavior. Default value suitable for most fingerings is 0.97, however in case when four or more finger holes are closed, gain parameter needs to be decreased or model becomes unstable. Figure 4.1 shows the spectrum of a D5 sound for the tone hole filter gain parameter equal to 0.92 (left) and 0.94 (right).

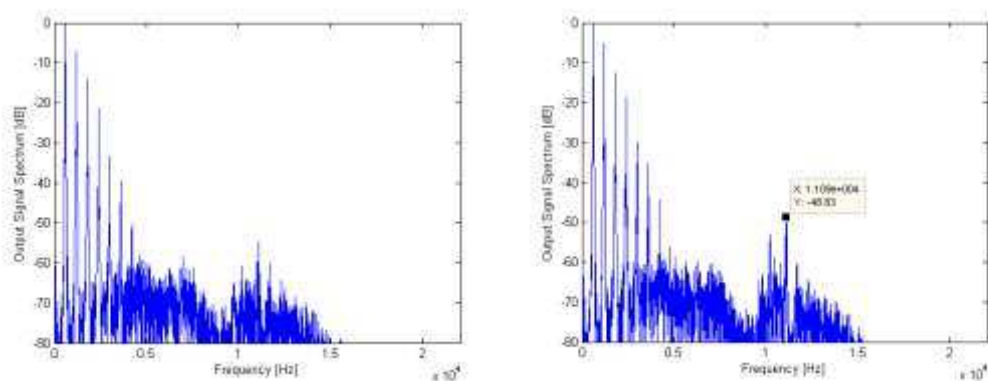


**Figure 4.1 D5 sound for tone hole filter gain equal to 0.92 (left) and 0.94 (right).**

The right hand side of the figure 4.1 shows a peak located around 11 kHz. Its amplitude is increasing proportionally to the filter gain parameter. For example for the note D5 the critical value of the filter gain is 0.94. If critical value is exceeded, the model becomes unstable and most of the energy in the system cumulates around frequency of 11 kHz as shown in the figure 4.2. In general, the described effect is much more common for fingerings representing many closed finger holes and is caused by the band-pass frequency response of the tone hole reflectance filter.

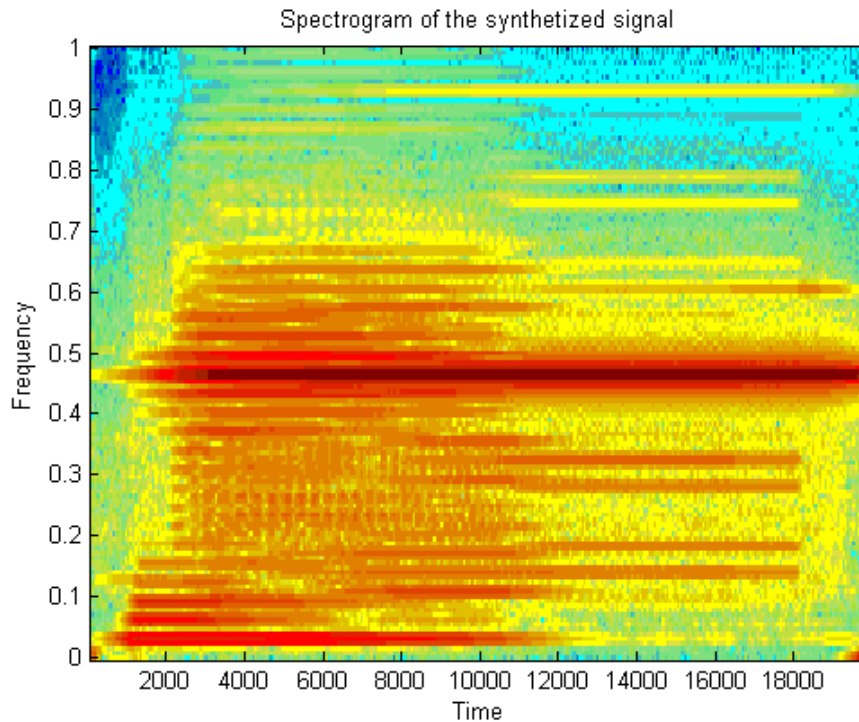


**Figure 4.2 Spectrogram illustrating an unstable behavior of the system.**

In case of difficult to produce notes like E5 or F#5, jet and bore feedback values need to be increased. However one has to be careful, because too high values might result in an unstable behavior. The same rule applies to parameters controlling the amplitude of the input pressure signal (vibrato and random pressure components and ADSR levels) and input gain factor.

### **4.3.3 Timbre control**

Once physical model parameters are set, instrument timbre depends on the amplitude and character of the excitation signal. As expected, the implemented model acts likewise to the majority of real instruments, following a simple rule that increasing the amplitude of an input signal results in the creation of an increased number of successive harmonics.

Figures 4.3, 4.4 and 4.5 present spectrums of output signals obtained for increasing input signal amplitude – starting from 0.8, through 1, finishing at 1.1.

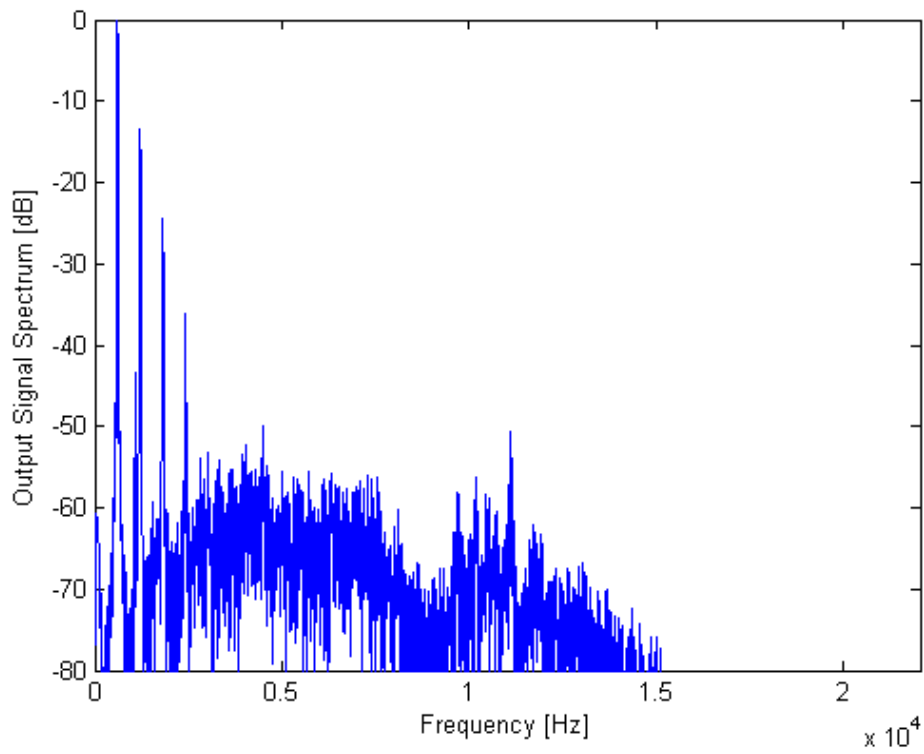


**Figure 4.3** Spectrum of the note D5 for the input signal amplitude equal to 0.8

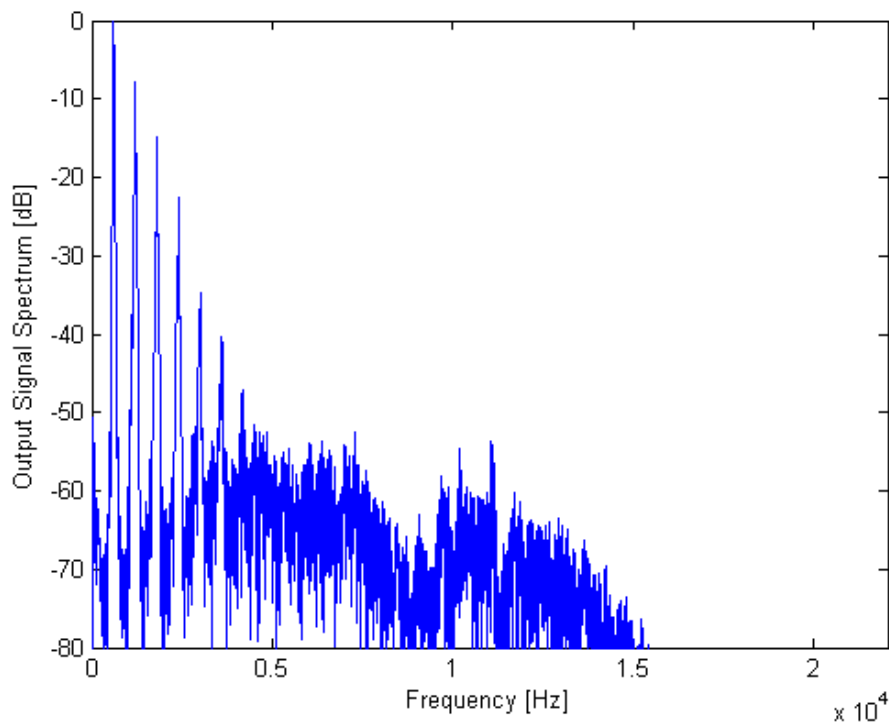


**Figure 4.4** Spectrum of the note D5 for the input signal amplitude equal to 1

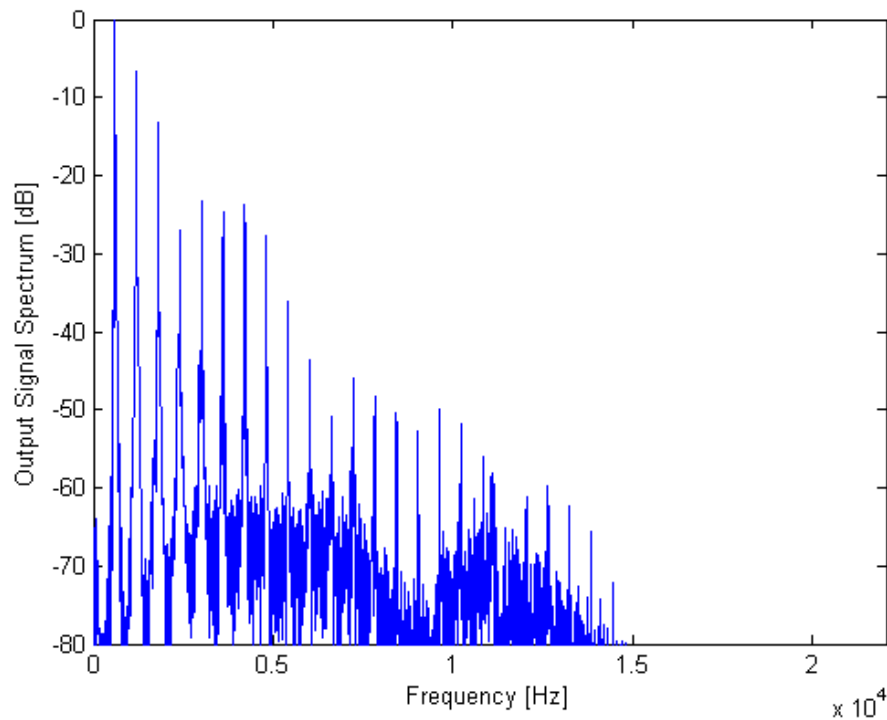


**Figure 4.5 Spectrum of the note D5 for the input signal amplitude equal to 1.1**

Figures 4.3 to 4.5 prove that the harmonic content of produced sound depends on the amplitude of the excitation signal.

Another way to vary harmonic richness is to tweak model parameters responsible for amount of the feedback in the system. Increasing bore or direct feedback factors induces extra harmonics in the generated signal. In other words - increasing feedback changes the "sensitivity" of the model, because lower input amplitudes are able to produce sounds with richer harmonic content.

Another element affecting perceived timbre is a noise component. The user may control its amount in the generated signal either by changing modulation coefficients  $c_1$  and  $c_3$  or mixing some white noise with an input signal. Figures 4.6 and 4.7 present the spectrogram and spectrum of the output signal without any noise added.

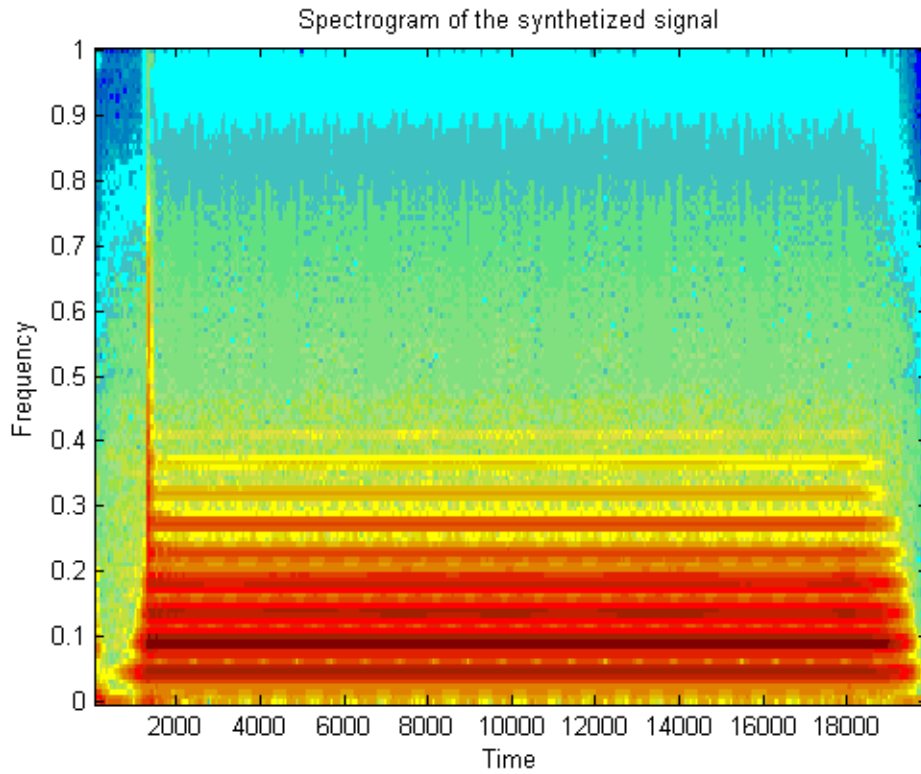


**Figure 4.6 Spectrogram of the note H5, no noise component used.**

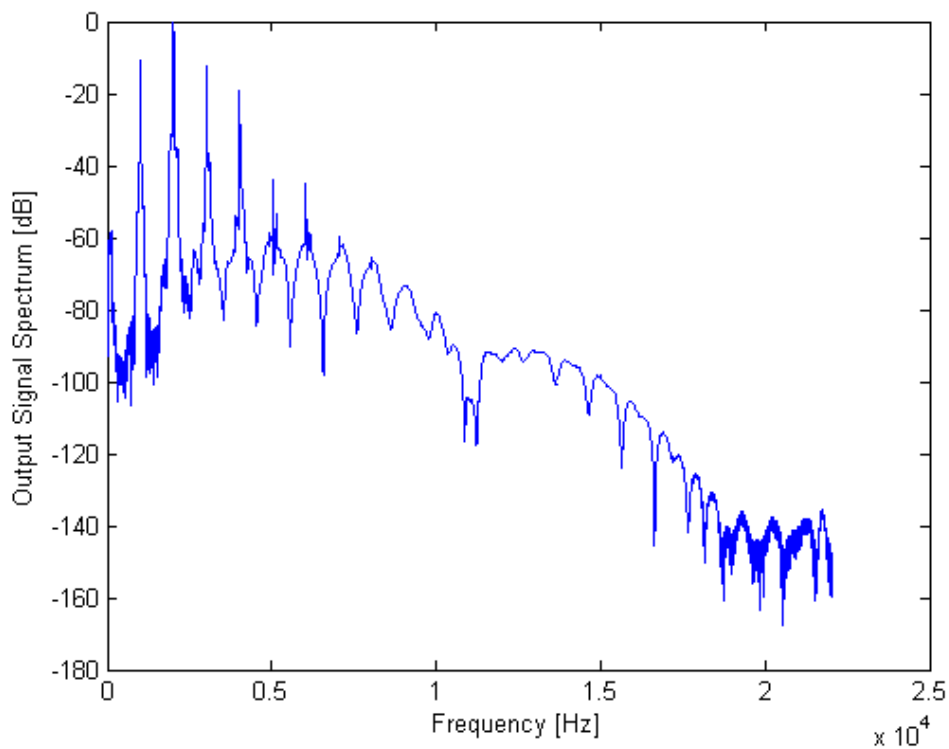


**Figure 4.7 Spectrum of the note H5, no noise component used.**

First method, which is adding a white noise to an input signal, does not produce very pleasant outcome. The injected noise, after propagating

through a system, sounds more like a hiss; especially high frequency content is missing. It is audible that the noise component comes from some other source and does not blend with the sound produced by the instrument. The remedy could be applying an appropriate filter before mixing with other input signal components.

Second method (Chaffe's noise model) produces a better outcome. Resulting sound has a more pleasant and subtle character. Figures 4.10 and 4.11 containing the spectrum and spectrogram of the output sound reveal that the characteristic shape of harmonic peaks is now better retained, comparing to the previous method (figure 4.8 and 4.9). When listened to, the energy of noise seems to be distributed in the higher frequency range than in the STK model.

For majority of fingerings, the noise coefficients  $c_1$  and  $c_3$  were set to -0.015 and 0.015, respectively. Further increase results in harsh, unpleasant sound. In practice both noise injection methods can be use in a complementary way, since the resulting noise affects slightly different frequency bands.

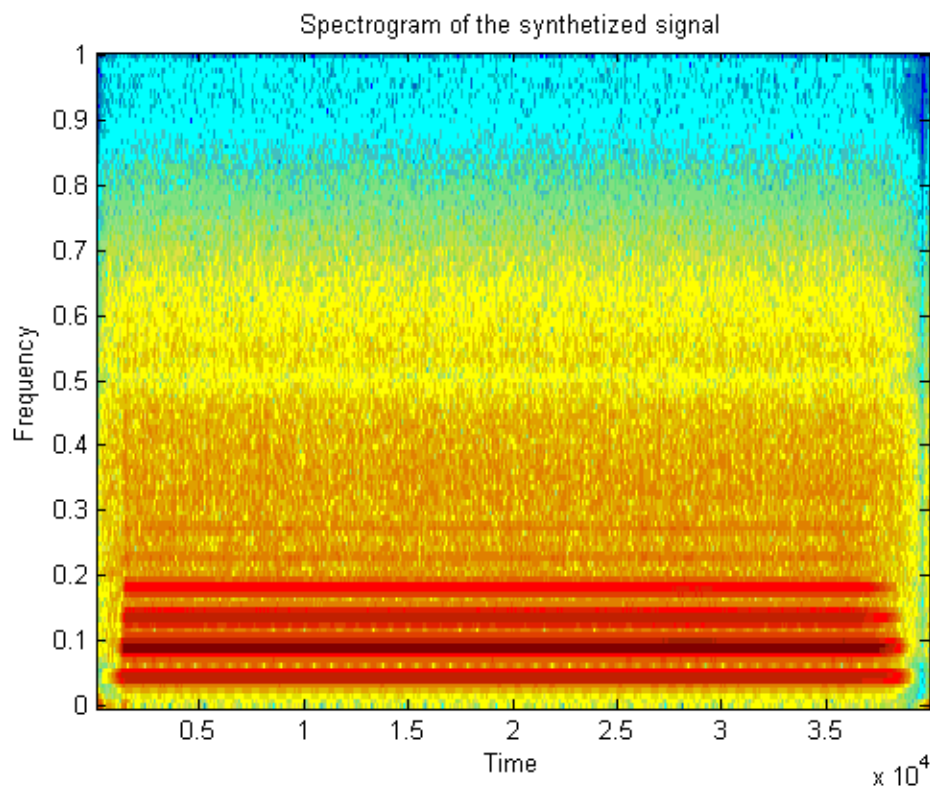


**Figure 4.8 Spectrogram of the h5 note, white noise mixed with the input signal. Noise intensity equal to 0.001.**

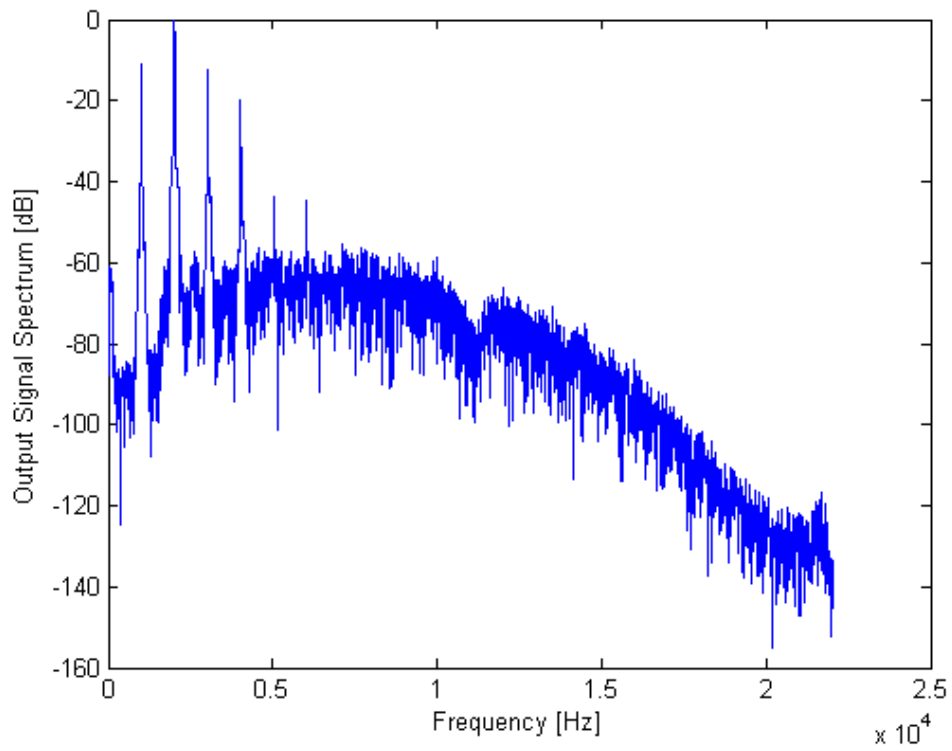


**Figure 4.9** Spectrum of the h5 note, white noise mixed with the input signal. Noise intensity equal to 0.001.

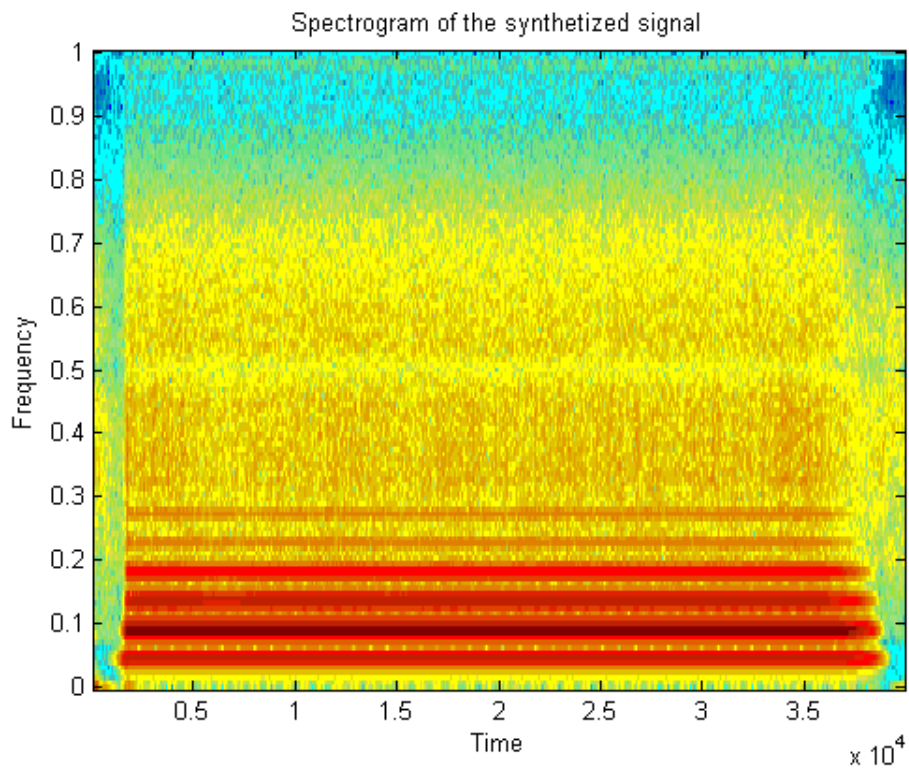


**Figure 4.10** Spectrogram of the h5 note, Chaffe's noise model used.  $C1 = -0.02$ ,  $C2 = 0.02$

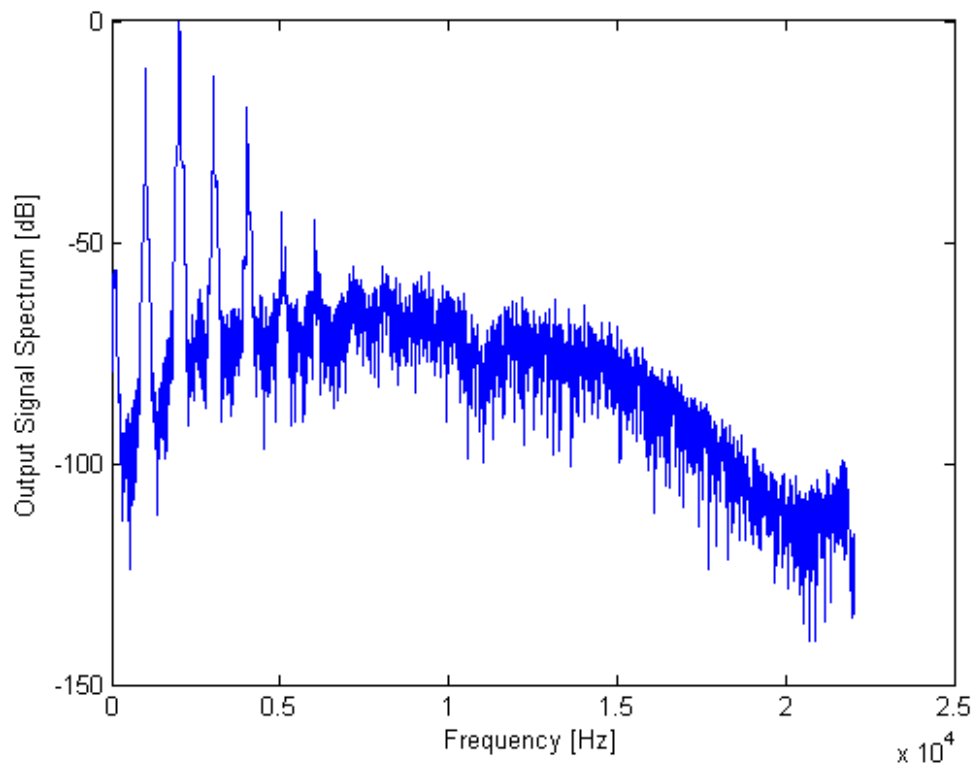


**Figure 4.11 Spectrum of the h5 note, Chaffe's noise model used.  $C1 = -0.02$ ,  $C2 = 0.02$**

#### 4.3.4 Overblowing

It is possible to force an Irish whistle to play in the higher register by blowing harder into the instrument. The fingering remains the same as in the lower octave.

Section 4.3.3 showed that blowing harder changed the frequency content, but did not affect the produced pitch, as in the case of the real instrument. However an overblowing phenomenon can be simulated by manipulating the length of the jet delay line.

For fingering D5, changing the jet ratio parameter from 0.33 to 0.2 results in a one octave higher sound. Analogically, further decrease to 0.16 drives the model to a generate two octaves higher sound. Unfortunately, some fingerings do not produce overtones resulting from changing jet ratio parameter. There is also a significant error in the frequency of produced higher modes, however it is not surprising as the model in general exhibits problems with appropriate tuning. Figures 4.12 and 4.13 illustrate D6 and D7 overtones in time and frequency domain.

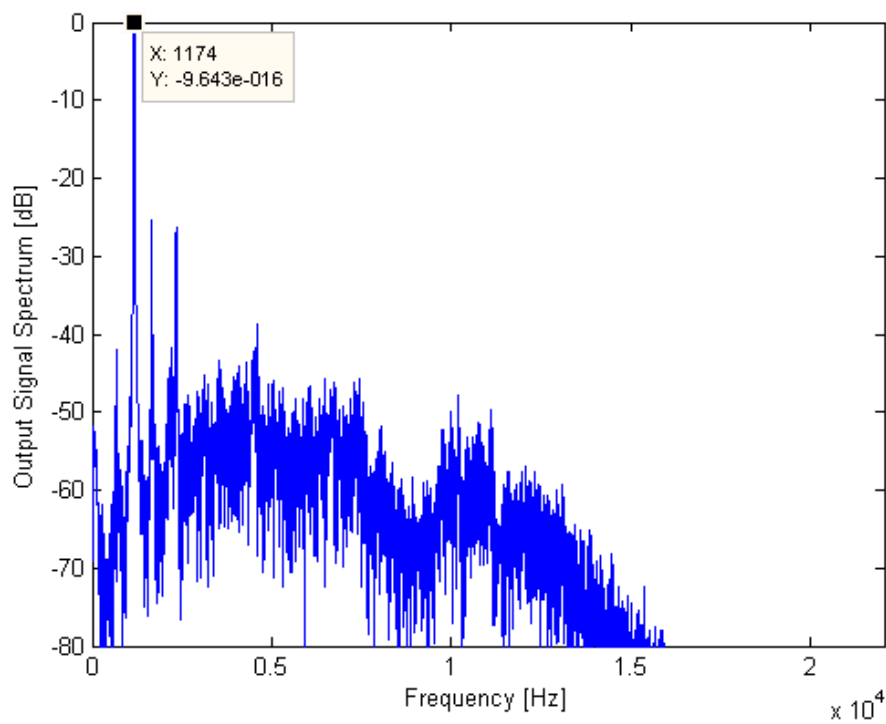
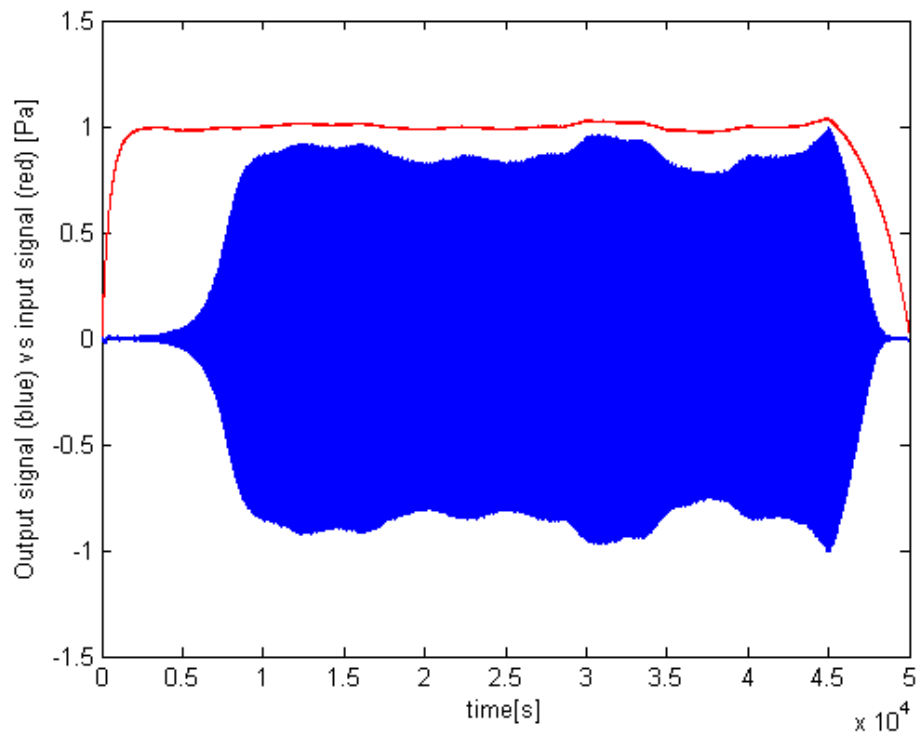


**Figure 4.12** Second oscillation mode produced for the fingering of D5 (600 Hz), 25 Hz tuning error present

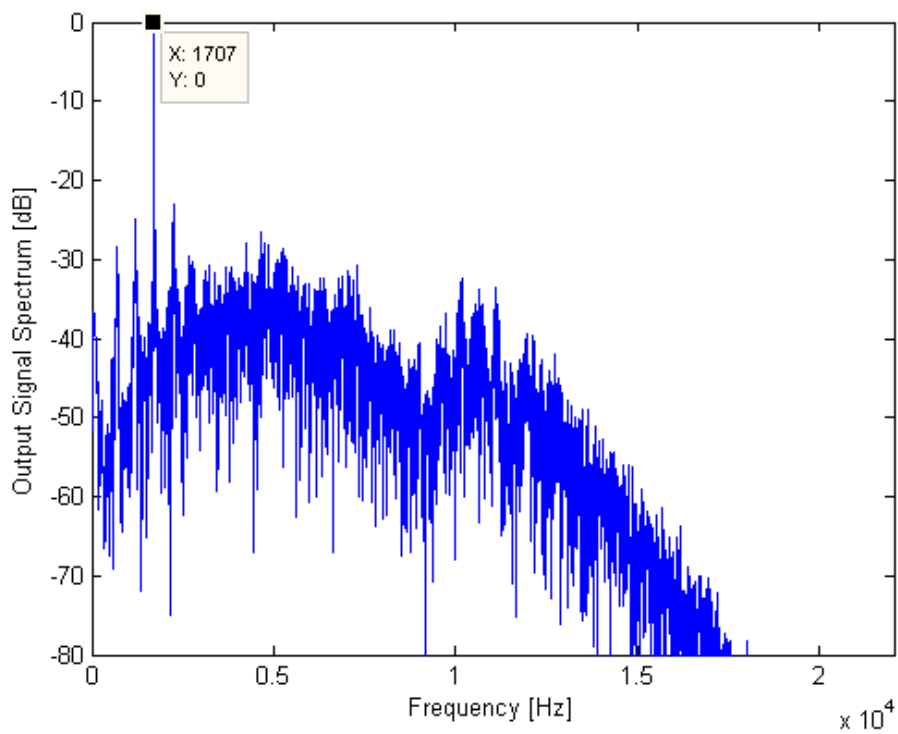
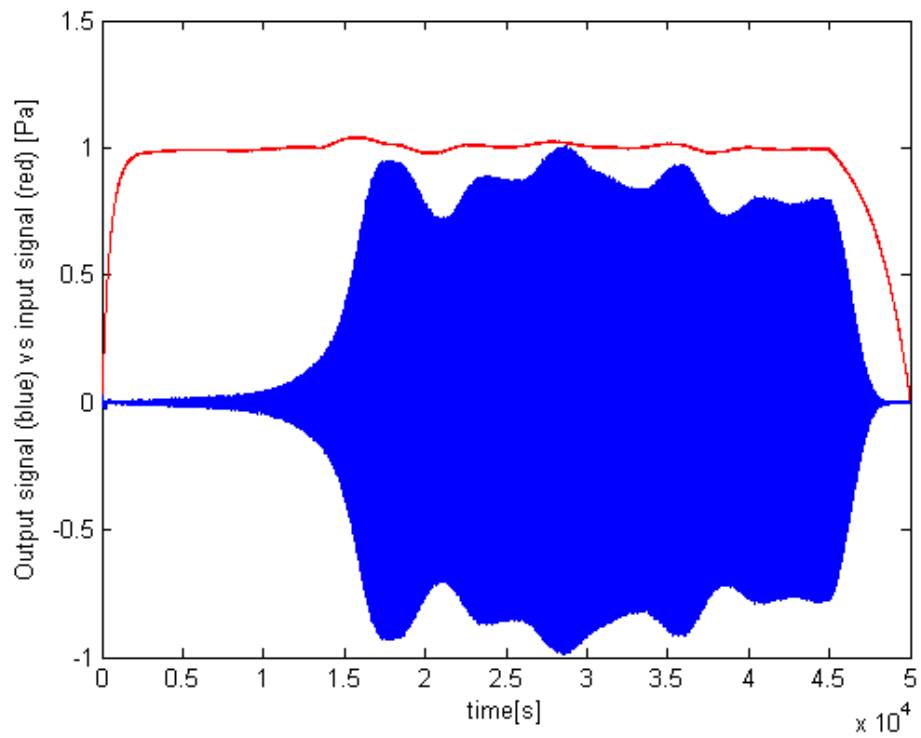


**Figure 4.13 Third oscillation mode produced for the fingering of D5 (600 Hz), around 90 Hz tuning error present**

## 4.4 Real vs. Virtual tin whistle comparison

This section deals with the evaluation of the tin whistle model by comparing its sounding frequencies and timbre characteristics with the natural instrument. The real Irish whistle used in tests is a 26.4 cm long metal tube with six tone holes. Bore radius is equal to 7.5 mm. Tests were limited to the notes resulting from the first mode of oscillation only. Interesting features like cross fingering and dynamic tone hole states were investigated. Produced sounds were compared with samples of original instrument in both frequency and time domain.

### 4.4.1 Tuning

The implemented model parameters like tone holes and bore dimensions have been set to match geometrical dimensions of the real instrument. The model is able to produce only one frequency per fingering, while the real instrument produces a range of frequencies depending on the blowing pressure amplitude. Table 4.2 presents results of the fundamental frequency measurements taken for natural instrument and corresponding values produced by the model. Measurements of the recorded sounds fundamental frequency are based on the spectrum graphs calculated with the Fast Fourier Transform in the Sound Forge audio processing software. Recorded samples were windowed with 32768 samples long Hamming window with 75 % of overlap.

**Table 4.2 Theoretical and measured fundamental frequencies from recorded and synthesized sounds of tin whistle in key D.**

Note	Fundamental frequency (theoretical)[Hz]	Real instrument fundamental frequency [Hz]	Physical model fundamental frequency [Hz]	Tuning [Hz]	Error
D5	587,33	595,8-600	656,8		58,9
E5	659,26	660-672	721		55
F#5	739,99	753-760	818		61,5
G5	783,99	790-805	883		85,5
A5	880	885-904	963		68,5
H5	987,77	995-1028	1039		27,5
C#6	1108,73	1080-1150	1120		-5

The first column contains values of the reference frequency for key D notes taken from [40]. The second column consist of frequency ranges produced by the instrument for successive fingerings. The third column shows values of fundamental frequencies produced by the implemented model having the

same virtual dimensions as its real counterpart. The last column contains the distance between the fundamental frequency generated by the model and the centre of frequency range produced by the real instrument for the same fingering. This distance measured in Hertz may be considered as the average tuning error.

The table 4.2 shows that the only fingering producing correct results is the one with all finger holes open (note C#6). As expected closing successive tone holes decreases produced fundamental frequency, but not sufficiently enough. One can see that sounds produced by the implemented model are in general too sharp comparing to the natural instrument. The amount of the tuning error varies from approximately 30 Hz for note H5 to almost 85 Hz for the note G5.

Real woodwind instruments are able to produce sounds that are the same in pitch, but result from different fingerings. To get the note c#6 three different fingering configurations are valid. One may improve tuning properties of a particular note by closing additional tone holes at the far end of the instrument as presented in the figure 4.14. The same rule applies to different notes like A5, G5 or B5. The advantage of such fingerings is an increased ability of the instrument to keep its fundamental frequency stable.



**Figure 4.14 Alternative fingerings producing sound C#6**

Cross fingering is also useful to get notes laying outside the principal major key. The same goal can be also achieved by a technique called "half-holing" (partially covering the highest open finger hole).

After several tests the general conclusion is that the implemented model successfully simulate the tone hole lattice impact and is able to produce sounds for the same fingerings as the natural instrument, including cross-fingerings and half-holing features. However produced sounds are in general too high in pitch comparing to the natural instrument, therefore the implemented tone hole model should be investigated in more details in

order to find the reason of detected error. Naturally in order to keep the model stable and able to oscillate some adjustments of parameters like feedback or input gain are necessary.

#### **4.4.2 Resonances and timbre**

As it was shown in the previous sections, model exhibits some tuning error. Therefore, before performing resonance and timbre tests, the length of the bore was appropriately changed to make the model and the real instrument play in tune in respect to each other.

The best match between synthesized and recorded sound was found for the note D5. Spectrum graphs of recorded and synthesized notes D5 and A5 are presented in the figures 4.15 to 4.20.

The D5 note spectrum exhibits descending series of harmonics and has a minimum of characteristics at 9 kHz reaching -80 dB.

In case of note A5 the match between harmonics location and their amplitude is even better, but synthesized sound spectrum minimum is now located around 12 kHz instead of 9 kHz.

One can also see that harmonic peaks of the recorded sound are wider comparing to ones produced by the physical model. The reason for that could be slight fluctuations of musician's breath pressure, resulting in pitch fluctuations widening harmonic stripes.

It is worth mentioning that all recorded samples have some noise component around 18 kHz, which is very close to the inaudible frequency range; hence has no impact on the quality of a recorded sound. The source of the detected peak is probably the air-conditioning device lately installed in the studio.

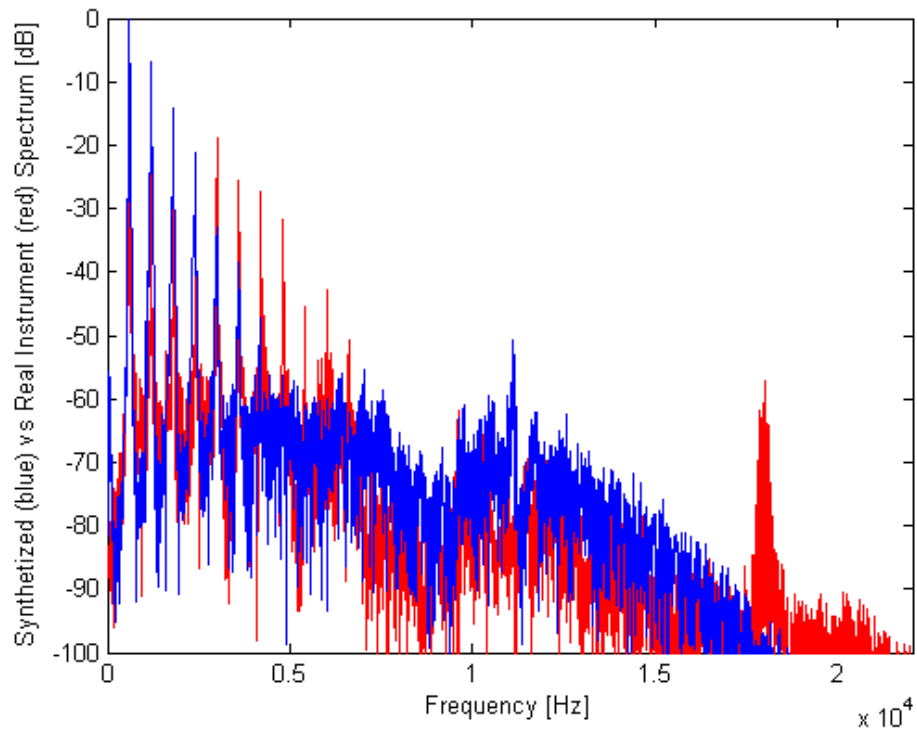


**Figure 4.15 Synthesized (blue) and recorded (red) note D5.**

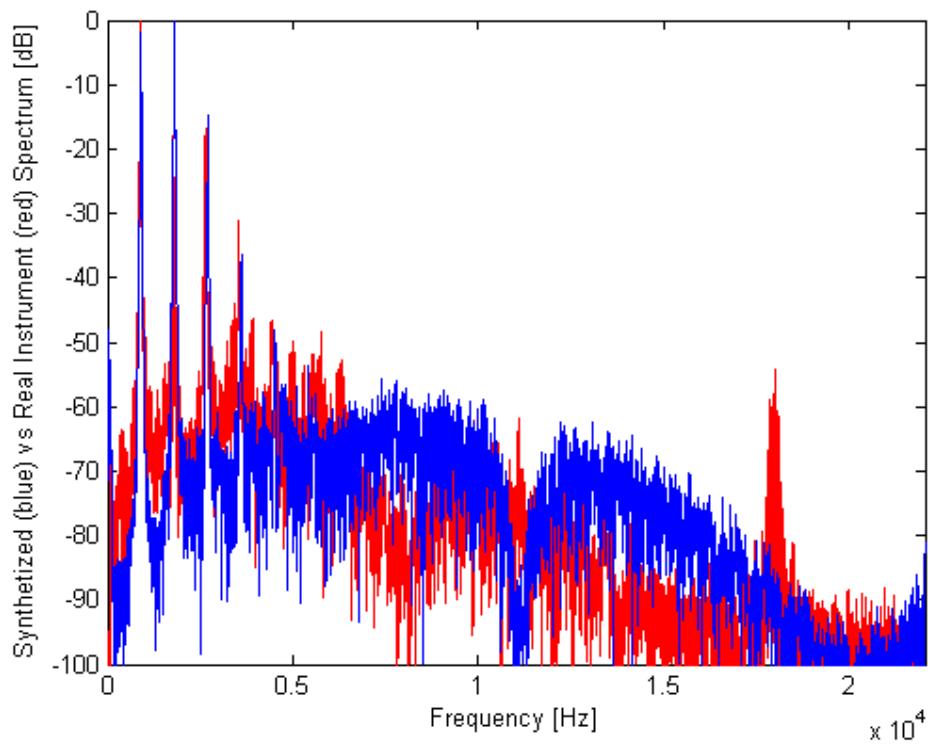


**Figure 4.16 Synthesized (blue) and recorded (red) note A5.**

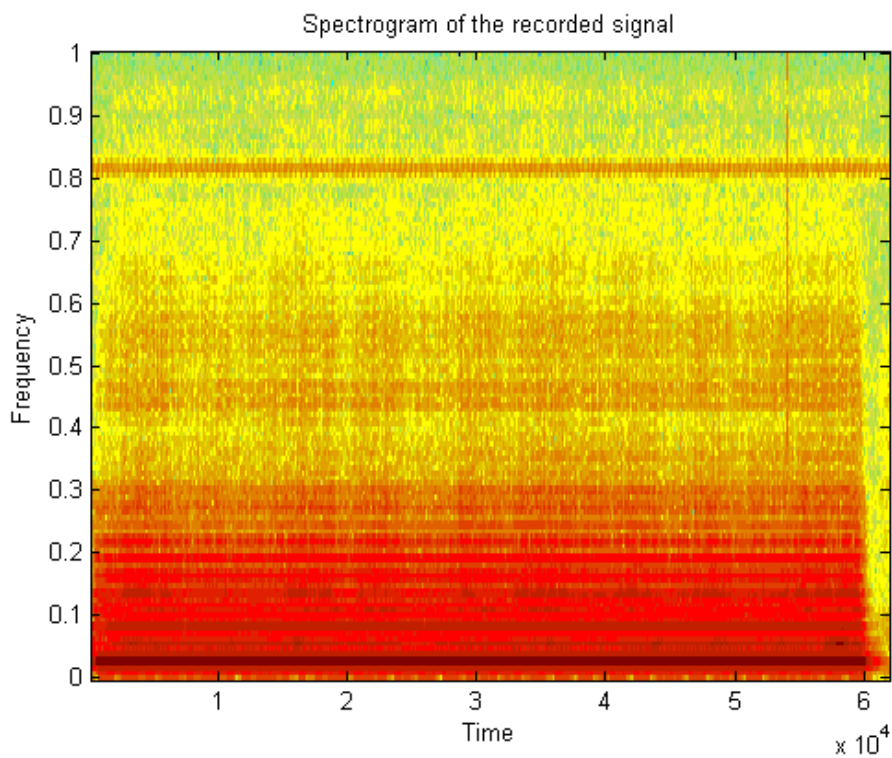


**Figure 4.17 Spectrogram of the recorded D5 note.**

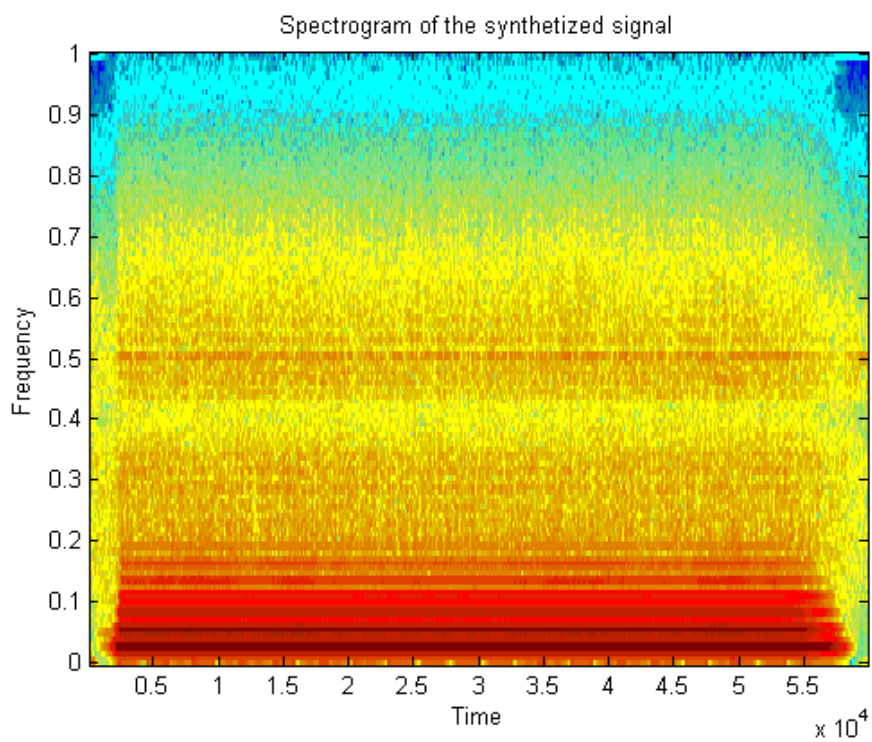


**Figure 4.18 Spectrogram of the synthesized D5 note.**

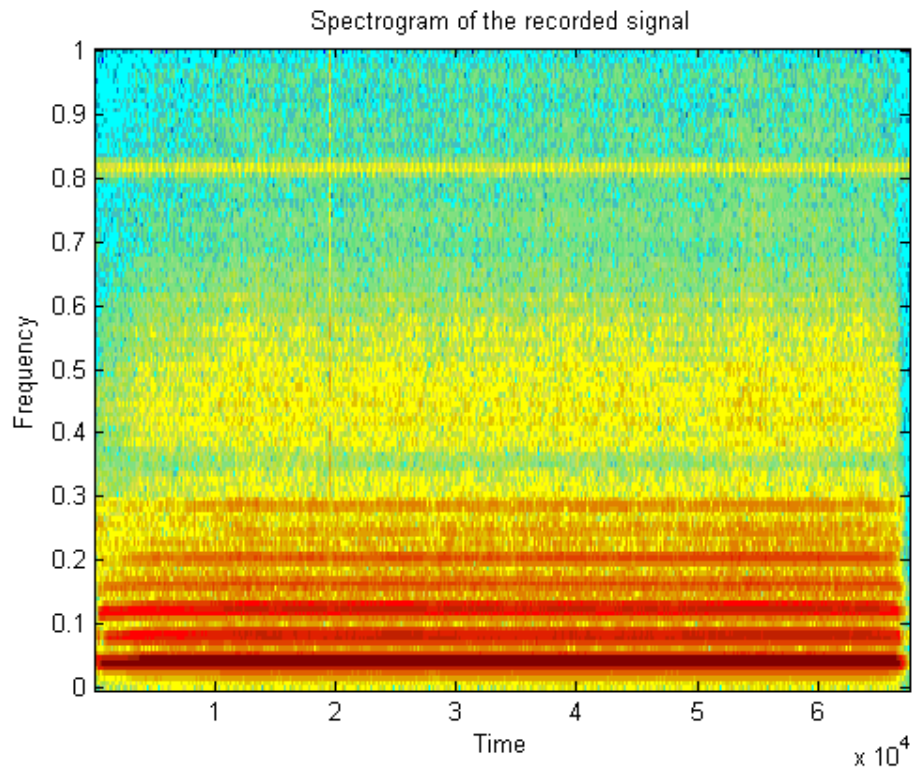


**Figure 4.19 Spectrogram of the recorded A5 note.**

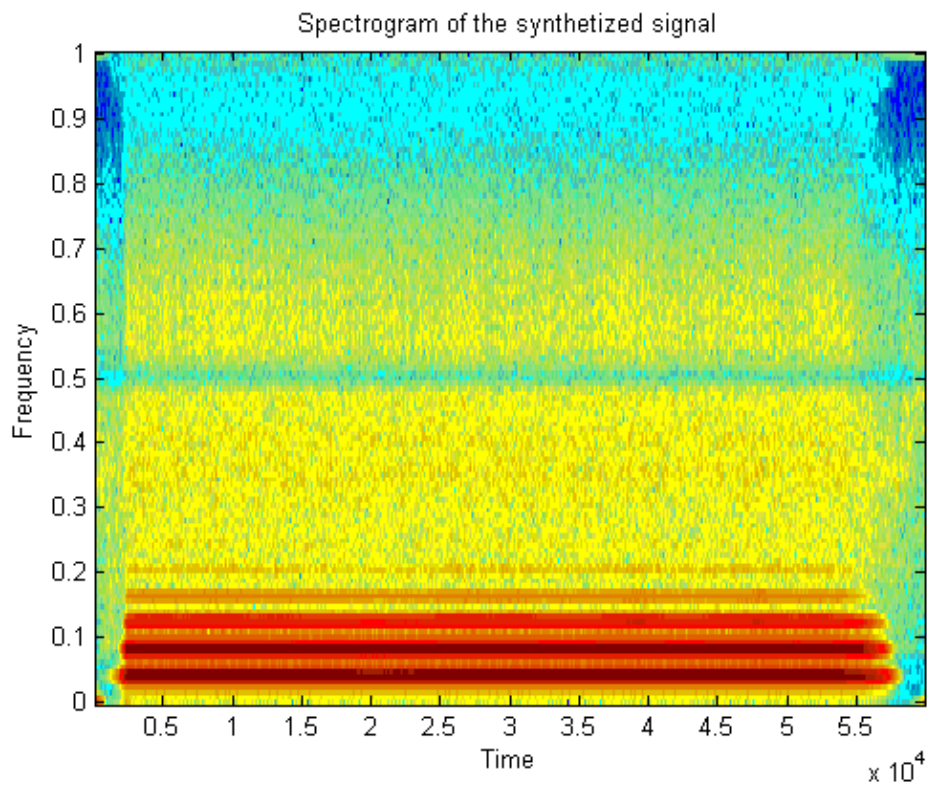


**Figure 4.20 Spectrogram of the synthesized A5 note.**

Another factor affecting the timbre of the instrument is the non-uniform distribution of harmonics along the frequency axis, in such a way that successive harmonics lay at imperfect multiples of the fundamental frequency. Table 4.3 contains three columns consisting of harmonics frequencies calculated as the perfect multiples of fundamental, measured from the physical model output spectrum and natural instrument output spectrum, respectively. The symbol "x" in the table represents harmonics which were non-measurable due to the noise present in the signal.

One can see that natural instrument harmonics are in general lower in frequency comparing to implemented model harmonics (not including harmonics numbered 17 and higher). Moreover, also synthesized sound harmonics exhibit lower frequencies than expected comparing to reference resonances in column one. Greater amount of inharmonicity in the natural instrument sound may be the reason of its more "warm" and peculiar character.

**Table 4.3 Comparison of physical model and natural instrument harmonics frequency location for the note D5.**

	Theoretic harmonic	Physical Model	Natural Instrument
Harmonic Number	Frequency[Hz]	Frequency [Hz]	Frequency [Hz]
1	602,9	602,9	602,9
2	1205,8	1204	1203
3	1808,7	1806	1803
4	2411,6	2409	2404
5	3014,5	3009	3007
6	3617,4	3612	3607
7	4220,3	4215	4210
8	4823,2	4815	4810
9	5426,1	x	5410
10	6029	x	6013
11	6631,9	x	x
12	7234,8	x	x
13	7837,7	x	x
14	8440,6	x	x
15	9043,5	x	x
16	9646,4	x	9620
17	10249,3	x	10301
18	10852,2	x	10910
19	11455,1	11111	11150
20	12058	11670	12110

### 4.4.3 Transient and stationary characteristics

The ADSR envelope generator enables only basic control over time domain characteristics of an input signal. Therefore the task of a realistic simulation of a mouth pressure signal is collectively managed by random pressure, vibrato and turbulent noise modules. However even such multi parameter control of an input signal encounters problems to simulate the diversity of natural excitation characteristics.

The model encounters problems when the slope of the attack envelope is too gentle. From the figure 4.21 and 4.22 one can see that there is an apparent delay between the beginning of an excitation and start of output oscillations. Apparently, the system will not start forming the output attack transient before the constant mouth pressure is applied at its input. Therefore selected shape of the curve is irrelevant.

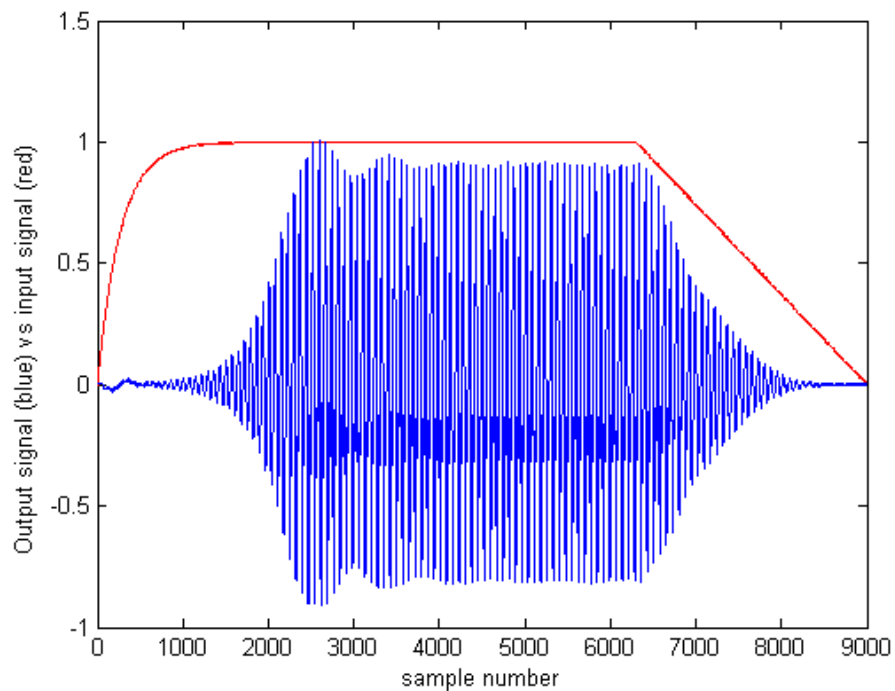


**Figure 4.21 Exponential attack of an input signal.**

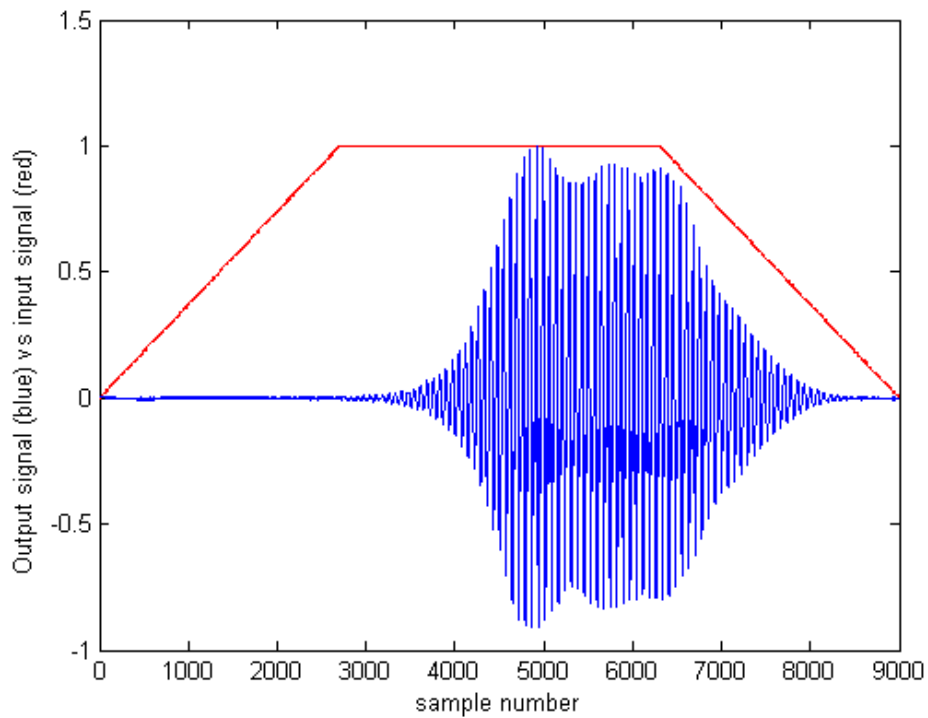


**Figure 4.22 Linear attack of an input signal. The shape of the output transient is the same as in case of exponential type of attack.**

Figure 4.23 shows the time domain plot of the recorded and synthesized D5 note. Both sounds are 0.2 seconds long and have a gentle character of attack and release phases. However, due to the reasons discussed earlier, modelling the exact time domain shape for both sounds was impossible. The synthesized sound exhibits interesting amplitude modulation after reaching its maximum value at the end of the attack transient. The recorded waveform in contrary to the generated one does not exhibit the x-axis symmetry.

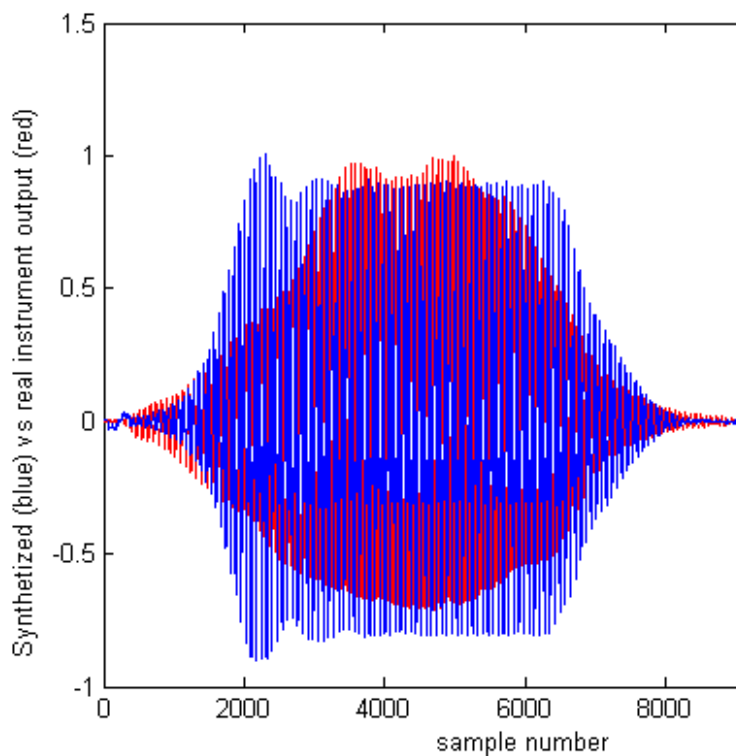


**Figure 4.23 Recorded vs. synthesized sound - short duration, gentle attack and release slopes.**

A detailed view of the transient attack characteristics can be found in the figure 4.24. Time domain plots reveal that the shape of a produced wave in the attack phase has a very similar shape to the wave produced by the system in the stationary phase. From the spectrogram one can deduce that the attack transient waveform is richer in higher harmonics and some extra amount of noise, but misses an unique and peculiar character comparing to the rest of the obtained sound.

An interesting behavior of attack phase harmonics can be observed on the recorded sound spectrogram in the figure 4.27. Frequencies greater than fundamental exhibit a rapid modulation of amplitude. In other words they seem to be competing to be the second strongest harmonic in the signal after the fundamental. This random behaviour is responsible for very peculiar character of an abrupt transient of a whistle and unfortunately implemented model is not able to reconstruct it.

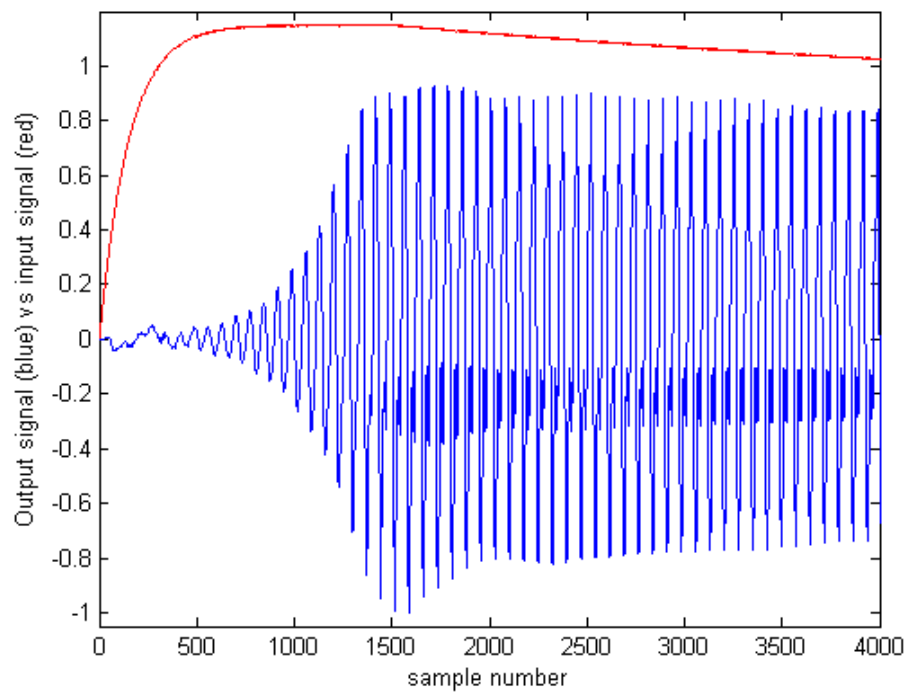


**Figure 4.24 Tin whistle synthesized sound characterized by an abrupt attack. Red curve is an input signal and blue is an output signal.**

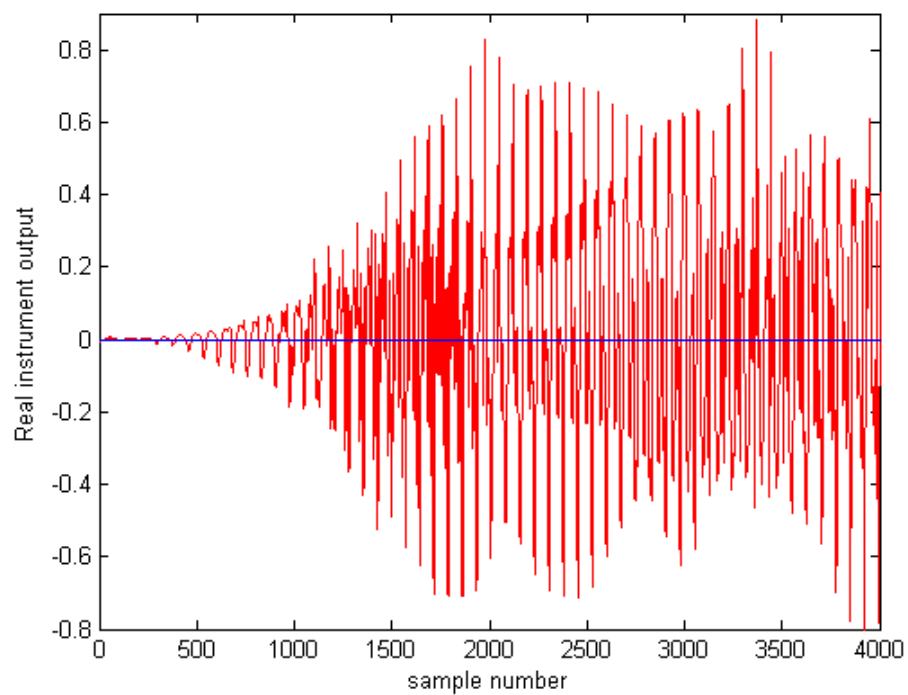


**Figure 4.25 Recorded sound of the Irish whistle characterised by an abrupt attack.**

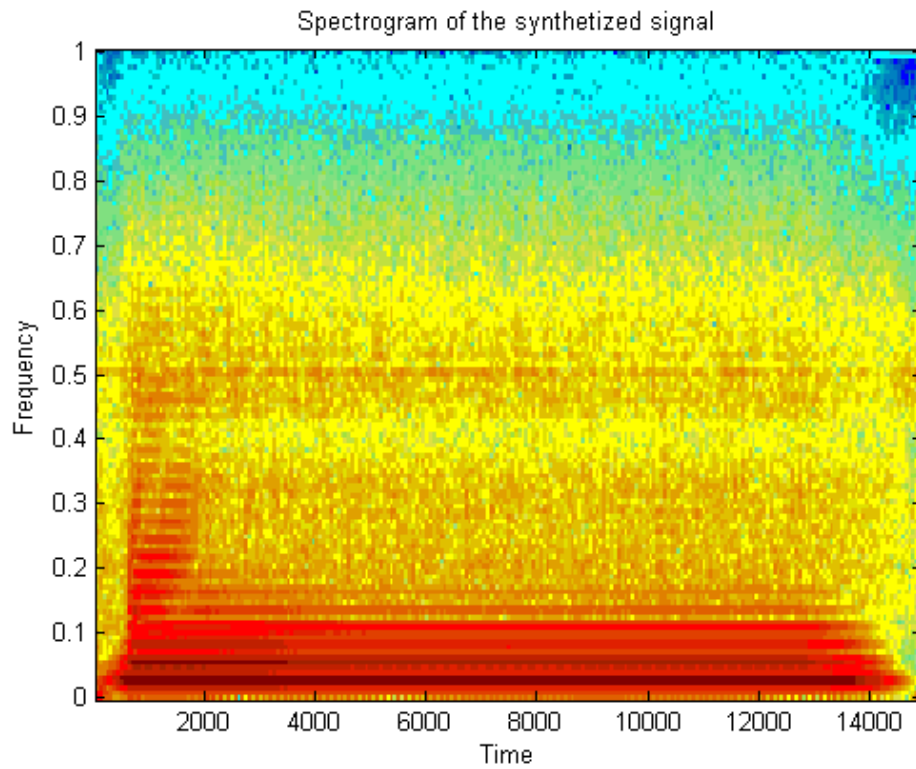


**Figure 4.26 Spectrogram of synthesized tin whistle sound characterized by an abrupt attack.**

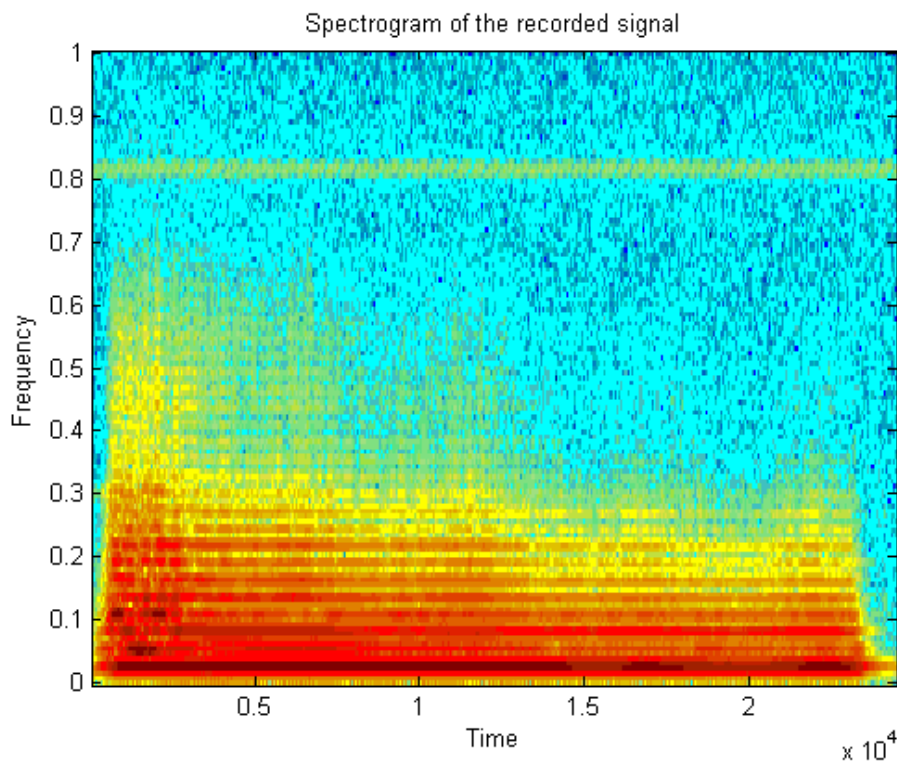


**Figure 4.27 Spectrogram of the recorded Irish whistle sound characterised by an abrupt attack.**

As expected there are perceptible discrepancies between the recorded and synthesized sounds in the stationary phase. Figures 4.28 to 4.29 point out lack of higher harmonics in the generated signal, differences in the phase characteristics and too homogeneous character of neighbouring periods.

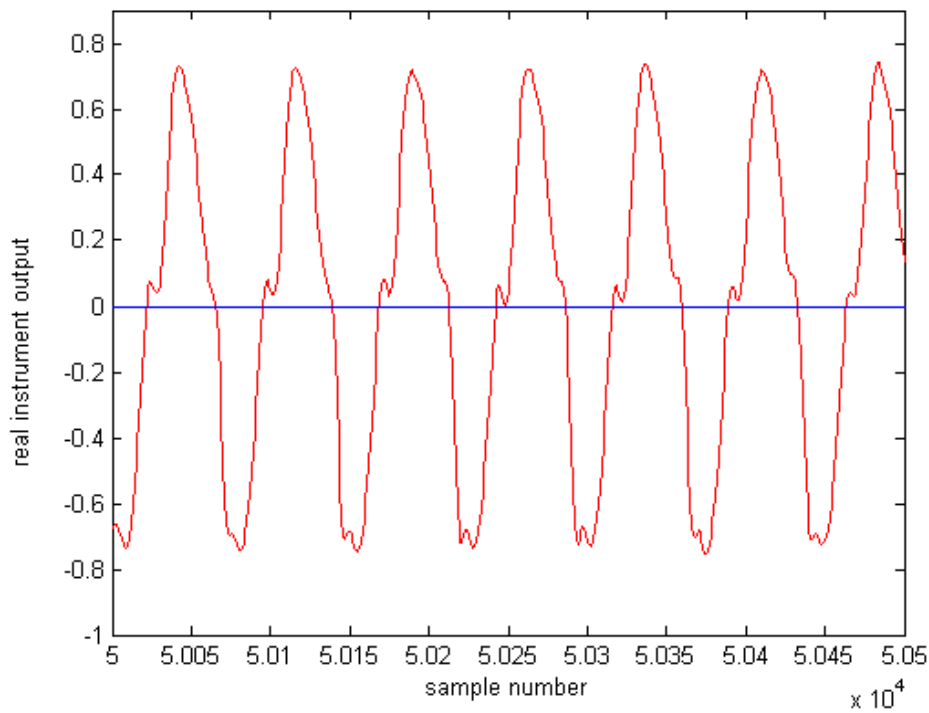


**Figure 4.28 Recorded tin whistle sound - stationary phase.**

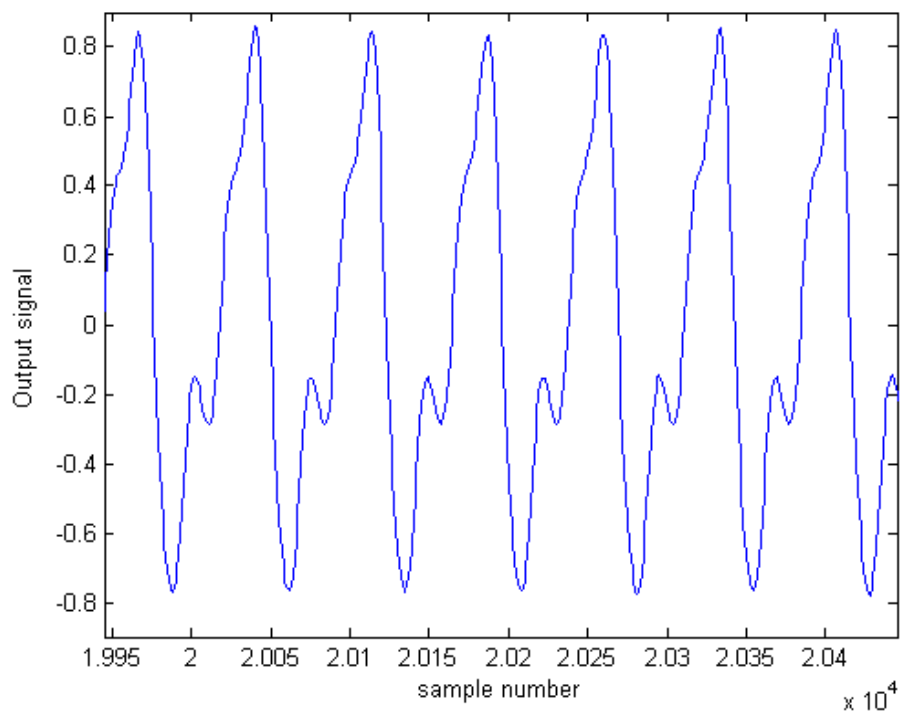


**Figure 4.29 Synthesized tin whistle sound - stationary phase.**

## 4.5 Imperfections of the tin whistle model

The conducted evaluation shows that the implementation may be considered successful. The model is able to produce whistle-like sounds and in general appropriately reacts to different types of excitations and available tone hole configurations. On the other hand, conducted tests have also pointed out several elements of the model which can be improved.

The process of collecting samples revealed that an Irish tin whistle is quite difficult instrument to play, comparing to the commonly known recorder. Even slight variations in the amount of the input mouth pressure cause significant changes in the pitch of produced sound. Hence, amateur musicians may encounter initial problems with the appropriate tuning while playing. The instrument is also prone to mouth pressure variations in the steady state resulting in the amplitude modulation effect, which is difficult to reproduce by the proposed physical model.

As discussed in section 4.4, the generated sound is constant in pitch regardless of the input signal amplitude. The reason lays in the properties of chosen excitation model. Replacing it with the model developed by Verge or De La Cudra may produce more realistic results and allow overblowing without jet length variations. Significant advantage of more advanced models is the possibility to simulate an edge-tone generator of the same virtual dimensions as the geometrical dimensions of natural instrument.

The reason for negligible errors in tuning may be errors in real instrument measurements. However, the implemented model exhibits serious differences in produced fundamental frequencies comparing to the natural whistle. The error increases proportionally to the number of closed tone holes. During tests, in order to keep the model and real instrument in tune in respect to each other, the length of the model bore was varied. This bore length manipulations can be possibly replaced by an appropriate jet length corrections in a function of the number of closed holes.

The WDF tone hole model is suspected to be responsible for tuning problems and timbre discrepancies, even though WDF model is considered to be the most advanced finger hole model available. The height of Irish whistle holes is relatively small comparing to the height of clarinet or transverse flute tone holes. The acoustic properties of typical cylindrically shaped finger hole are different that in the couple millimetre high whistle

hole and the effectiveness of WDF simulation of latter is not completely clear. Moreover musician fingers closing the holes, modify the ideal cylindrical shape of the bore in the unknown manner. Possible improvements of the tone hole model are beyond the scope of this project. During the recording process the high pass radiation characteristics of instrument tone holes came to light. Ignoring that property may be one of the reasons behind the lack of the peculiar noise component in the synthesized sounds. Hence, another possible improvement is a more advanced simulation of the tone hole lattice sound radiation. Each open or partially open tone hole acts as an isotropic source of sound, therefore the sound produced by a natural instrument depends on the number of opened holes, their geometrical dimensions and distances from the sound receiver. In the future simple calculation of the physical model output can be replaced by the radiation model proposed by Scavone and van Walstjin [20], which includes an accurate modelling of the instrument position in respect to the microphone.

## **5 Conclusions and future research**

### **5.1 Research summary**

The project goal formulated as the creation and evaluation of the woodwind instrument physical model has been met at the satisfactorily level. The implemented Irish whistle model is able to generate range of sounds of various timbre and temporal characteristics. Chapter 4 considering evaluation process enlists imperfections responsible for discrepancies between natural and synthesized sounds, with some suggestions considering detected problems.

### **5.2 Recommendations and future research**

The most urgent improvements were discussed in the section 4.5. One can also consider extending the model with the functionality of playing a simple melody, by allowing fingering variations, with the accordant reshape of the input mouth pressure.

The painstaking process of tuning could be greatly improved, if the model would be able to work in real time. Another element increasing the level of excitement during tuning process would be implementing a MIDI control of various parameters and especially a real-time input signal generation using the MIDI breath controller. In such environment the tone hole lattice could be replaced by the simple delay line of varying length. Such solution would eliminate tuning errors and problems with unstable behaviour of the model, both being caused by the tone hole modelling elements.

## 6 Bibliography

- [1] Tolonen, T., Valimaki, V., Karljalainen, M. (1998) *Evaluation of Modern Synthesis Methods*, Laboratory of Acoustics and Audio Signal Processing, Department of Electrical and Communications Engineering, Helsinki University of Technology
- [2] Verge, M. (1995) *Aeroacoustics of confined jets, with application to the physical modeling of recorder-like instruments*, Ph.D thesis, Technische Universiteit Eindhoven
- [3] Yamaha - The team and the technology behind the sound  
[http://www.yamahaproaudio.com/topics/leading\\_technology/addon\\_effects/index.html](http://www.yamahaproaudio.com/topics/leading_technology/addon_effects/index.html)
- [4] Smith, J. O., *Digital Waveguide Synthesis - Selected Tutorials, Papers, Programming Examples, Sound Samples and Related Links*.  
<https://ccrma.stanford.edu/~jos/wg.html>
- [5] Scavone, G. P. , Cook, P. C. , *The Synthesis ToolKit in C++ (STK)*.  
<https://ccrma.stanford.edu/software/stk/>
- [6] Scavone, G. P. (1997) *An acoustic analysis of single-reed woodwind instruments with an emphasis on design and performance issues and digital waveguide modeling techniques*, Ph.D thesis, CCRMA, Stanford University
- [7] Cook, P. R. (2002) *Real Sound Synthesis for Interactive Applications*, A K Peters Ltd.
- [8] Wolfe, J. *How do woodwind instruments works*  
<http://www.phys.unsw.edu.au/jw/woodwind.html>
- [9] Wolfe, J. *Introduction to flute acoustics*  
<http://www.phys.unsw.edu.au/jw/fluteacoustics.html>.
- [10] Wolfe, J. *Introduction to clarinet acoustics*  
<http://www.phys.unsw.edu.au/jw/clarinetacoustics.html>
- [11] Hirschberg, S.W. , Rienstra, A. (2004) *An introduction to acoustics*, Eindhoven University of Technology
- [12] Ystad, S. (2005) *Sound modelling applied to flute sounds*, CNRS Laboratoire de Mecanique et d'Acoustique Marseille
- [13] ISO/IEC 14496-3:1999, *Information technology – Coding of audio-visual objects – Part 3: Audio, Subpart 5: Structured Audio*, Geneva 1999
- [14] MPEG-4 Description

<http://mpeg.chiariglione.org/standards/mpeg-4/mpeg-4.htm>

[15] Lewandowski, M. *AKAI EWI USB/4000S test*. „Estrada i studio magazine”, August 2009

[16] Smith, J. O. *D'Alembert formula derivation*,

[https://ccrma.stanford.edu/~jos/pasp/Traveling\\_Wave\\_Solution\\_I.html](https://ccrma.stanford.edu/~jos/pasp/Traveling_Wave_Solution_I.html)

[17] Levine, H, Schwinger, J. (1947) *On the Radiation of Sound from an Unflanged Circular Pipe*. Harvard University and Cambridge Massachusetts

[18] Smith, J. O., *Tonehole modeling*.

[https://ccrma.stanford.edu/~jos/pasp/Tonehole\\_Modeling.html](https://ccrma.stanford.edu/~jos/pasp/Tonehole_Modeling.html).

[19] Smith, J. O., Scavone, G. P. (1997), *The One-Filter Keefe Clarinet Tonehole*. CCRMA, Stanford

[20] van Walstijn, M., Scavone, G. P. (2000) *The Wave Digital Tonehole Model*, CCRMA, Stanford

[21] Smith, J.O., *Explicit Lagrange Coefficient Formulas*

[https://ccrma.stanford.edu/~jos/pasp/Explicit\\_Lagrange\\_Coefficient\\_Formulas.html](https://ccrma.stanford.edu/~jos/pasp/Explicit_Lagrange_Coefficient_Formulas.html)

[22] Valimaki, V. (1995) *Discrete-Time Modeling of Acoustic Tubes Using Fractional Delay Filters*, Laboratory of Acoustics and Audio Signal Processing, Department of Electrical and Communications Engineering, Helsinki University of Technology

[23] McIntyre, M.E., Schumacher, R.T., Woodhouse, J. (1983) *On the oscillations of musical instruments*

[24] Smith, J. O. (1986) *Efficient simulation of the reed-bore and bow-string mechanisms*. ICMC papers

[25] van Waljstin, M. (2002) *Discrete time modeling of brass and reed instruments with application to musical sound synthesis*. Ph.D thesis, University of Edinburgh

[26]. Avanzini, F. (2001) *Computational issues in physically-based sound models.*, Ph.D thesis, University of Padova

[27] Smyth, T., Abel, J. and Smith, J. O., (2004) *The feathered clarinet reed*. CCRMA, Stanford

[28] Nave, C. R., *Flow controlled valve model for pipe excitation*.  
<http://hyperphysics.phy-astr.gsu.edu/hbase/music/edge3.html>

[29] Coltman, J. W. (1976) *Jet drive mechanisms in edge tones and organ pipes*

- [30] Fletcher, N.H. (1998) *The nonlinear physics of musical instruments*. Research School of Physical Sciences and Engineering, Australian National University.
- [31] de la Cuadra, P. (2006) *Sound of oscillating air jets; physics, modelling and simulation in flute-like instruments*. Ph.D thesis, CCRMA, Stanford
- [32] Wawrzynek, J. (1987) *VLSI concurrent computation for music synthesis*. Ph.D thesis, California Institute of Technology
- [33] Le Brun, M. (1979) *Digital Waveshaping Synthesis*, Journal of the Audio Engineering Society, 27(4), p. 250-266
- [34] Chafe, C. (1995) *Adding vortex noise to wind instrument physical model*, ICMC recordings
- [35] Tymony, J. and others (2004) *Timbral attributes for objective quality assessment of the Irish tin whistle*, Int. Conference of Digital Audio Effects, Naples
- [36] Wood, S. G. (2008) *Objective test methods for digital waveguide synthesis*. M.Sc Thesis, Brigham Young University, York
- [37] Bartsch, M. A. (1999) *A hybrid waveguide model of the transverse flute*, J. Acoust. Soc. Am. Volume 106, Issue 4, pp. 2142-2142
- [38] Karlajainen, M. *Communication acoustics lecture notes*  
<http://www.acoustics.hut.fi/>
- [39] *The official website of Irish flute manufacturer Feadog*.  
<http://www.feadog.ie/>
- [40] *Fundamental frequency tone chart*  
[http://www.daktik.rubikon.pl/muzyka/muzyka\\_tabela\\_czestotliwosci\\_tonow.htm](http://www.daktik.rubikon.pl/muzyka/muzyka_tabela_czestotliwosci_tonow.htm)